OSU-HEP-20-12

arXiv:2009.01771v3 [hep-ph] 24 Mar 2021

Unified Framework for B-Anomalies, Muon $g − 2$, and Neutrino Masses

K.S. Babu,[a] **P.S. Bhupal Dev,**[b] **Sudip Jana,**[c] **Anil Thapa**[a]

[a]*Department of Physics, Oklahoma State University, Stillwater, OK 74078, USA*

[b]*Department of Physics and McDonnell Center for the Space Sciences, Washington University, St. Louis, MO 63130, USA*

[c]*Max-Planck-Institut für Kernphysik, Saupfercheckweg 1, 69117 Heidelberg, Germany*

E-mail: babu@okstate.edu, bdev@wustl.edu, sudip.jana@mpi-hd.mpg.de, thapaa@okstate.edu

ABSTRACT: We present a model of radiative neutrino masses which also resolves anomalies reported in B-meson decays, $R_{D^{(\star)}}$ and $R_{K^{(\star)}}$, as well as in muon $g − 2$ measurement, Δa_μ. Neutrino masses arise in the model through loop diagrams involving TeV-scale leptoquark (LQ) scalars R_2 and S_3. Fits to neutrino oscillation parameters are obtained satisfying all flavor constraints which also explain the anomalies in $R_{D^{(\star)}}$, $R_{K^{(\star)}}$ and Δa_μ within $1\,\sigma$. An isospin-3/2 Higgs quadruplet plays a crucial role in generating neutrino masses; we point out that the doubly-charged scalar contained therein can be produced in the decays of the S_3 LQ, which enhances its reach to 1.1 (6.2) TeV at $\sqrt{s} = 14$ TeV high-luminosity LHC ($\sqrt{s} = 100$ TeV FCC-hh). We also present flavor-dependent upper limits on the Yukawa couplings of the LQs to the first two family fermions, arising from non-resonant dilepton ($pp \to \ell^+\ell^-$) processes mediated by t-channel LQ exchange, which for 1 TeV LQ mass, are found to be in the range $(0.15 − 0.36)$. These limits preclude any explanation of $R_{D^{(\star)}}$ through LQ-mediated B-meson decays involving ν_e or ν_μ in the final state. We also find that the same Yukawa couplings responsible for the chirally-enhanced contribution to Δa_μ give rise to new contributions to the SM Higgs decays to muon and tau pairs, with the modifications to the corresponding branching ratios being at $(2–6)\%$ level, which could be tested at future hadron colliders, such as HL-LHC and FCC-hh.

KEYWORDS: Neutrino Mass, Flavor Anomalies, LHC

Contents

1 Introduction

Among the many reasons to consider physics beyond the Standard Model (SM), an understanding of the origin of neutrino masses stands out, as neutrino oscillations have been firmly established [1] which require nonzero neutrino masses, in contradiction with the SM. While neutrino masses may be accommodated at tree-level simply by the addition of three SM-singlet right-handed neutrino fields having large Majorana masses via the type-I seesaw mechanism [2–7], or by the addition of an $SU(2)_L$-triplet scalar (or fermion) via the type-II [7–9] (or type-III [10]) seesaw, there are other interesting scenarios where small neutrino masses arise naturally as quantum corrections [11–14]. These models of radiative neutrino masses, which we focus on in this paper, are more likely to be accessible for direct experimental tests at colliders. (For recent reviews on radiative neutrino mass models and constraints, see Refs. [15, 16].) Here we show that the new particles that are present in these models to induce neutrino masses can also play an important role in explaining certain persistent experimental anomalies, viz. the anomalous magnetic moment of the muon (Δa_μ), and the lepton-flavor-universality violating decays of the B meson ($R_{D^{(\star)}}$ and $R_{K^{(\star)}}$).

There has been a long-standing discrepancy in the measured value of the anomalous magnetic moment of the muon by the E821 experiment at Brookhaven National Laboratory [17] and the SM theory prediction [18], resulting in a value for $\Delta a_\mu \equiv a_\mu^{\exp} - a_\mu^{\mathrm{SM}} = (27.4 \pm 7.3) \times 10^{-10}$, which indicates a 3.7 σ discrepancy. The muon $g-2$ experiment at Fermilab [19] which is currently in the data accumulation stage, in conjunction with more precise calculations of the dominant hadronic vacuum polarization contribution [20–26], is expected to settle in the near future whether this discrepancy is indeed due to new physics [27]. Meanwhile, it appears to be productive to envision TeV-scale new physics that can account for the observed anomaly. We shall pursue this line of thought here in the presence of an $R_2(\mathbf{3}, \mathbf{2}, 7/6)$ leptoquark (LQ) scalar (in the notation of Ref. [28], where the numbers in parenthesis denote $SU(3)_c \times SU(2)_L \times U(1)_Y$ quantum numbers) that also takes part in radiative neutrino mass generation.

Independently, various anomalies have been reported in the semi-leptonic rare decays of the B-meson by BaBar [29, 30], Belle [31–33] and LHCb [34–37] experiments. The combined average ratio of branching ratios for the charged-current decay, $R_{D^{(\star)}} = \mathrm{BR}(B \to D^{(\star)}\tau\nu)/\mathrm{BR}(B \to D^{(\star)}\ell\nu)$ (with $\ell = e, \mu$) [29–35] differs from the SM prediction [38] by $1.4\,(2.7)\,\sigma$. The ratio of branching ratios for the neutral-current decay $R_{K^{(\star)}} = \mathrm{BR}(B \to K^{(\star)}\mu^+\mu^-)/\mathrm{BR}(B \to K^{(\star)}e^+e^-)$ [36, 37] differs from the SM predictions [39–42] by $2.6\,(2.4)\,\sigma$ in the high-momentum range, while the discrepancy is $2.2\,\sigma$ in the lower-momentum range for $R_{K^\star}$. These anomalies, while taken together, appear to suggest some lepton-flavor-universality violating new physics beyond the SM. The most popular explanation of these anomalies is in terms of scalar LQs. While the charged-current

B-anomaly requires the relevant LQ to have a mass around 1 TeV, the neutral-current anomaly may be explained with a LQ that is somewhat heavier.

A single scalar LQ solution to both $b \to s\ell^+\ell^-$ and $b \to c\tau\nu$ anomalies [43–46] seems to be ruled out when such models are confronted with global fits to $b \to s\mu^+\mu^-$ observables, as well as perturbativity constraints and direct limits from the LHC [47] (see also Refs. [48, 49]). The $R_{D^{(\star)}}$ anomaly may be explained by either an $S_1(\bar{\mathbf{3}}, \mathbf{1}, 1/3)$ or an $R_2(\mathbf{3}, \mathbf{2}, 7/6)$ LQ, while the $R_{K^{(\star)}}$ anomaly may be explained in terms of an $S_3(\bar{\mathbf{3}}, \mathbf{3}, 1/3)$ LQ.[1] Thus, in order to explain both $R_{D^{(\star)}}$ and $R_{K^{(\star)}}$ anomalies, there are two logical options: Addition of (i) $R_2(\mathbf{3}, \mathbf{2}, 7/6)$ and $S_3(\bar{\mathbf{3}}, \mathbf{3}, 1/3)$ LQs, or (ii) $S_1(\bar{\mathbf{3}}, \mathbf{1}, 1/3)$ and $S_3(\bar{\mathbf{3}}, \mathbf{3}, 1/3)$ LQs. Among these options, we find it more compelling to adopt (i) as there is a direct connection with neutrino masses induced radiatively in this case, since both the LQs are essential to generate neutrino mass, unlike option (ii) where only one such LQ is sufficient, along with a color-sextet diquark to ensure lepton number violation [50]. Therefore, we adopt here a radiative neutrino mass model involving $R_2(\mathbf{3}, \mathbf{2}, 7/6)$ and $S_3(\bar{\mathbf{3}}, \mathbf{3}, 1/3)$ LQs, along with an isospin-3/2 Higgs field $\Delta(\mathbf{1}, \mathbf{4}, 3/2)$ which is needed to induce an R_2–$S_3^\star$ mixing that leads to lepton number violation, a requirement to generate Majorana neutrino masses.

We show by explicit construction that a model with $R_2(\mathbf{3}, \mathbf{2}, 7/6)$ and $S_3(\bar{\mathbf{3}}, \mathbf{3}, 1/3)$ LQs plus $\Delta(\mathbf{1}, \mathbf{4}, 3/2)$ Higgs field [46] can simultaneously explain the $R_{D^{(\star)}}$, $R_{K^{(\star)}}$ and Δa_μ anomalies, while being consistent with all low-energy flavor constraints, as well as with the LHC limits. We propose a minimal Yukawa flavor structure that achieves these, while also providing excellent fits to neutrino oscillation parameters. We have also evaluated constraints from $\sqrt{s} = 13$ TeV LHC data on the LQ Yukawa couplings to fermions of the first two families arising from non-resonant $pp \to \ell_i^+ \ell_j^-$ processes mediated by t-channel exchange of LQs. These limits on the couplings are found to be in the range $(0.15 - 0.36)$ for a 1 TeV LQ, which would preclude any solution of $R_{D^{(\star)}}$ with new LQ-mediated decays of the B meson involving ν_e or ν_μ, an *a priori* logical possibility. We also show that the Δ^{++} scalar from the $\Delta(\mathbf{1}, \mathbf{4}, 3/2)$ multiplet, which decays to same-sign dileptons for much of the parameter space, can be probed to masses as large as 1.1 TeV at the high-luminosity (HL) phase of the $\sqrt{s} = 14$ TeV LHC with 3000 fb^{-1} of data, as it can be produced via strong interactions in the decay of $S_3^{4/3} \to (R_2^\star)^{-2/3} + \Delta^{++}$. The mass reach in this new mode is somewhat better than in the standard Drell-Yan (DY) channel. We also find that the same Yukawa couplings responsible for the chirally-enhanced contribution to Δa_μ give rise to new contributions to the SM Higgs decays to muon and tau pairs, with the modifications to the corresponding branching ratios being at a few percent level with opposite signs, which could be tested at future hadron colliders, such as HL-LHC and FCC-hh.

There have been various attempts to explain radiative neutrino masses and a subset of the anomalies in $R_{D^{(\star)}}$, $R_{K^{(\star)}}$ and Δa_μ using scalar LQs. For instance, Ref. [45] has studied neutrino masses, $R_{D^{(\star)}}$ and Δa_μ, whereas Refs. [51–56] address neutrino masses and $R_{K^{(\star)}}$. Similarly, Refs. [57, 58] explain radiative neutrino masses, $R_{D^{(\star)}}$ and $R_{K^{(\star)}}$, while Ref. [59] explains neutrino masses and lepton $g - 2$. In some cases such explanations

---

[1]The R_2 LQ can also explain $R_{K^{(\star)}}$ [46], but only by modifying $b \to se^+e^-$ at tree-level and thus cannot explain the other $b \to s\mu^+\mu^-$ anomalies like P_5' [42].

are disconnected from neutrino mass generation, in the sense that removing certain particle from the model would still result in nonzero neutrino masses [60, 61]. Our approach here is similar in spirit to Ref. [62], which address all three anomalies, viz., $R_{D^{(\star)}}$, $R_{K^{(\star)}}$ and Δa_μ, in the context of radiative neutrino masses; but unlike Ref. [62] we do not introduce new vector-like fermions into the model. In the model proposed here there is a close-knit connection between the $R_{D^{(\star)}}$ and $R_{K^{(\star)}}$ anomalies, Δa_μ and neutrino mass. In particular, neutrino mass generation requires all particles that play a role in explaining these anomalies. Removing any new particle from the model would render the neutrino to be massless. For other models of radiative neutrino mass using LQ scalars, see Refs. [63–68].

The rest of the paper is organized as follows. In Section 2 we present the basic features of the model, including the Yukawa Lagrangian (cf. Section 2.1), scalar potential (cf. Section 2.2), radiative neutrino mass generation mechanism (cf. Section 2.3) and a desired texture for the Yukawa coupling matrices (cf. Section 2.4) consistent with flavor constraints that can explain the flavor anomalies. In Section 3 we discuss how the LQ scalars present in the model explain the $R_{D^{(\star)}}$ and $R_{K^{(\star)}}$ flavor anomalies. In Section 4 we show how the R_2 LQ explains the Δa_μ anomaly. In this section, we also point out the difficulty in simultaneously explaining the electron $g-2$ (cf. Section 4.1), as well as the model predictions for related processes, namely, Higgs decay to lepton pairs (cf. Section 4.2) and muon electric dipole moment (cf. Section 4.3). Section 5 summarizes the low-energy constraints on the LQ couplings and masses. Section 6 analyzes the LHC constraints on the LQs. In Section 7 we present our numerical results for two benchmark fits to the neutrino oscillation data that simultaneously explain $R_{D^{(\star)}}$, $R_{K^{(\star)}}$ and $(g-2)_\mu$ anomalies, while being consistent with all the low-energy and LHC constraints. Section 8 further analyzes the collider phenomenology of the model relevant for the Δ^{++} scalar, and makes testable predictions for HL-LHC and future hadron colliders. Our conclusions are given in Section 9.

2 The Model

The model proposed here aims to explain the B-physics anomalies $R_{D^{(\star)}}$ and $R_{K^{(\star)}}$, as well as the muon $(g-2)$ anomaly Δa_μ, and at the same time induce small neutrino masses as radiative corrections. To this end, we choose the gauge symmetry and the fermionic content of the model to be identical to the SM, while the scalar sector is extended to include three new states, apart from the SM Higgs doublet H:

$$R_2\ (\mathbf{3},\mathbf{2},7/6)\ =\ \left(\omega^{5/3}\ \omega^{2/3}\right)^T, \qquad S_3\ (\bar{\mathbf{3}},\mathbf{3},1/3)\ =\ \left(\rho^{4/3}\ \rho^{1/3}\ \rho^{-2/3}\right)^T,$$

$$\Delta\ (\mathbf{1},\mathbf{4},3/2)\ =\ \left(\Delta^{+++}\ \Delta^{++}\ \Delta^+\ \Delta^0\right)^T, \quad H\ (\mathbf{1},\mathbf{2},1/2)\ =\ \left(H^+\ H^0\right)^T. \qquad (2.1)$$

Here the numbers within brackets represent the transformation properties under the SM gauge group $SU(3)_c \times SU(2)_L \times U(1)_Y$. The superscripts on various fields denote their respective electric charge Q defined as $Q = I_3 + Y$, with I_3 being the third-component of $SU(2)_L$-isospin. The R_2 and S_3 LQs are introduced to explain $R_{D^{(\star)}}$ and $R_{K^{(\star)}}$ anomalies respectively. The R_2 LQ also explains Δa_μ through a chirally-enhanced operator it induces, which is proportional to the top quark mass. The $SU(2)_L$-quadruplet Δ field mixes $\omega^{2/3}$

from R_2 with $\bar{\rho}^{2/3}$ from $S_3^\star$ (the complex conjugate of $\rho^{-2/3}$), which is needed to generate Majorana neutrino masses radiatively. This multiplet, with its characteristic triply-charged component, was introduced to generate tree-level neutrino masses from dimension (d)-7 effective operators in Ref. [69]; here we use it for radiative mass generation, also via $d = 7$ operators.

2.1 Yukawa Couplings

In addition to the SM Yukawa couplings of the fermions involving the Higgs-doublet field H, the following Yukawa couplings of the R_2 and S_3 LQs are allowed in the model:[2]

$$\mathcal{L}_Y = \hat{f}_{ab}(u_a^{cT}C\psi_b^i)R_2^j\epsilon_{ij} - \hat{f}'_{ab}(Q_a^{iT}Ce_b^c)\widetilde{R}_2^j\epsilon_{ij} + \hat{y}_{ab}(Q_a^T C\tau_\alpha\psi_b)S_{3\alpha} - \hat{y}'_{ab}(Q_a^T C\tau_\alpha Q_b)S_{3\alpha}^\star + \text{H.c.} \tag{2.2}$$

Here we have adopted a notation where all fermion fields are left-handed. $Q = (u\ d)^T$ and $\psi = (\nu\ e)^T$ are the SM quark and lepton doublets respectively, $\{i, j\}$ are $SU(2)$ indices, $\{a, b\}$ are flavor indices, C is the charge conjugation matrix, ϵ_{ij} is the $SU(2)$ Levi-Civita tensor, $\widetilde{R}_2 = i\tau_2 R_2^\star$, and τ_α (with $\alpha = 1, 2, 3$) are the Pauli matrices in the doublet representation of $SU(2)$. The color contraction is unique in each term, which is not shown. It is to be noted that S_3 possesses both leptoquark and diquark couplings, as shown in Eq. (2.2), which would lead to potentially dangerous proton decay operators. Therefore, we set the diquark coupling $\hat{y}'_{ab}$ to zero in Eq. (2.2), so that baryon number remains unbroken. This is achieved by assigning baryon number $B = -1/3$ to S_3 and $R_2^\star$, along with $B = 1/3$ for quarks and $-1/3$ for anti-quarks, and 0 for leptons and anti-leptons.

We redefine fields to go from the flavor basis (u, d, e) to the mass eigenstates (u^0, d^0, e^0) for the charged fermions (and similarly for the (u^c, d^c, e^c) fields) via the following unitary rotations in family space:

$$u = V_u u^0, \quad d = V_d d^0, \quad e = V_e e^0, \quad \nu = V_e \nu^0,$$
$$u^c = V_{u^c} u^{c0}, \quad d^c = V_{d^c} d^{c0}, \quad e^c = V_{e^c} e^{c0}. \tag{2.3}$$

The Cabibbo-Kobayashi-Maskawa (CKM) quark mixing matrix V_{CKM} is generated in the process and is given by

$$V = V_u^\dagger V_d = P V_{\text{CKM}} Q, \tag{2.4}$$

where P, Q are diagonal phase matrices which are unphysical in the SM, but become physical in non-SM interactions, such as the ones involving the LQs. These phases will have an effect on CP-violating observables, such as the muon electric dipole moment (EDM), see Section 4.3. Note that the unitary rotation on the neutrino fields in Eq. (2.3) is the same as for left-handed lepton fields e, and therefore no Pontecorvo-Maki-Nakagawa-Sakata (PMNS) mixing in the charged weak-current interactions of leptons is induced at this stage. For explaining the anomalies in B-decays and in muon $g - 2$, there is no need to go to the mass eigenstates of the neutrinos; the distinction between the mass and flavor eigenstates

---

[2]The field Δ has no Yukawa couplings with fermions at the tree-level, but couples to the leptons at one-loop level (cf. Eq. (2.52)).

will only affect neutrino oscillation phenomenology. For convenience, we also redefine the Yukawa couplings as follows:

$$V_{u^c}^T \hat{f} V_e \ \equiv \ f, \quad V_u^T \hat{f}' V_{e^c} \ \equiv \ V^T f', \quad V_u^T \hat{y} V_e \ \equiv \ V^T y. \tag{2.5}$$

Eq. (2.2) can now be written in terms of mass eigenstate fermions (except for neutrinos which are still flavor eigenstates) and the redefined Yukawa couplings as

$$
\begin{aligned}
\mathcal{L}_Y \ = \ & u^{cT} C f \nu \omega^{2/3} - u^{cT} C f e \omega^{5/3} + u^T C (V^\star f') e^c \omega^{-5/3} + d^T C f' e^c \omega^{-2/3} \\
& - u^T C (V^\star y) \nu \rho^{-2/3} + u^T C (V^\star y) e \frac{\rho^{1/3}}{\sqrt{2}} + d^T C y \nu \frac{\rho^{1/3}}{\sqrt{2}} + d^T C y e \rho^{4/3} + \text{H.c.} \quad (2.6)
\end{aligned}
$$

Here we have dropped the superscript ^{0} in the labeling of mass eigenstates. In the discussions that follow, the quark and lepton fields are to be identified as mass eigenstates. Note that the Yukawa coupling matrices f' and y, which respectively appear in the $d - e^c$ and $d - e$ couplings, also appear in the $u - e^c$ and $u - e$ couplings, along with the generalized CKM matrix V. Any texture adopted for f' and y should therefore be consistent with flavor violation in both down-type and up-type quark sectors. The flavor indices i and j in f_{ij} (and similarly for f' and y) refer to the quark flavor and the lepton flavor respectively. We shall make use of these interactions in explaining the B-anomalies, Δa_μ and radiative neutrino masses.

2.2 Scalar Sector

The most general renormalizable Higgs potential involving H, R_2, S_3 and Δ is given by:

$$
\begin{aligned}
V \ = \ & -\mu_H^2 H^\dagger H + \mu_R^2 R_2^\dagger R_2 + \mu_S^2 S_3^\dagger S_3 + \mu_\Delta^2 \Delta^\dagger \Delta + \frac{\lambda_H}{2}(H^\dagger H)^2 + \frac{\lambda_R}{2}(R_2^\dagger R_2)^2 \\
& + \frac{\widetilde{\lambda}_R}{2}(R_2^{\dagger\alpha} R_{2\beta})(R_2^{\dagger\beta} R_{2\alpha}) + \frac{\lambda_S}{2}(S_3^\dagger S_3)^2 + \frac{\lambda_S'}{2}(S_3^\dagger T_a S_3)^2 + \frac{\widetilde{\lambda}_S}{2}(S_3^{\dagger\alpha} S_{3\beta})(S_3^{\dagger\beta} S_{3\alpha}) \\
& + \frac{\widetilde{\lambda}_S'}{2}(S_3^{\dagger\alpha} T_a S_{3\beta})(S_3^{\dagger\beta} T_a S_{3\alpha}) + \frac{\lambda_\Delta}{2}(\Delta^\dagger \Delta)^2 + \frac{\lambda_\Delta'}{2}(\Delta^\dagger T_a' \Delta)^2 + \lambda_{HR}(H^\dagger H)(R_2^\dagger R_2) \\
& + \lambda_{HR}'(H^\dagger \tau_a H)(R_2^\dagger \tau_a R_2) + \lambda_{HS}(H^\dagger H)(S_3^\dagger S_3) + \lambda_{HS}'(H^\dagger \tau_a H)(S_3^\dagger T_a S_3) \\
& + \lambda_{H\Delta}(H^\dagger H)(\Delta^\dagger \Delta) + \lambda_{H\Delta}'(H^\dagger \tau_a H)(\Delta^\dagger T_a' \Delta) + \lambda_{RS}(R_2^\dagger R_2)(S_3^\dagger S_3) \\
& + \lambda_{RS}'(R_2^\dagger \tau_a R_2)(S_3^\dagger T_a S_3) + \widetilde{\lambda}_{RS}(R_2^{\dagger\alpha} R_{2\beta})(S_3^{\dagger\alpha} S_{3\beta}) + \widetilde{\lambda}_{RS}'(R_2^{\dagger\alpha} \tau_a R_{2\beta})(S_3^{\dagger\alpha} T_a S_{3\beta}) \\
& + \lambda_{R\Delta}(R_2^\dagger R_2)(\Delta^\dagger \Delta) + \lambda_{R\Delta}'(R_2^\dagger \tau_a R_2)(\Delta^\dagger T_a' \Delta) + \lambda_{S\Delta}(S_3^\dagger S_3)(\Delta^\dagger \Delta) \\
& + \lambda_{S\Delta}'(S_3^\dagger T_a S_3)(\Delta^\dagger T_a' \Delta) + \lambda_{S\Delta}''(S_3^\dagger T_a T_b S_3)(\Delta^\dagger T_a' T_b' \Delta) \\
& + \left(\mu \Delta^{\star ijk} R_{2_i} S_{3_{jk}} + \lambda_{RHS^2} R_2^{i*} S_{3ij} S_{3kl} H_m \epsilon^{jk} \epsilon^{lm} + \lambda_{\Delta H^3} \Delta^{\star ijk} H_i H_j H_k + \text{H.c.} \right).
\end{aligned}
\tag{2.7}
$$

Here $\{i, j\}$ are $SU(2)_L$ indices, $\{\alpha, \beta\}$ are $SU(3)_c$ indices, τ_a are the Pauli matrices, and T_a, T_a' (with $a = 1, 2, 3$) are the normalized generators of $SU(2)$ in the triplet and quadruplet representations, respectively.[3] Color-singlet contractions not shown explicitly are to be

---

[3]This potential differs considerably from the one given in Ref. [46], which is missing many terms.

assumed among two colored fields within the same bracket. For example, the λ'_{RS} term has the color contraction $(R_2^{\dagger\alpha}\tau_a R_{2\alpha})(S_3^{\dagger\beta}T_a S_{3\beta})$. Here $S_{3_{ij}}$ and Δ^{ijk} are the completely symmetric rank-2 and rank-3 tensors of $SU(2)$, with their components related to those given in Eq. (2.1) as:

$$S_{3_{11}} = \rho^{4/3}, \quad S_{3_{12}} = \frac{\rho^{1/3}}{\sqrt{2}}, \quad S_{3_{22}} = \rho^{-2/3},$$

$$\Delta_{111} = \Delta^{+++}, \quad \Delta_{112} = \frac{\Delta^{++}}{\sqrt{3}}, \quad \Delta_{122} = \frac{\Delta^{+}}{\sqrt{3}}, \quad \Delta_{222} = \Delta^{0}. \quad (2.8)$$

The presence of the quartic coupling with coefficient $\lambda_{\Delta H^3}$ in Eq. (2.7) will induce a vacuum expectation value (VEV) for the neutral component of Δ, even when $\mu_\Delta^2 > 0$ is chosen. The cubic coupling with coefficient μ would then lead to mixing of $\omega^{2/3}$ and $\bar{\rho}^{2/3}$ components of R_2 and $S_3^\star$ LQ fields. Such a mixing is required to realize lepton number violation and to generate neutrino masses. We shall be interested in the choice $\mu_H^2 > 0$ (which leads to electroweak symmetry breaking), and $\mu_R^2, \mu_S^2 > 0$ (so that electric charge and color remain unbroken), and $\mu_\Delta^2 > 0$ – so that Δ^0 acquires only an induced VEV. To ensure that this desired vacuum is indeed a local minimum of the potential, we now proceed to derive the masses of all scalars in the model.

2.2.1 Scalar Masses

We denote the VEVs of H^0 and Δ^0 fields as

$$\langle H^0 \rangle = \frac{v}{\sqrt{2}}, \qquad \langle \Delta^0 \rangle = \frac{v_\Delta}{\sqrt{2}}, \quad (2.9)$$

with $(v^2 + 3\,v_\Delta^2) \simeq (246.2 \text{ GeV})^2$ determined from the Fermi constant G_F. While v can be taken to be real by a gauge rotation, v_Δ is complex in general. However, all the complex-valued couplings of the potential, i.e. terms in the last line of Eq. (2.7), can be made real by field redefinitions, which we adopt, and consequently minimization of the potential would make v_Δ real as well.

We obtain the following conditions for the potential to be an extremum around the VEVs of Eq. (2.9), assuming that $v \neq 0$:

$$-\mu_H^2 + \frac{1}{2}\lambda_H v^2 + \frac{v_\Delta}{4}\left(6\lambda_{\Delta H^3} v + 2\lambda_{H\Delta} v_\Delta + 3\lambda'_{H\Delta} v_\Delta\right) = 0, \quad (2.10)$$

$$\mu_\Delta^2 v_\Delta + \frac{1}{2}\lambda_{\Delta H^3} v^3 + \left(\frac{1}{2}\lambda_{H\Delta} + \frac{3}{4}\lambda'_{H\Delta}\right) v^2 v_\Delta + \left(\frac{1}{2}\lambda_\Delta + \frac{9}{8}\lambda'_\Delta\right) v_\Delta^3 = 0. \quad (2.11)$$

We eliminate μ_H^2 and μ_Δ^2 using these two conditions. To derive the scalar mass spectrum, we construct the mass matrices from the bilinear terms resulting from expanding the potential in Eq. (2.7) around the VEVs v and v_Δ.

The 2×2 mass matrix involving the mixing of the charge-2/3 LQs in the basis $(\omega^{2/3}, \bar{\rho}^{2/3})$ is found to be:

$$M_{2/3}^2 = \begin{pmatrix} m_{\omega^{2/3}}^2 & \mu\frac{v_\Delta}{\sqrt{2}}, \\ \mu\frac{v_\Delta}{\sqrt{2}} & m_{\rho^{2/3}}^2 \end{pmatrix}, \quad (2.12)$$

where

$$m^2_{\omega^{2/3}} = \mu^2_R + \frac{v^2}{2}(\lambda_{HR} + \lambda'_{HR}) + \frac{v^2_\Delta}{4}(2\lambda_{R\Delta} + 3\lambda'_{R\Delta}), \tag{2.13}$$

$$m^2_{\rho^{2/3}} = \mu^2_S + \frac{v^2}{2}(\lambda_{HS} + \lambda'_{HS}) + \frac{v^2_\Delta}{8}(4\lambda_{S\Delta} + 6\lambda'_{S\Delta} + 9\lambda''_{S\Delta}). \tag{2.14}$$

The mass eigenstates denoted as $X_{1,2}$ are given by

$$X_1 = \cos\varphi\,\omega^{2/3} + \sin\varphi\,\bar\rho^{2/3}, \tag{2.15}$$

$$X_2 = -\sin\varphi\,\omega^{2/3} + \cos\varphi\,\bar\rho^{2/3}, \tag{2.16}$$

where the mixing angle φ is defined as

$$\tan 2\varphi = \frac{\sqrt{2}v_\Delta\mu}{(m^2_{\omega^{2/3}} - m^2_{\rho^{2/3}})}. \tag{2.17}$$

The mass eigenvalues of the charge-2/3 LQ fields are then given as

$$m^2_{X_1,X_2} = \frac{1}{2}\left[m^2_{\omega^{2/3}} + m^2_{\rho^{2/3}} \pm \sqrt{(m^2_{\omega^{2/3}} - m^2_{\rho^{2/3}})^2 + 2\mu^2 v^2_\Delta}\right]. \tag{2.18}$$

The masses for the remaining LQ components ($\omega^{5/3}$, $\rho^{1/3}$, $\rho^{4/3}$) are obtained as follows:

$$m^2_{\omega^{5/3}} = \mu^2_R + \frac{v^2}{2}(\lambda_{HR} - \lambda'_{HR}) + \frac{v^2_\Delta}{4}(2\lambda_{R\Delta} - 3\lambda'_{R\Delta}), \tag{2.19}$$

$$m^2_{\rho^{1/3}} = \mu^2_S + \frac{v^2}{2}\lambda_{HS} + \frac{v^2_\Delta}{4}(2\lambda_{S\Delta} + 3\lambda''_{S\Delta}), \tag{2.20}$$

$$m^2_{\rho^{4/3}} = \mu^2_S + \frac{v^2}{2}(\lambda_{HS} - \lambda'_{HS}) + \frac{v^2_\Delta}{8}(4\lambda_{S\Delta} - 6\lambda'_{S\Delta} + 15\lambda''_{S\Delta}). \tag{2.21}$$

As for the Δ fields, the masses of the triply and doubly-charged components are given by

$$m^2_{\Delta^{+++}} = -\frac{3\lambda'_{H\Delta}v^2}{2} - \frac{9\lambda'_\Delta v^2_\Delta}{4} - \frac{\lambda_{\Delta H^3}v^3}{2v_\Delta}, \tag{2.22}$$

$$m^2_{\Delta^{++}} = -\lambda'_{H\Delta}v^2 - \frac{3\lambda'_\Delta v^2_\Delta}{2} - \frac{\lambda_{\Delta H^3}v^3}{2v_\Delta}. \tag{2.23}$$

The singly-charged components of H and Δ will mix, with a mass matrix given by:

$$M^2_+ = \frac{1}{2}\left(\lambda_{\Delta H^3}v + \lambda'_{H\Delta}v_\Delta\right)\begin{pmatrix} -3v_\Delta & \sqrt{3}v \\ \sqrt{3}v & -\frac{v^2}{v_\Delta} \end{pmatrix}. \tag{2.24}$$

One combination of $(H^\pm, \Delta^\pm)$ fields is the Goldstone boson $(G^\pm)$ eaten up by the $W^\pm$ gauge boson, while the other combination $(\delta^\pm)$ is a physical charged Higgs field. These fields are

$$G^+ = \frac{vH^+ + \sqrt{3}v_\Delta\Delta^+}{\sqrt{v^2 + 3v^2_\Delta}}, \qquad \delta^+ = \frac{\sqrt{3}v_\Delta H^+ - v\Delta^+}{\sqrt{v^2 + 3v^2_\Delta}}, \tag{2.25}$$

with the mass of δ^+ given by[4]

$$m_{\delta^+}^2 = -\frac{\lambda'_{H\Delta}\left(v^2 + 3v_\Delta^2\right)}{2} - \frac{\lambda_{\Delta H^3}\left(v^3 + 3v_\Delta^2 v\right)}{2v_\Delta}. \tag{2.26}$$

The neutral CP-even scalars do not mix with the CP-odd scalars, since all couplings and VEVs are real. The mass matrix for the CP-even states in the basis (Re H^0, Re Δ^0) reads as:

$$M_{\text{even}}^2 = \begin{pmatrix} \lambda_H v^2 + \frac{3}{2}\lambda_{\Delta H^3}vv_\Delta & \frac{v}{2}\left[3\lambda_{\Delta H^3}v + (2\lambda_{H\Delta} + 3\lambda'_{H\Delta})v_\Delta\right] \\ \frac{v}{2}\left[3\lambda_{\Delta H^3}v + (2\lambda_{H\Delta} + 3\lambda'_{H\Delta})v_\Delta\right] & -\frac{\lambda_{\Delta H^3}v^3}{2v_\Delta} + \left(\lambda_\Delta + \frac{9}{4}\lambda'_\Delta\right)v_\Delta^2 \end{pmatrix}. \tag{2.27}$$

The resulting mass eigenvalues are given by

$$m_{h,H}^2 = \frac{1}{2}\left[\lambda_H v^2 + (\lambda_\Delta + \frac{9}{4}\lambda'_\Delta)v_\Delta^2 - \frac{\lambda_{\Delta H^3}v(v^2 - 3v_\Delta^2)}{2v_\Delta} \pm \sqrt{A}\right] \tag{2.28}$$

where

$$A = \left\{\lambda_H v^2 - \left(\lambda_\Delta + \frac{9}{4}\lambda'_\Delta\right)v_\Delta^2 + \frac{\lambda_{\Delta H^3}v(v^2 + 3v_\Delta^2)}{2v_\Delta}\right\}^2$$
$$+ v^2\left[3\lambda_{\Delta H^3}v + (2\lambda_{H\Delta} + 3\lambda'_{H\Delta})v_\Delta\right]^2. \tag{2.29}$$

The corresponding mass eigenstates are given by

$$h = \cos\alpha\,\text{Re}(H^0) + \sin\alpha\,\text{Re}(\Delta^0), \tag{2.30}$$
$$H = -\sin\alpha\,\text{Re}(H^0) + \cos\alpha\,\text{Re}(\Delta^0), \tag{2.31}$$

with

$$\sin 2\alpha = \frac{v\left[3\lambda_{\Delta H^3}v + (2\lambda_{H\Delta} + 3\lambda'_{H\Delta})v_\Delta\right]}{(m_H^2 - m_h^2)}. \tag{2.32}$$

The field h is to be identified as the SM-like Higgs boson of mass 125 GeV.

Similarly, the CP-odd scalar mass matrix, in the basis (Im H^0, Im Δ^0) is given by

$$M_{\text{odd}}^2 = \frac{1}{2}\lambda_{\Delta H^3}v\begin{pmatrix} -9v_\Delta & 3v \\ 3v & -\frac{v^2}{v_\Delta} \end{pmatrix}. \tag{2.33}$$

We identify the Goldstone mode G^0 eaten up by the Z^0 gauge boson and the physical pseudoscalar Higgs boson A^0 as

$$G^0 = \frac{v\,\text{Im}(H^0) + 3v_\Delta\text{Im}(\Delta^0)}{\sqrt{v^2 + 9v_\Delta^2}}, \qquad A^0 = \frac{3v_\Delta\text{Im}(H^0) - v\,\text{Im}(\Delta^0)}{\sqrt{v^2 + 9v_\Delta^2}}, \tag{2.34}$$

with the mass of A^0 given by

$$m_A^2 = -\frac{\lambda_{\Delta H^3}v^3}{2v_\Delta} - \frac{9\lambda_{\Delta H^3}vv_\Delta}{2}. \tag{2.35}$$

---

[4]In the limit $v_\Delta \ll v$, the physical δ^+ field is nearly identical to the original Δ^+ field. So we will use the same notation for m_{δ^+} and m_{Δ^+}.

The VEV v_Δ must obey the condition $v_\Delta \ll v$ from electroweak T-parameter constraint. In presence of v_Δ, the electroweak ρ parameter deviates from unity at tree-level, with the deviation given by [69]

$$\delta\rho \simeq -6\frac{v_\Delta^2}{v^2} . \tag{2.36}$$

Although there are also loop-induced contributions to $\delta\rho$, arising from the mass splittings among components of Δ, R_2, S_3 fields which typically have the opposite sign compared to Eq. (2.36), we assume that there is no precise cancellation between these two types of contributions. A parameter ρ_0, defined as

$$\rho_0 = \frac{m_W^2}{m_Z^2 \hat{c}_Z^2 \hat{\rho}} \tag{2.37}$$

(where $\hat{c}_Z \equiv \cos\theta_W(m_Z)$ in the $\overline{\text{MS}}$ scheme, θ_W being the weak mixing angle, and $\hat{\rho}$ includes leading radiative corrections from the SM), has a global average $\rho_0 = 1.00038 \pm 0.00020$ [1]. Eq. (2.36) can be compared to this global value, with $\rho_0 = 1$ in the SM, which sets a limit of $|v_\Delta| \leq 1.49$ GeV, allowing for $3\,\sigma$ variation, and ignoring loop contributions proportional to mass splitting among multiplets.

In the approximation $|v_\Delta| \ll |v|$, one can solve for v_Δ from Eq. (2.11), to get

$$v_\Delta \simeq -\frac{\lambda_{\Delta H^3} v^3}{2\mu_\Delta^2} . \tag{2.38}$$

Substituting this into the masses of the Higgs quadruplet components, we obtain [69]

$$m_{\Delta_i}^2 \simeq \mu_\Delta^2 - q_i \frac{\lambda'_{H\Delta} v^2}{2} , \tag{2.39}$$

where q_i is the (non-negative) electric charge of the component field Δ_i (with $i = 1, 2, 3, 4$ denoting the four components of Δ given in Eq. (2.1)). We note that there are two possibilities for mass ordering among these components, depending on the sign of the quartic coupling $\lambda'_{H\Delta}$, with $m_{\Delta^{+++}}$ being either the heaviest or the lightest member. Phenomenology of these scenarios has been studied extensively in Refs. [69–72].

By choosing all the bare mass parameters μ_X^2 (for $X = H, R_2, S_3, \Delta$) in Eq. (2.7) to be positive, and the quartic coupling λ_H to be positive, the desired minimum can be shown to be a local minimum, as long as the masses of Δ, R_2, S_3 are well above $v \simeq 246$ GeV. To verify that this minimum is also the absolute minimum of the potential for some range of parameters, further work has to be done, which is beyond the scope of this paper. Since none of the quartic couplings, except for $\lambda_{\Delta H^3}$, plays any crucial role for our analysis, it appears possible to achieve this condition. Similarly, there is enough freedom to choose the quartic couplings so that the potential remains bounded from below. We shall discuss below a set of necessary conditions for the potential to be bounded, which will find application in Section 4.2 in the discussion of modified rates for $h \to \ell^+\ell^-$ in the model.

2.2.2 Necessary Conditions for Boundedness of the Potential

While the full set of necessary and sufficient conditions on the quartic couplings of Eq. (2.7) for the Higgs potential to be bounded from below is not easily tractable, certain necessary

conditions of phenomenological interest (cf. Section 4.2) can be analyzed analytically. We focus on the quartic couplings involving only the H and R_2 fields, which will turn out to be of phenomenological interest. With $SU(2)_L$ and $SU(3)_c$ rotations, these fields can be brought to the form

$$H \; = \; \begin{pmatrix} 0 \\ v \end{pmatrix}, \qquad R_2 \; = \; \begin{pmatrix} x & 0 & 0 \\ y\sin\alpha e^{i\phi} & y\cos\alpha & 0 \end{pmatrix}, \tag{2.40}$$

where in R_2, the color indices run horizontally. Here v, x, y can be taken to be real. The quartic terms $V^{(4)}(H, R_2)$ can be then written as

$$V^{(4)}(H, R_2) \; = \; \frac{1}{2} \left(v^2 \; x^2 \; y^2 \right) \hat{\lambda} \begin{pmatrix} v^2 \\ x^2 \\ y^2 \end{pmatrix}, \tag{2.41}$$

where $\hat{\lambda}$ is defined as

$$\hat{\lambda} \; = \; \begin{pmatrix} \lambda_H & \lambda_{HR} - \lambda'_{HR} & \lambda_{HR} + \lambda'_{HR} \\ \lambda_{HR} - \lambda'_{HR} & \lambda_R + \tilde{\lambda}_R & \lambda_R + \tilde{\lambda}_R \sin^2\alpha \\ \lambda_{HR} + \lambda'_{HR} & \lambda_R + \tilde{\lambda}_R \sin^2\alpha & \lambda_R + \tilde{\lambda}_R \end{pmatrix}. \tag{2.42}$$

The necessary and sufficient conditions for boundedness of this potential can now be derived from the co-positivity of real symmetric matrices [73–75]:

$$\lambda_H \; \geq \; 0\,, \tag{2.43}$$

$$\lambda_R + \tilde{\lambda}_R \; \geq \; 0\,, \tag{2.44}$$

$$\lambda_{HR} - \lambda'_{HR} \; \geq \; -\sqrt{\lambda_H(\lambda_R + \tilde{\lambda}_R)}\,, \tag{2.45}$$

$$\lambda_{HR} + \lambda'_{HR} \; \geq \; -\sqrt{\lambda_H(\lambda_R + \tilde{\lambda}_R)}\,, \tag{2.46}$$

$$\lambda_R + \tilde{\lambda}_R \sin^2\alpha \; \geq \; -(\lambda_R + \tilde{\lambda}_R)\,, \tag{2.47}$$

$$(\lambda_{HR} - \lambda'_{HR})\sqrt{\lambda_R + \tilde{\lambda}_R} + (\lambda_R + \tilde{\lambda}_R \sin^2\alpha)\sqrt{\lambda_H}$$
$$+ (\lambda_{HR} + \lambda'_{HR})\sqrt{\lambda_R + \tilde{\lambda}_R} + (\lambda_R + \tilde{\lambda}_R)\sqrt{\lambda_H} \; \geq \; 0 \quad \text{or} \quad \det(\hat{\lambda}) \; \geq \; 0\,. \tag{2.48}$$

These conditions should hold for any value of the angle α.

Note that from Eq. (2.45) it follows that if $(\lambda_{HR} - \lambda'_{HR})$ is negative, its magnitude cannot exceed about 1.33, if we demand that none of the quartic couplings should exceed $\sqrt{4\pi}$ in magnitude from perturbativity considerations, and using the fact that $\lambda_H \simeq 0.25$ is fixed from the mass of h, $m_h = 125$ GeV. This result will be used in the calculation of the modified Higgs branching ratio $h \to \ell^+\ell^-$ in Section 4.2.

2.3 Radiative Neutrino Masses

Neutrino masses are zero at the tree-level in the model. However, since lepton number is not conserved, nonzero M_ν will be induced as quantum corrections. The leading diagrams generating M_ν are shown in Fig. 1, mediated by the charge-2/3 LQs. The Yukawa couplings
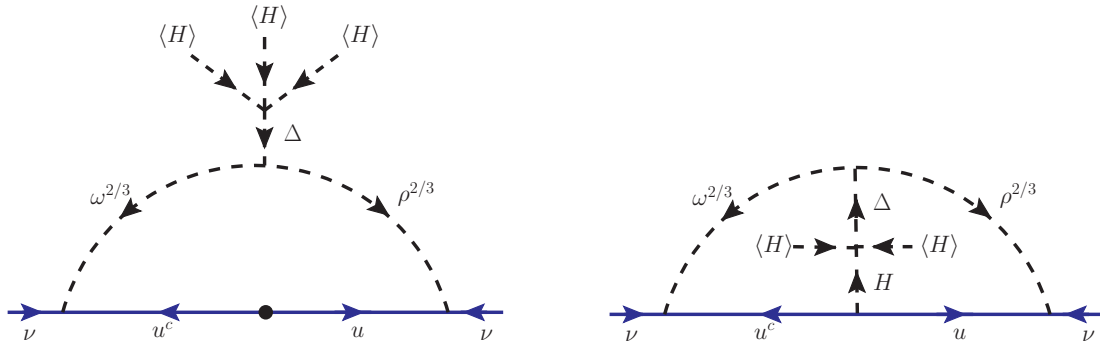
Figure 1: Feynman diagram generating neutrino masses through the exchange of LQs in the model. The one-loop diagram shown is the leading contribution, while the two-loop diagram can be important. The dot (•) on the SM fermion line in the one-loop diagram indicates mass insertion arising from the SM Higgs doublet VEV. There is a second set of diagrams obtained by reversing the arrows on the internal particles.

in Eq. (2.6), together with the $\Delta^\star R_2 S_3$ trilinear term and the $\Delta^\star HHH$ quartic term in the scalar potential (2.7), guarantee lepton number violation. These interactions result in an effective $d = 9$ operator that violates lepton number by two units, given by $\widetilde{\mathcal{O}}_1 = (\psi Q)(\psi u^c)(HH)H$ [16, 76–78]. Smallness of neutrino mass can be loosely understood even when the new particles have TeV scale masses, owing to a loop suppression factor and a chiral suppression affecting M_ν.

The induced neutrino mass matrix arising from Fig. 1 can be evaluated to be

$$M_\nu \;=\; (\kappa_1 + \kappa_2)(f^T M_u V^\star y + y^T V^\dagger M_u f)\,, \tag{2.49}$$

where $M_u = \mathrm{diag}\{m_u, m_c, m_t\}$ is the diagonal up-quark mass matrix, and κ_1, κ_2 are respectively the one-loop and two-loop factors given by

$$\kappa_1 \;=\; \frac{1}{16\pi^2} \sin 2\varphi \log\left(\frac{m_{X_2}^2}{m_{X_1}^2}\right), \tag{2.50}$$

$$\kappa_2 \;\approx\; \frac{1}{(16\pi^2)^2} \frac{\lambda_{\Delta H^3} v \mu}{M^2}\,. \tag{2.51}$$

The leading contribution to M_ν is the one-loop term proportional to κ_1. In evaluating this loop integral we have ignored the masses of the up-type quarks in relation to the LQ masses. In Eq. (2.50) the parameter φ is the $\omega^{2/3} - \bar\rho^{2/3}$ mixing angle given in Eq. (2.17). Since the effective operator for M_ν arising from the one-loop diagram is of the type $\mathcal{O}_{\mathrm{eff}}^{d=7} = \psi\psi HHH^\dagger H$, which is of $d = 7$, one should also consider the lower dimensional $d = 5$ operator $\mathcal{O}_{\mathrm{eff}}^{d=5} = \psi\psi HH$ that can be induced at the two-loop level as shown in Fig. 1. In the approximate expression for κ_2 given in Eq. (2.51), the relevant mass scale is that of the heaviest particle in the loop, denoted here by M, defined as $M = \max(m_{X_1}, m_{X_2}, m_{\Delta^0})$, with m_{X_1, X_2} being the physical masses of the charge-2/3 LQs (cf. Eq. (2.18)) and m_{Δ^0} being the physical masses of the quadruplet (cf. Eq. (2.39)). When $m_{X_1, X_2} \gg m_{\Delta^0}$, the ratio

$\kappa_2/\kappa_1 \sim m_{\Delta^0}^2/(16\pi^2 v^2)$, which becomes of order unity for $m_{\Delta^0} < 3$ TeV or so. However, as we will see later in Section 7, the R_2 LQ is required to have a mass not larger than about 1 TeV in order for it to explain the $R_{D^{(\star)}}$ anomaly. In this case the two-loop diagram is negligible, and therefore, we only include the one-loop contribution in the neutrino fit described in Section 7.2, although the κ_2 term can be important in a more general setting. The overall factor κ_1 in Eq. (2.49) is a free parameter which needs to be of $\mathcal{O}(10^{-8})$ to get the correct order of magnitude for the neutrino masses. Note that the Yukawa matrix elements f_{ij} and y_{ij} must have at least some entries that are of order one in order to explain the B-decay anomalies. $\kappa_1 \sim 10^{-8}$ can be achieved by taking either the cubic coupling μ in Eq. (2.7) or the induced VEV v_Δ to be small. Both these choices are technically natural, since if either of these parameters is set to zero, lepton number becomes a good symmetry.

We note that the same operator that leads to neutrino masses in this model also induces an effective Δ-quadruplet coupling to the SM leptons. (Recall that Δ cannot couple to fermions at the tree level in the model.) This can be seen from partner diagrams of Fig. 1, where the $SU(2)_L$ components are chosen differently. Ignoring small $SU(2)_L$-breaking effects, these couplings would all arise from the same effective operator $(\psi\psi H^\dagger \Delta)$. Therefore, one can write these couplings as being proportional to M_ν. Explicitly, we find that the Δ^{++} coupling to leptons has the Yukawa coupling matrix given by

$$(Y_{\Delta^{++}\ell\ell})_{ij} = \frac{\sqrt{2}}{\sqrt{3}} \frac{(M_\nu)_{ij}}{v_\Delta}, \tag{2.52}$$

where the $1/\sqrt{3}$ is a Clebsch-Gordan factor for the Δ^{++} component of the quadruplet in the expansion of the $(\psi\psi H^\dagger \Delta)$ operator. Eq. (2.52) will play a crucial role in the collider phenomenology of the quadruplet, as discussed in Section 8.

2.4 Yukawa Textures

In order to minimize the number of parameters in our numerical fit to R_D, $R_{D^\star}$, R_K, $R_{K^\star}$, $(g-2)_\mu$, and the neutrino oscillation observables, while satisfying all flavor and LHC constraints, we choose the following economical textures for the Yukawa matrices f', f and y defined as in Eq. (2.6) with the first (second) index corresponding to quark (lepton) flavors:

$$f' = \begin{pmatrix} 0 & 0 & 0 \\ 0 & 0 & 0 \\ 0 & f'_{32} & f'_{33} \end{pmatrix}, \quad f = \begin{pmatrix} 0 & 0 & 0 \\ 0 & f_{22} & f_{23} \\ 0 & f_{32} & f_{33} \end{pmatrix}, \tag{2.53}$$

$$y = \begin{pmatrix} 0 & 0 & 0 \\ 0 & y_{22} & y_{23} \\ y_{31} & y_{32} & 0 \end{pmatrix} \quad (\texttt{Fit}-\texttt{I}), \quad \text{or} \quad y = \begin{pmatrix} 0 & 0 & 0 \\ 0 & y_{22} & 0 \\ y_{31} & y_{32} & y_{33} \end{pmatrix} \quad (\texttt{Fit}-\texttt{II}). \tag{2.54}$$

Our motivation for the above textures is as follows: Nonzero (f'_{32}, f_{32}) can explain the anomalous magnetic moment of the muon via chirally-enhanced top-quark loops. The couplings $(f'_{33}, f_{22}, f_{23})$ are responsible for $R_{D^{(\star)}}$, while (y_{22}, y_{32}) can explain $R_{K^{(\star)}}$. Similarly, the coupling f_{33} is required to suppress the lepton-flavor-violating (LFV) constraint from chirally-enhanced $\tau \to \mu\gamma$, while simultaneously explaining $(g-2)_\mu$. The remaining parameters $(y_{23\,(33)}, y_{31})$ in Eq. (2.54) are needed to satisfy the six neutrino oscillation observables

$(\Delta m_{21}^2, \Delta m_{31}^2, \sin^2\theta_{13}, \sin^2\theta_{23}, \sin^2\theta_{12}, \delta_{\mathrm{CP}})$. For more details, see Section 7. We also note that the zeros in the coupling matrices of Eqs. (2.53)-(2.54) need not be exactly zero; but they need to be sufficiently small so that the flavor changing processes remain under control (cf. Section 5).

3 B-physics Anomalies

In this section, we present our strategy to reconcile the observed tension between experiment and theory in the lepton flavor universality violating observables in the charged-current decays $B \to D^{(\star)} \ell \nu$ (with $\ell = e, \mu, \tau$) and the neutral-current decays $B \to K^{(\star)} \ell^+ \ell^-$ (with $\ell = e, \mu$) by making use of the R_2 and S_3 LQs.

3.1   Charged-current Observables

The relevant lepton universality violating ratios R_D and $R_{D^\star}$ are defined as

$$R_{D^{(\star)}} \;=\; \frac{\mathrm{BR}(B \to D^{(\star)}\tau\nu)}{\mathrm{BR}(B \to D^{(\star)}\ell\nu)} \qquad (\text{with } \ell = e, \mu)\,. \tag{3.1}$$

These observables have been measured by both BaBar [29, 30] and Belle [31–33] in the $\bar{B}^0 \to D^{+(\star)}\ell^-\bar{\nu}_\ell$ decays, while LHCb has measured only the $R_{D^\star}$ parameter using both $\bar{B}^0 \to D^{+\star}\ell^-\bar{\nu}_\ell$ [79] and $\bar{B}^0 \to D^{-\star}\ell^+\nu_\ell$ decays [35]. Combining all these measurements, the average of these ratios are found to be [38]:

$$R_D^{\mathrm{Exp}} \;=\; 0.340 \pm 0.027 \pm 0.013\,, \tag{3.2}$$

$$R_{D^\star}^{\mathrm{Exp}} \;=\; 0.295 \pm 0.011 \pm 0.008\,, \tag{3.3}$$

which induce tensions at the levels of $1.4\,\sigma$ and $2.5\,\sigma$ respectively with respect to the corresponding SM predictions [80–88] given by:

$$R_D^{\mathrm{SM}} \;=\; 0.299 \pm 0.003\,, \tag{3.4}$$

$$R_{D^\star}^{\mathrm{SM}} \;=\; 0.258 \pm 0.005\,. \tag{3.5}$$

Considering the R_D and $R_{D^\star}$ total correlation of -0.38, the combined difference with respect to the SM is about $3.08\,\sigma$.

A related observable is the ratio $R_{J/\psi}$ defined as

$$R_{J/\psi} \;=\; \frac{\mathrm{BR}(B \to J/\psi\tau\bar{\nu}_\tau)}{\mathrm{BR}(B \to J/\psi\ell\bar{\nu}_\ell)} \qquad (\text{with } \ell = e, \mu)\,, \tag{3.6}$$

which also shows a mild discrepancy of $1.7\,\sigma$ between the experimental measurement [34]

$$R_{J/\psi}^{\mathrm{Exp}} \;=\; 0.71 \pm 0.17 \pm 0.184\,, \tag{3.7}$$

and the corresponding SM prediction [89–96]

$$R_{J/\psi}^{\mathrm{SM}} \;=\; 0.289 \pm 0.01\,. \tag{3.8}$$

However, the experimental uncertainty on this measurement is rather large at the moment, and any new physics scenario that explains the $R_{D^{(\star)}}$ anomaly automatically explains the $R_{J/\psi}$ anomaly. Therefore, we will not explicitly discuss $R_{J/\psi}$ in what follows.

In order to confront our model with the experimental data for the charged-current processes, we shall consider LQ contributions to the flavor specific process $b \to c\tau^-\bar\nu$. Thus, only the numerator of Eq. (3.1) is modified by the new LQ interactions. To this end, we consider the general low-energy effective Hamiltonian induced by SM interactions as well as the R_2 and S_3 LQs, which is given by

$$
\mathcal{H}_{\text{eff}} = \frac{4G_F}{\sqrt{2}} V_{cb} \Big[(\bar\tau_L \gamma^\mu \nu_{\tau L})(\bar c_L \gamma_\mu b_L) + g_V^\ell(\mu_R)(\bar\tau_L \gamma^\mu \nu_{\ell L})(\bar c_L \gamma_\mu b_L) + g_S^\ell(\mu_R)(\bar\tau_R \nu_{\ell L})(\bar c_R b_L)
$$
$$
+ g_T^\ell(\mu_R)(\bar\tau_R \sigma^{\mu\nu} \nu_{\ell L})(\bar c_R \sigma_{\mu\nu} b_L) \Big] + \text{H.c.}, \tag{3.9}
$$

where the first term is the SM contribution, while the remaining terms correspond to new physics contribution, with $g_{V,S,T}^\ell$ being the Wilson coefficients defined at the appropriate renormalization scale μ_R. As shown in Fig. 2, left panel, the $\omega^{2/3}$ component of the R_2 LQ mediates the $b \to c\tau^- \bar\nu_\ell$ semileptonic decay via a tree-level contribution. After integrating out the R_2 field, we obtain the following Wilson coefficients at the matching scale $\mu_R = m_{R_2}$:

$$
g_S^\ell(\mu_R = m_{R_2}) = 4 g_T^\ell(\mu_R = m_{R_2}) = \frac{f_{2\ell} f_{33}'^\star}{4\sqrt{2} m_{R_2}^2 G_F V_{cb}}, \tag{3.10}
$$

where $\ell = e, \mu, \tau$ correspond to the outgoing neutrino flavors ν_e, ν_μ, ν_τ respectively. These Wilson coefficients are then run down in momentum to the B-meson mass scale in the leading logarithm approximation, yielding [97]

$$
g_S(\mu_R = m_b) = \left[\frac{\alpha_s(m_b)}{\alpha_s(m_t)}\right]^{-\frac{\gamma_s}{2\beta_0^{(5)}}} \left[\frac{\alpha_s(m_t)}{\alpha_s(m_{R_2})}\right]^{-\frac{\gamma_s}{2\beta_0^{(6)}}} g_S(\mu_R = m_{R_2}), \tag{3.11}
$$

$$
g_T(\mu_R = m_b) = \left[\frac{\alpha_s(m_b)}{\alpha_s(m_t)}\right]^{-\frac{\gamma_T}{2\beta_0^{(5)}}} \left[\frac{\alpha_s(m_t)}{\alpha_s(m_{R_2})}\right]^{-\frac{\gamma_T}{2\beta_0^{(6)}}} g_T(\mu_R = m_{R_2}), \tag{3.12}
$$

where $\beta_0^{(n_f)} = 11 - 2n_f/3$ is the running coefficient, with n_f being the number of quark flavors effective in the relevant momentum regime [98, 99]. γ_S and γ_T are anomalous dimension coefficients given by $\gamma_S = -8$ and $\gamma_T = 8/3$. Thus, using $\alpha_s(m_Z) = 0.118$, which yields (using QCD running at four loops) $\alpha_s(m_b) = 0.2169$, $\alpha_s(m_t) = 0.1074$ and $\alpha_s(m_{R_2}) = 0.09$ for our benchmark value of $m_{R_2} = 900$ GeV, we obtain the following renormalization factors:[5]

$$
g_S(\mu_R = m_b) = 1.596 \, g_S(\mu_R = m_{R_2}), \tag{3.13}
$$

$$
g_T(\mu_R = m_b) = 0.855 \, g_T(\mu_R = m_{R_2}). \tag{3.14}
$$

We see that the tensorial coupling g_T becomes less important at $\mu_R = m_b$, with its value given by $g_S(\mu_R = m_b) \approx 7.56 \, g_T(\mu_R = m_b)$ [101]. We also note that we have ignored here the mixing between between the Wilson coefficients g_S and g_T, which is an excellent
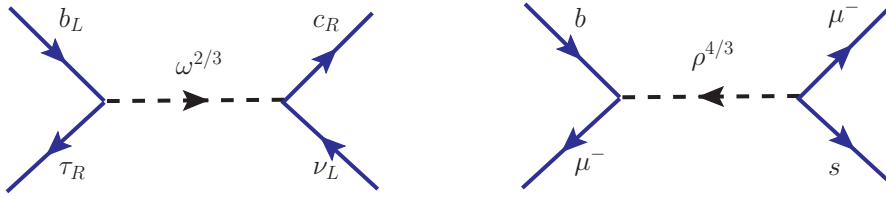
Figure 2: Feynman diagrams for the dominant LQ contributions to the $b \to c\tau^-\bar{\nu}$ (left) and $b \to s\mu^-\mu^+$ (right) transitions.

approximation, as these off-diagonal terms are much smaller than the diagonal terms [101].

The $\rho^{1/3}$ component of the S_3 LQ can also contribute in principle to $b \to c\tau\bar{\nu}_\ell$ via the Wilson coefficient g_V^ℓ given by

$$g_V^\ell(\mu_R = m_{S_3}) \;=\; -\frac{y_{3\ell}(V^\star y)_{23}^\star}{8\, m_{S_3}^2\, G_F V_{cb}} \,. \tag{3.15}$$

However, this contribution cannot accommodate $R_{D^{(\star)}}$ as the relevant Yukawa couplings are highly constrained from flavor physics. Any nonzero $y_{2\ell}$ is subject to $D^0 - \bar{D}^0$ mixing and must be small (cf. Section 5.5), while LHC limits constrain both y_{31} and y_{32} (cf. Section 6). Furthermore, the product of the Yukawa couplings $y_{2\ell}$ and $y_{3\ell'}$ is strongly constrained by processes such as $B \to K\nu\bar{\nu}$. It is also worth mentioning that one can induce Wilson coefficient g_V^ℓ of Eq. (3.15) proportional to $y_{3\ell}y_{33}^\star$, in conjunction with CKM mixing. However, for $\ell = 3$, this contribution has an opposite sign compared to the SM, and therefore would require the new contribution to be twice as large as the SM one, bringing it to the non-perturbative regime. For $\ell = 1$ or 2, there is no interference with the SM term, which would again require large non-perturbative values from the S_3 contribution. Thus we shall ignore these S_3-induced contributions to $R_{D^{(\star)}}$. In Section 7.1, we have shown two best fit values of the Yukawa coupling matrices. For these choices of Yukawa couplings, shown in Eqs. (7.3) and (7.4), we get negligible contribution to $g_V^\ell = -5 \times 10^{-5}$ for Fit I and $g_V^\ell = 6 \times 10^{-6}$ for Fit II from the S_3 LQ, whereas the allowed $1\,\sigma$ range to explain $R_{D^{(\star)}}$ is $[0.072, 0.11]$. Therefore, we will only focus on the R_2 contribution to $R_{D^{(\star)}}$ induced through the Wilson coefficients g_S^ℓ and g_T^ℓ. R_D and $R_{D^\star}$ induced through the Wilson coefficients g_S^ℓ and g_T^ℓ at $\mu_R = m_b$ with ν_τ in the final state are approximately given by [102]

$$R_D \;\simeq\; R_D^{\rm SM} \left(1 + 1.54\,{\rm Re}[g_S^\tau] + 1.09\,|g_S^\tau|^2 + 1.04\,{\rm Re}[g_T^\tau] + 0.75\,|g_T^\tau|^2\right), \tag{3.16}$$

$$R_{D^\star} \;\simeq\; R_{D^\star}^{\rm SM} \left(1 - 0.13\,{\rm Re}[g_S^\tau] + 0.05\,|g_S^\tau|^2 - 5.0\,{\rm Re}[g_T^\tau] + 16.27\,|g_T^\tau|^2\right), \tag{3.17}$$

where the numerical coefficients arise from the relevant form factors. These expressions are applicable for $\nu_{e,\mu}$ final states as well, but by setting the ${\rm Re}[g_S^\tau]$ and ${\rm Re}[g_T^\tau]$ terms in Eqs. (3.16) and (3.17) to zero. This is because the new physics and the SM contributions interfere only when $\nu_\ell = \nu_\tau$.

---

[5]The running of g_S is identical to that of the b-quark mass, see for e.g., Ref. [100].

The required values for the Wilson coefficient to get a simultaneous fit for both R_D and $R_{D^\star}$ is depicted in Fig. 3. We make use of `Flavio` package [103] that has NNLO QCD and NLO electroweak corrections coded in it, in generating Fig. 3. The left panel shows the $1\,\sigma$ allowed range of R_D (light blue band) and $R_D^\star$ (light coral band) in the complex plane of g_S^τ with $g_S^{e,\mu} = 0$, i.e., with $f_{23} \neq 0$ and $f_{21} = f_{22} = 0$ in Eq. (3.10). The intersection between the two bands, highlighted by the purple shaded regions, represents the allowed region that satisfies both anomalies. From this plot, we find that $\text{Im}(g_S^\tau)$ must be nonzero, as first noted in Ref. [104], while $\text{Re}(g_S^\tau)$ should be nearly zero to fit $R_{D^{(\star)}}$. From Eqs. (3.16) and (3.17) it is clear that any nonzero $\text{Re}[g_s^\tau]$ would pull R_D and R_D^* in opposite directions, in contradiction with experimental values (cf. Eqs. (3.2) and (3.3)), which is what forces $\text{Re}(g_S^\tau) \simeq 0$. In the right panel, we set $\text{Re}(g_S^\tau) = 0$, i.e., we set g_S^τ (or, equivalently, the f_{23} coupling) to be purely imaginary, and switch on the f_{22} coupling as well, as is the case with our texture in Eq. (2.53). Again, the $1\,\sigma$ allowed ranges for R_D and $R_{D^\star}$ are shown by the light blue and light coral bands, respectively. The same result is obtained by replacing f_{22} with f_{21}, i.e., by using g_S^e instead of g_S^μ. In our numerical fit to $R_{D^{(\star)}}$ in Section 7, we fix m_{R_2} (f_{22}) close to its minimum (maximum) allowed value from LHC constraints (discussed in Section 6), and find a neutrino mass fit for f_{23} and f'_{33} such that the $g_S^{\mu,\tau}$ values are within the allowed region for both R_D and $R_{D^{(\star)}}$ shown in Fig. 3.

The same effective Hamiltonian (3.9) relevant for $R_{D^{(*)}}$ also gives rise to the exclusive decay $B_c \to \tau\nu$. Within our model, the branching ratio for this decay is given by [94, 105]:

$$\text{BR}(B_c \to \tau\nu) \;=\; 0.023\,|1 - 4.068\,g_S(\mu_R = m_{B_c})|^2 \;. \tag{3.18}$$

Here we have used $\tau[B_c] = (0.507 \pm 0.009)$ ps, $f_{B_c} = 0.43$ GeV, and $m_{B_c} = 6.2749$ GeV. The branching ratio $\text{BR}(B_c \to \tau\nu)$ has not been measured experimentally. Thus, B_c lifetime needs to be compared with theoretical calculations [106–110]. With the benchmark fits shown in Section 7, we obtain branching ratio at the level of 12 %, which is consistent with the limit quoted in Refs. [102, 105, 111, 112].

3.2 Neutral-current Observables

The relevant lepton flavor universality violation ratios R_K and $R_{K^\star}$ are defined as

$$R_K \;=\; \frac{\text{BR}(B^+ \to K^+ \mu^+ \mu^-)}{\text{BR}(B^+ \to K^+ e^+ e^-)}\,, \qquad R_{K^\star} \;=\; \frac{\text{BR}(B^0 \to K^{\star 0} \mu^+ \mu^-)}{\text{BR}(B^0 \to K^{\star 0} e^+ e^-)}\,. \tag{3.19}$$

The latest LHCb measurement of R_K in the $q^2 \in [1.1, 6]$ GeV^2 region (q^2 is the invariant mass of the lepton pair in the decays) is [36][6]

$$R_K^{\text{LHCb}} \;=\; 0.846^{+0.060+0.016}_{-0.054-0.014}\,, \tag{3.20}$$

which shows a discrepancy at the level of $2.6\,\sigma$ from its SM prediction [39, 114]

$$R_K^{\text{SM}} \;=\; 1.0003 \pm 0.0001\,. \tag{3.21}$$

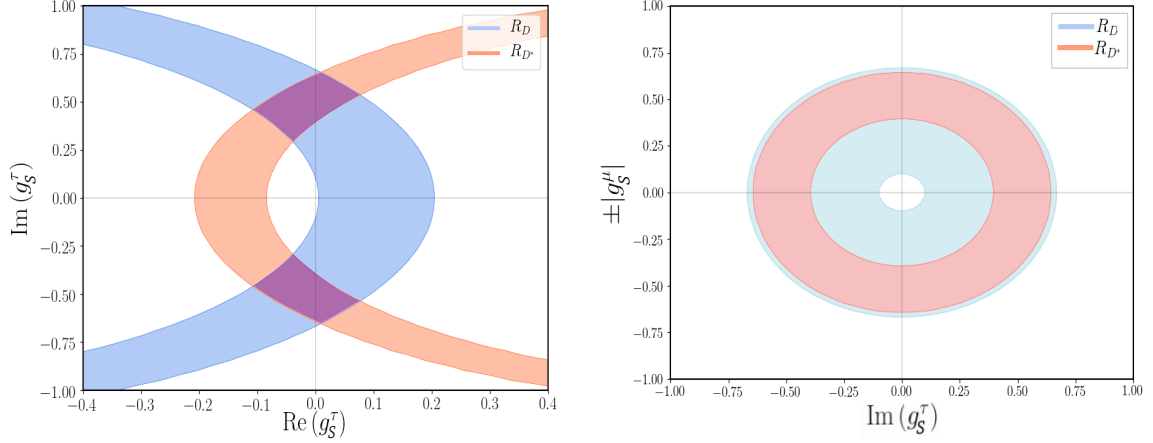[6]For the recent update, see Ref. [113].

Figure 3: *Left:* The 1σ allowed ranges for R_D and $R_{D^\star}$ in the complex plane of g_S^τ with $g_S^{e,\mu} = 0$. The purple shaded regions correspond to the allowed region that explains both R_D and $R_{D^\star}$. *Right:* The 1σ allowed ranges for R_D and $R_{D^\star}$ in the plane of (g_S^τ, g_S^μ) (with $g_S^e = 0$). The same result is obtained by replacing g_S^μ with g_S^e.

Analogously, the LHCb Collaboration has also measured the $R_{K^\star}$ ratio in two bins of low-q^2 region [37]:

$$R_{K^\star}^{\text{LHCb}} = \begin{cases} 0.660^{+0.110}_{-0.070} \pm 0.024 & q^2 \in [0.045, 1.1]\ \text{GeV}^2\,, \\ 0.685^{+0.113}_{-0.069} \pm 0.047 & q^2 \in [1.1, 6.0]\ \text{GeV}^2\,. \end{cases} \tag{3.22}$$

which have respectively $2.2\,\sigma$ and $2.4\,\sigma$ deviations from their corresponding SM results [40]:

$$R_{K^\star}^{\text{SM}} = \begin{cases} 0.92 \pm 0.02 & q^2 \in [0.045, 1.1]\ \text{GeV}^2\,, \\ 1.00 \pm 0.01 & q^2 \in [1.1, 6.0]\ \text{GeV}^2\,. \end{cases} \tag{3.23}$$

In addition to these LHCb results, Belle has recently announced new measurements on both R_K [115] and $R_{K^\star}$ [116], but these results have comparatively larger uncertainties than the LHCb measurements on $R_{K^\star}$.

The effective Hamiltonian describing the new physics contribution to the neutral-current process $b \to s\mu^+\mu^-$, in presence of S_3 LQ, is given by

$$\mathcal{H}_{\text{eff}} = -\frac{4G_F}{\sqrt{2}} V_{tb} V_{ts}^\star \frac{e^2}{(4\pi)^2} \Big[C_9^{\mu\mu}(\bar{s}\gamma_\mu P_L b)(\bar{\mu}\gamma^\mu \mu) + C_{10}^{\mu\mu}(\bar{s}\gamma_\mu P_L b)(\bar{\mu}\gamma^\mu\gamma^5 \mu) \Big] + \text{H.c.}, \tag{3.24}$$

with $C_9^{\mu\mu}$ and $C_{10}^{\mu\mu}$ being the Wilson coefficients. Here we have assumed that the new physics couplings to electrons are negligible. We focus on new physics contributions in the $b \to s\mu^+\mu^-$ channel, i.e. modifying only the numerator of Eq. (3.19). This is motivated by the fact that an explanation of $R_{K^{(\star)}}$ by modifying the $b \to s\mu^+\mu^-$ decay provides a better global fit to other observables, as compared to modifying the $b \to se^+e^-$ decay [42]. It is known that both R_K and $R_{K^\star}$ can be explained by either a purely vectorial Wilson

coefficient $C_9^{\mu\mu} < 0$, or a purely left-handed combination, $C_9^{\mu\mu} = -C_{10}^{\mu\mu} < 0$ [47], with the latter combination performing better in the global analysis due to a $\sim 2\sigma$ tension in the $\mathrm{BR}(B_s \to \mu\mu)$ decay which remains unresolved in the $C_9^{\mu\mu}$ scenario [42]. In our model, the dominant contribution to $b \to s\mu^+\mu^-$ comes at tree level via the mediation of the $\rho^{4/3}$ component of the S_3 LQ, as shown in Fig. 2, right panel. After integrating out the S_3 field, one can extract the Wilson coefficient for $b \to s\mu^-\mu^+$ decay as:

$$C_9^{\mu\mu} \;=\; -C_{10}^{\mu\mu} \;=\; \frac{\pi v^2}{V_{tb}V_{ts}^\star \alpha_{\mathrm{em}}} \frac{y_{22}y_{32}^\star}{m_{S_3}^2} \,. \tag{3.25}$$

The required best fit values of the Wilson coefficients at $\mu = m_b$ are $C_9 = -C_{10} = -0.53$, with the 1σ range being $[-0.61, -0.45]$ [42]. In our numerical fit, y_{22} and y_{32} are fixed by the neutrino mass fit (up to an overall factor), which is then used to fix m_{S_3} such that the best-fit value of $C_9 = -C_{10}$ is obtained from Eq. (3.25).

Note that the R_2 LQ can also give rise to $b \to s\ell^+\ell^-$ transition at tree-level with the corresponding Wilson coefficient given by:

$$C_9^{\mu\mu} \;=\; C_{10}^{\mu\mu} \;=\; -\frac{\pi v^2}{V_{tb}V_{ts}^\star \alpha_{\mathrm{em}}} \frac{f'_{22}f'^\star_{32}}{m_{R_2}^2} \,. \tag{3.26}$$

There is no acceptable fit to $R_{K^{(*)}}$ with $C_9 = C_{10}$. Thus, taking the product of couplings $f'_{2\alpha}$ and $f'_{3\alpha}$ to be zero (or very small), one can suppress R_2 contribution to $R_{K^{(*)}}$. On the other hand, a loop-level contribution to $b \to s\ell^+\ell^-$ transition can in principle accommodate $R_{K^{(*)}}$, but not simultaneously with $R_{D^{(*)}}$, due to the stringent limits from $\tau \to \mu\gamma$ [117]. In our numerical fit, therefore, the R_2 contribution will not play a role in explaining $R_{K^{(*)}}$.

4 Muon Anomalous Magnetic Moment and Related Processes

Virtual corrections due to the LQ states can modify the electromagnetic interactions of charged leptons. The contribution from scalar LQ to anomalous magnetic moments has been extensively studied [118–120]. In particular, the $\omega^{5/3}$ component of the R_2 LQ can explain the muon (or electron) anomalous magnetic moment, as it couples to both left-handed and right-handed fermions, see Eq. (2.6). The new contribution to the anomalous magnetic moment arising from $\omega^{5/3}$ LQ can be written as [118, 121]:

$$\Delta a_\ell \;=\; -\frac{3}{16\pi^2}\frac{m_\ell^2}{m_{R_2}^2}\sum_q \Big[\left(|f_{q\ell}|^2 + |(V^\star f')_{q\ell}|^2\right)\left(Q_q F_5(x_q) + Q_S F_2(x_q)\right)$$
$$-\frac{m_q}{m_\ell}\mathrm{Re}[f_{q\ell}\,(V^\star f')^\star_{q\ell}]\left(Q_q F_6(x_q) + Q_S F_3(x_q)\right) \Big] \tag{4.1}$$

where $Q_q = 2/3$ and $Q_S = 5/3$ are respectively the electric charges of the up-type quark and the LQ propagating inside the loop, as shown in Fig. 4.[7] Here $x_q = m_q^2/m_{R_2}^2$ and

---

[7]The last term in Eq. (4.1) appears with a negative sign, as f and f' in the Lagrangian have opposite signs, see Eq. (2.6).
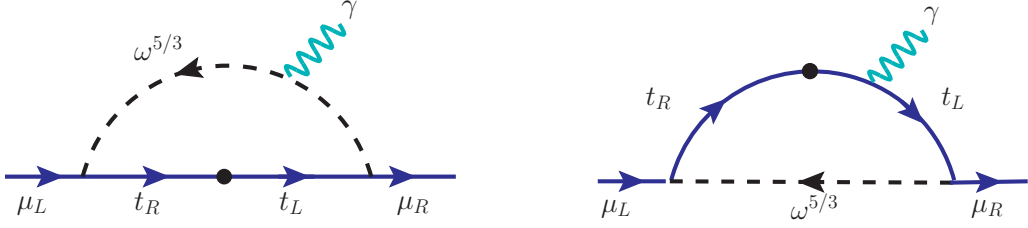
Figure 4: Chirally-enhanced contribution from the R_2 LQ to the muon anomalous magnetic moment.

we have ignored terms proportional to $m_\ell^2/m_{R_2}^2$ in the loop integral. The loop functions appearing in Eq. (4.1) are:

$$F_2(x_q) = \frac{1}{6(1-x_q)^4} \left(1 - 6x_q + 3x_q^2 + 2x_q^3 - 6x_q^2 \ln x_q\right) , \qquad (4.2)$$

$$F_3(x_q) = \frac{1}{(1-x_q)^3} \left(1 - x_q^2 + 2x_q \ln x_q\right) , \qquad (4.3)$$

$$F_5(x_q) = \frac{1}{6(1-x_q)^4} \left(2 + 3x_q - 6x_q^2 + x_q^3 + 6x_q \ln x_q\right) , \qquad (4.4)$$

$$F_6(x_q) = \frac{1}{(1-x_q)^3} \left(-3 + 4x_q - x_q^2 - 2\ln x_q\right) . \qquad (4.5)$$

Note that the first term in Eq. (4.1) is the LQ contribution to the anomalous magnetic moment without chiral enhancement, whereas the second term is the chirally-enhanced one, which in our case will be proportional to the top-quark mass.

4.1 Difficulty with Explaining Δa_e

A discrepancy has also been reported in the anomalous magnetic moment of the electron, denoted as Δa_e, with a somewhat lower significance of $2.4\,\sigma$ [122]. The signs of Δa_e and Δa_μ are opposite. We have investigated whether Δa_e can also also explained in our framework, but found that the model does not admit a simultaneous explanation of both anomalies, as introducing couplings of the type $f_{\alpha e}$ would lead to a chirally-enhanced contribution to the decay $\mu \to e\gamma$, which is highly constrained. One can attempt to explain both anomalies by simply avoiding chirally-enhanced $\ell_i \to \ell_j\gamma$ decays by adopting a redefinition of $V^\star f' \equiv f'$ in Eq. (2.6). However, one introduces V_{CKM} in the down sector leading to strong constraints arising from processes such as $K_L \to e^\pm\mu^\mp$, $K_L \to \ell^+\ell^-$, and $K - \bar{K}$ mixing.

A logical option to explain Δa_e would be to choose the Yukawa coupling f_{21} to be of $\mathcal{O}(1)$, and rely on the charm-quark loop (proportional to $f_{21}f'_{21}$), while being consistent with all the flavor constraints and $R_{D^{(*)}}$. However, it turns out that the required values of the Yukawa couplings in this case have been excluded by the latest LHC dilepton constraints on LQ Yukawa couplings and masses from the non-resonant t-channel process $pp \to \ell^+\ell^-$. These constraints are discussed later in Section 6, and are summarized in Fig. 8. Therefore, simultaneous explanation of the electron and muon anomalous magnetic moments, together with $R_{D^{(*)}}$, is not possible in our setup. Thus, we focus on the parameter space required to
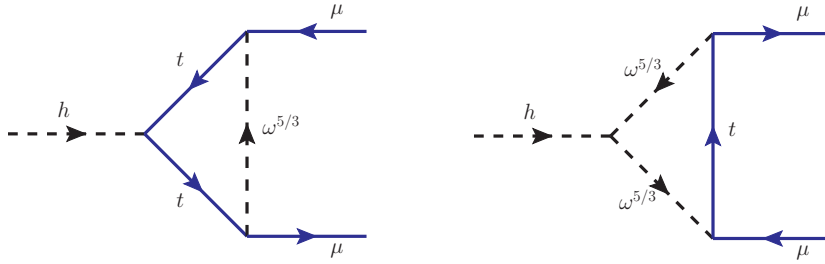
Figure 5: Feynman diagrams for the LQ contribution to $h \to \mu^+\mu^-$ (and also $\tau^+\tau^-$) in our model.

explain Δa_μ, but not Δa_e, as the former is the more persistent and significant discrepancy. In particular, we set $f_{\alpha e} = f'_{\alpha e} = 0$ in Eq. (2.53) to avoid any Δa_e contribution for our numerical fits discussed in Section 7.

4.2 Modified Higgs Decays to Lepton Pairs

The same R_2 LQ interactions that lead to the chirally-enhanced m_t/m_μ contribution to the muon $g-2$ in Fig. 4 will also induce a loop-level correction to the decay of the SM Higgs boson $h \to \mu^+\mu^-$. The Feynman diagrams are shown in Fig. 5. In addition to these diagrams which modify the Yukawa couplings directly, one should also take into account correction to the muon mass arising from the R_2 interactions. The relevant diagram is obtained from Fig. 5 by removing the Higgs boson line. The significance of the LQ diagrams in modifying $h \to \mu^+\mu^-$ decay has been noted recently in Ref. [123]. We have carried out this calculation independently, and found full agreement with the results of Ref. [123]. It is sufficient to compute the coefficient of the $d=6$ operator $(\overline{\psi}_{\mu L}\,\mu_R)H(H^\dagger H)$ which is finite, as any loop correction to the $d=4$ operator $(\overline{\psi}_{\mu L}\,\mu_R)H$ will only renormalize the SM operator. The modification to the branching ratio $\mathrm{BR}(h \to \mu^+\mu^-)$ is found to be

$$
\begin{aligned}
\mu_{\mu^+\mu^-} &\equiv \frac{\mathrm{BR}(h \to \mu^+\mu^-)}{\mathrm{BR}(h \to \mu^+\mu^-)_{\mathrm{SM}}} \\
&= \left| 1 - \frac{3}{8\pi^2}\frac{m_t}{m_\mu}\frac{f_{32}(V^\star f')^\star_{32}}{m_{R_2}^2}\left\{ \frac{m_t^2}{8}\mathcal{F}\left(\frac{m_h^2}{m_t^2},\frac{m_t^2}{m_{R_2}^2}\right) + v^2\left(\lambda_{HR} - \lambda'_{HR}\right) \right\} \right|^2 .
\end{aligned}
\tag{4.6}
$$

The loop function $\mathcal{F}(x,y)$ can be expanded to first order in $y = m_t^2/m_{R_2}^2$ (so that the coefficient of the $d=6$ operator is picked out), and also to the required order in $x = m_h^2/m_t^2$. Although $m_h^2/m_t^2 \sim 1$, the actual expansion parameter is some factor k times this ratio, with $k \sim 1/10$, leading to a rapidly converging series. The function $\mathcal{F}(x,y)$ to third order in m_h^2/m_t^2 is found to be

$$
\mathcal{F}(x,y) = -8 + \frac{13}{3}x - \frac{1}{5}x^2 - \frac{1}{70}x^3 + 2(x-4)\log y .
\tag{4.7}
$$

For our benchmark fits (see Eqs. (7.3) and (7.4)) with $m_{R_2} = 0.9\,\mathrm{TeV}$, the model predictions for $\mu_{\mu^+\mu^-}$ as a function of the quartic coupling combination $(\lambda_{HR} - \lambda'_{HR})$ is shown in Fig. 6.

Collider	$\mu_{\mu^+\mu^-}$	$\mu_{\tau^+\tau^-}$
HL-LHC [127]	9.2%	3.8%
HE-LHC [127]	3.4%	2.2%
ILC (1000) [128]	12.4%	1.1%
CLIC (3000) [129]	11.6%	1.8%
CEPC [130]	17.8%	2.6%
FCC-hh [131]	0.82%	0.88%

Table I: Expected relative precision of the Higgs signal strengths for future colliders. The numbers shown here are for the kappa-0 scenario of Ref. [126].

These predictions are essentially the same for the two benchmark points, so we present our results for Fit I (cf. Eq. (7.3)) in Fig. 6.

The coupling λ'_{HR} is responsible for the mass splitting between the $\omega^{2/3}$ and $\omega^{5/3}$ components of the R_2 LQ (cf. Eqs. (2.13) and (2.19))), which yields a positive contribution to the electroweak ρ-parameter:

$$\delta\rho \simeq \frac{N_c G_F}{8\sqrt{2}\pi^2}(\Delta m)^2 \,, \tag{4.8}$$

where $N_c = 3$ for color-triplets like R_2. Using the current global-fit result for $\rho_0 = 1.00038 \pm 0.00020$ [1] (with $\rho_0 = 1$ in the SM) and allowing for $3\,\sigma$ uncertainty, we obtain an upper bound on the mass splitting $\Delta m \leq 55.9$ GeV (assuming that $v_\Delta \leq$ few MeV, adopted in our collider physics analysis), which yields a corresponding bound on $|\lambda'_{HR}| \leq 1.66$. As discussed in Section 2.2.2, a necessary condition for the Higgs potential to be bounded from below (cf. Eq. (2.45)) is that for negative values of $(\lambda_{HR} - \lambda'_{HR})$, its magnitude should be below about 1.33, assuming that the magnitudes of all quartic couplings lie below $\sqrt{4\pi}$ to satisfy perturbativity. Using the same constraint, we would then have $-1.33 \leq (\lambda_{HR} - \lambda'_{HR}) \leq 5.20$ as the preferred range, which is what we shall choose for our numerical study.

Our model prediction for $\mu_{\mu^+\mu^-}$ is shown in Fig. 6 by the solid blue line. We see that the deviation from the SM predictions in this branching is typically at the (2-6)% level. This is fully consistent with the current LHC measurements: $\mu^{\rm ATLAS}_{\mu^+\mu^-} = 1.2 \pm 0.6$ [124] and $\mu^{\rm CMS}_{\mu^+\mu^-} = 1.19^{+0.41}_{-0.39}(\text{stat.})^{+0.17}_{-0.16}(\text{syst.})$ [125]. For comparison, we quote in Table I the future collider sensitivities for $\mu_{\mu^+\mu^-}$ from Ref. [126], and the relevant ones are also shown in Fig. 6 by the horizontal dotted lines. Thus, our predictions for the modified $h \to \mu^+\mu^-$ signal strength can be tested at the HL-LHC, HE-LHC, as well as at the FCC-hh colliders.

It is also worth pointing out that the Yukawa textures needed to simultaneously explain B-anomalies, muon $g - 2$, and neutrino mass require the f_{33} entry to be nonzero, leading to a new contribution to $h \to \tau^+\tau^-$. This is also shown in Fig. 6 by the solid red line for our benchmark points. Our predictions for $\mu_{\tau^+\tau^-} \equiv \frac{\text{BR}(h\to\tau^+\tau^-)}{\text{BR}(h\to\tau^+\tau^-)_{\rm SM}}$ are consistent with the current LHC measurements: $\mu^{\rm ATLAS}_{\tau^+\tau^-} = 1.09^{+0.18}_{-0.17}(\text{stat.})^{+0.26}_{-0.22}(\text{syst.})^{+0.16}_{-0.11}(\text{theory syst.})$ [132] and $\mu^{\rm CMS}_{\tau^+\tau^-} = 0.85^{+0.12}_{-0.11}$ [133]. For comparison, we quote in Table I the future collider sensitivities for $\mu_{\tau^+\tau^-}$ from Ref. [126]. Some of these are also shown in Fig. 6 by the
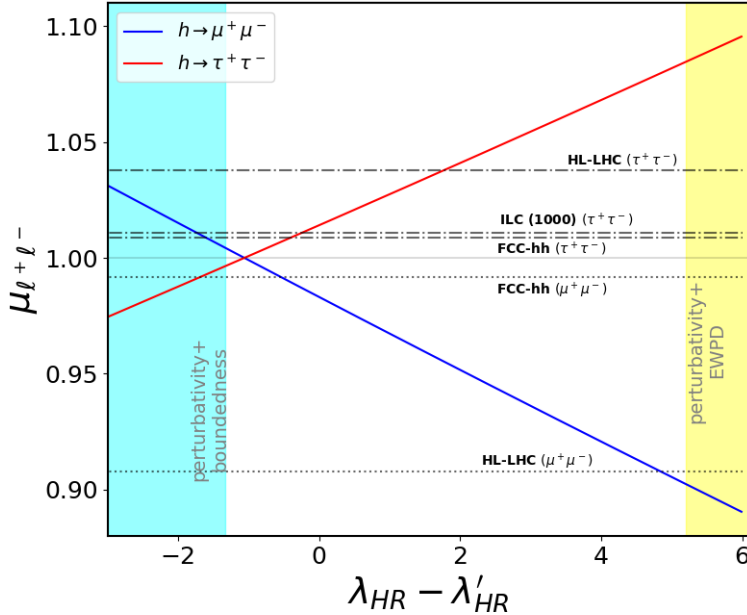
Figure 6: Branching ratios of Higgs to dimuon (blue) and ditau (red) decays with respect to the SM predictions in our model as a function of the quartic coupling parameter ($\lambda_{HR} - \lambda'_{HR}$). The horizontal dotted (dot-dashed) lines show the sensitivities of future colliders for the $\mu^+\mu^-$ ($\tau^+\tau^-$) channel. The shaded regions in yellow and blue are excluded by perturbativity plus electroweak precision data, and by perturbativity plus boundedness of the potential constraints, respectively.

horizontal dot-dashed lines. Thus, our predictions for the modified $h \to \tau^+\tau^-$ signal strength are potentially detectable at future colliders.

As can be seen from Fig. 6, a characteristic feature of the model in the allowed parameter space accessible to future colliders is that while the shift in the branching ratio of $h \to \mu^+\mu^-$ is downward compared to the SM, it is upward for the branching ratio of $h \to \tau^+\tau^-$.

4.3 Muon and Neutron Electric Dipole Moments

LQ interactions can also lead to electric dipole moments (EDM) of the charged leptons (as well as quarks). Existing limits from electron and muon EDMs would place strong constraints on the imaginary part of the Yukawa couplings of the R_2 LQ [134, 135]. These constraints are significant only when the LQ couples to both left- and right-handed charged leptons, as depicted in Fig. 4. The lepton EDM arising from these diagrams is given by [118]

$$|d_\ell| = \frac{3e}{32\pi^2} \sum_q \frac{m_q}{m_{R_2}^2} \left| \text{Im}[-f_{q\ell}(V^\star f')^\star_{q\ell}] \left(Q_q F_6(x_q) + Q_S F_3(x_q)\right) \right|. \tag{4.9}$$

In particular, the constraint arising from electron couplings is quite stringent due to the ACME limit $|d_e| \leq 1.1 \times 10^{-29}$ e.cm [136]. However, since our model does not give additional

contribution to $(g-2)_e$, we can simply avoid the electron EDM limit by setting the relevant couplings $f_{\alpha e} = f'_{\alpha e} = 0$ in Eq. (2.53). Furthermore, the muon EDM arising from the CKM phase, and from the phases in the matrices P and Q of Eq. (2.4) when varied in their full range $[0, 2\pi]$, is found to be at most 3×10^{-22} e-cm, which is well below the current experimental limit of $|d_\mu| \leq 1.9 \times 10^{-19}$ e-cm [137], but may be potentially measurable in future experiments [19, 138, 139] with high-intensity muon sources [140].

The large Yukawa couplings necessary to explain anomalies in $b \to c\tau\nu$ decay can also lead to EDM of the tau lepton d_τ, which is closely related to $\mathrm{Im}(g_s^\tau)$ appearing in the R_{D^*} calculation in Eq. (3.10). It is found to be at most 4.7×10^{-21} e-cm when the phases in the matrices P and Q of Eq. (2.4) are varied in their full range $[0, 2\pi]$, which is below the current experimental limit of $|d_\tau| \leq 2.5 \times 10^{-17}$ e-cm [141].

Similarly, the same Yukawa couplings that lead to tau EDM can also lead to charm quark EDM d_c proportional to $\mathrm{Im}(g_s^\tau)$. The relevant expression is obtained by replacing m_q by m_τ, x_q by x_ℓ, Q_q by $Q_\ell = -1$ and Q_S by $-5/3$ in Eq. (4.9). It is found to be at most 3.1×10^{-22} e-cm. It is below the current experimental limit of $|d_c| \leq 1.5 \times 10^{-21}$ e-cm [142], obtained from the limit on neutron EDM, $d_n < 3.0 \times 10^{-26}$ e-cm [143]. There is also a chromoelectric dipole moment of the charm quark $(\tilde{d}_c)$, arising from diagrams where the photon emitted by the leptoquark is replaced by a gluon. This contribution in the model is obtained from Eq. (4.9) by keeping only the second term, and making the substitutions mentioned above. We find that $\tilde{d}_c$ is at most $2.1 \times 10^{-23} g_s$-cm, which is below the experimental limit, $|\tilde{d}_c| < 1.0 \times 10^{-22}$ cm [142]. Improving the neutron EDM limit by one order of magnitude can therefore directly test the leptoquark explanation of the R_{D^*} anomaly.

5 Low-energy Constraints

This section summarizes the most stringent low-energy flavor constraints that are relevant for our model.

5.1 $\ell_\alpha \to \ell_\beta \gamma$

These LFV radiative decays arising from LQ loops set some of the most stringent constraints on the couplings of the LQs to μ and τ. As can be seen from Eq. (2.6), the R_2 LQ has both left- and right-handed couplings to charged leptons via the f and f' couplings; thus, it can lead to lepton decays both with and without chiral enhancement. The S_3 LQ on the other hand, only couples to left-handed charged leptons, so it cannot induce $\ell_\alpha \to \ell_\beta \gamma$ processes with chiral enhancement.

The decay width for the $\ell_\alpha \to \ell_\beta \gamma$ mediated by LQ loops is given by [119, 121, 144]

$$\Gamma(\ell_\alpha \to \ell_\beta \gamma) = \frac{\alpha_{\mathrm{em}}(m_{\ell_\alpha}^2 - m_{\ell_\beta}^2)^3}{4 m_{\ell_\alpha}^3} \sum_q \left(|\sigma_R^{\alpha\beta q}|^2 + |\sigma_L^{\alpha\beta q}|^2 \right). \tag{5.1}$$

The amplitudes $\sigma_{R,L}$ arising from the exchange of R_2 LQ can be written as

$$\sigma_R^{\alpha\beta q} = \frac{3}{32\pi^2 m_{R_2}^2} \left\{ \left[m_{\ell_\alpha} f_{q\alpha} f_{q\beta}^\star + m_{\ell_\beta} (V^\star f')_{q\beta} (V^\star f')_{q\alpha}^\star \right] \left[Q_q F_5(x_q) + Q_S F_2(x_q) \right] \right.$$

$$-m_q f_{qi} \left(V^\star f'\right)^\star_{qi} \left[Q_q F_6(x_q) + Q_S F_3(x_q)\right]\Big\} , \tag{5.2}$$

$$\sigma_L^{\alpha\beta q} = \frac{3}{32\pi^2 m_{R_2}^2} \Big\{ \left[m_{\ell_\alpha}(V^\star f')_{q\alpha}(V^\star f')^\star_{q\beta} + m_{\ell_\beta} f_{q\beta} f^\star_{q\alpha}\right] \left[Q_q F_5(x_q) + Q_S F_2(x_q)\right]$$

$$-m_q(V^\star f')_{qi}\, f^\star_{qi}\left[Q_q F_6(x_q) + Q_S F_3(x_q)\right]\Big\} , \tag{5.3}$$

with the loop functions $F_i(x_q)$ defined in Eqs. (4.2)-(4.5). Here we generically denote the masses of both 2/3 and 5/3 components of R_2 as m_{R_2}, assuming them to be degenerate. Note that the amplitude σ_L^q can be obtained from σ_R^q with the substitution $f \leftrightarrow V^\star f'$. The last terms in Eqs. (5.2) and (5.3) which are proportional to m_q are the chirally-enhanced contributions. Similarly, one can obtain the S_3 LQ contribution by replacing the f couplings in the first term of Eq. (5.2) by y, assigning proper charges for the quark (Q_q) and scalar LQ (Q_S), and dropping the f' terms in Eq. (5.2).

In the limit $m_{\ell_\beta} \to 0$, which is a very good approximation for both $\mu \to e\gamma$ and $\tau \to \ell\gamma$ (with $\ell = e, \mu$), and taking into account the $u^{cT} f e \omega^{5/3}$, $u^T (V^\star f') e^c \omega^{-5/3}$, and $d^T y e \rho^{4/3}$ terms in Eq. (2.6), the full expression for $\ell_\alpha \to \ell_\beta \gamma$ in our model can be written as

$$\Gamma = \frac{9 m_\alpha^5 \alpha_{\rm em}}{16(16\pi^2)^2} \left[\sum_{q=u,c,t} \left\{ \left| \frac{f_{q\beta} f^\star_{q\alpha}}{2m_{R_2}^2} + \left(\frac{(V^\star f')_{q\alpha} f^\star_{q\beta} + f_{q\alpha}(V^\star f')^\star_{q\beta}}{3m_{R_2}^2} \right) \frac{m_q}{m_\alpha}\left(1 + 4\log x_q\right) \right|^2 \right.$$

$$+ \left| \frac{(V^\star f')_{q\beta}(V^\star f')^\star_{q\alpha}}{2m_{R_2}^2} + \left(\frac{(V^\star f')_{q\alpha} f^\star_{q\beta} + f_{q\alpha}(V^\star f')^\star_{q\beta}}{3m_{R_2}^2} \right) \frac{m_q}{m_\alpha}\left(1 + 4\log x_q\right) \right|^2 \right\}$$

$$+ \sum_{q'=d,s,b} \left| \frac{y_{q'\beta} y^\star_{q'\alpha}}{3m_{S_3}^2} \right|^2 \right] . \tag{5.4}$$

Here we have not included the S_3 contribution from the $\bar{u}_L^c e_L \rho^{1/3}$ term, because it is suppressed compared to the $d_L^T y e_L \rho^{4/3}$ contribution because of smaller electric charge, as well as due to a CKM-suppression factor and by a Clebsch factor of 2, as can be seen from Eq. (2.6). Similarly, the $\omega^{2/3}$ component of the R_2 LQ gives sub-dominant contribution proportional to $m_b^2/m_{R_2}^2$ compared to the $\omega^{5/3}$ component, owing to a GIM-like cancellation [64]; so we have not included it in Eq. (5.4). We have displayed the constraint on the Yukawa coupling f from this process in Table II.

5.2 $\mu - e$ Conversion

$\mu - e$ conversion in nuclei provides a stringent constraint on the product of the Yukawa couplings in our model. The couplings of the S_3 LQ, in conjunction with CKM rotation, is subject to the LFV process from coherent $\mu - e$ conversion in nuclei. The branching ratio for this conversion, normalized to muon capture rate, is given by. [16, 64, 147]:

$$\text{BR}(\mu N \to eN) \simeq \frac{|\vec{p}_e|\, E_e m_\mu^3 \alpha_{\rm em}^3 Z_{\rm eff}^4\, F_p^2}{64\pi^2 Z \Gamma_N} (2A - Z)^2 \left| \frac{(V^\star y)_{11}(y^\star V)_{12}}{2m_{S_3}^2} \right|^2 \tag{5.5}$$

Process	Experimental limit	Constraint
$\mu \to e\gamma$	BR$< 4.2 \times 10^{-13}$ [145]	$\|f_{q1}f_{q2}^{\star}\| < 4.82 \times 10^{-4}\left(\frac{m_{R_2}}{\text{TeV}}\right)^2$
$\tau \to e\gamma$	BR$< 3.3 \times 10^{-8}$ [146]	$\|f_{q1}f_{q3}^{\star}\| < 0.32\left(\frac{m_{R_2}}{\text{TeV}}\right)^2$
$\tau \to \mu\gamma$	BR$< 4.4 \times 10^{-8}$ [146]	$\|f_{q2}f_{q3}^{\star}\| < 0.37\left(\frac{m_{R_2}}{\text{TeV}}\right)^2$

Table II: Constraints on the Yukawa couplings as a function of LQ mass from $\ell_\alpha \to \ell_\beta\gamma$ decay. Constraints on f' couplings are obtained by replacing f with $(V^{\star}f')$ for the $\omega^{5/3}$ LQ. Constraints on the S_3 Yukawa coupling y $(V^{\star}y)$ arising from $\bar{d}_L^c e_L \rho^{4/3}$ $(\bar{u}_L^c e_L \rho^{1/3})$ are weaker by a factor of $3/2$ (6) in comparison to those shown here for the f couplings, suppressed by smaller electric charge and Clebsch factor of 2, as can be seen from Eq. (2.6).

where Γ_N is the muon capture rate of the nucleus, $\vec{p}_e$ and E_e are respectively the momentum and energy of the outgoing electron, A, Z, and Z_{eff} are atomic number, mass number and effective atomic number of the nucleus, whereas F_p is the nuclear matrix element. The experimental limit from gold nucleus provides the most stringent bound [148] of BR $< 7.0 \times 10^{-13}$ leading to a constraint on the Yukawa coupling:

$$\left|(V^{\star}y)_{11}(y^{\star}V)_{12}\right| \;<\; 8.58 \times 10^{-6}\left(\frac{m_{S_3}}{\text{TeV}}\right)^2 . \tag{5.6}$$

5.3 $Z \to \tau\tau$ Decay

Modifications of $Z-$boson decays to fermion pairs through one-loop radiative corrections mediated by LQs provide another important constraint on the Yukawa couplings of the LQ fields in the model. We focus our study on the leptonic Z boson couplings as they are the most precisely determined by experiments [1, 149]. Within our model, we require the f'_{33} coupling to be of $\mathcal{O}(1)$ to explain the $R_{D^{(\star)}}$ anomaly. Thus we focus on the $Z \to \tau\tau$ decay which provides a constraint of f'_{33}. The shift in the coupling of τ_R with the Z boson arising through loop corrections involving the R_2 LQ is given by [150]

$$\text{Re}[\delta g_R^{\tau\tau}] \;=\; \frac{3|f'_{33}|^2}{16\pi^2}\left[\frac{1}{2}x_t(1 + \log x_t) - \frac{x_z}{12}\left\{\log x_t\left(2 + 8/3\sin^2\theta_W\right) + \left(4 + 10/3\sin^2\theta_W\right)\right\}\right.$$

$$\left. + \frac{x_z}{108}\left\{(-3 + 4\sin^2\theta_W) + \log x_z(18 + 12\sin^2\theta_W)\right\}\right]. \tag{5.7}$$

Here we have used the definitions $x_t = \frac{m_t^2}{m_{R_2}^2}$ and $x_z = \frac{m_Z^2}{m_{R_2}^2}$, and kept terms only to linear orders in these parameters. Using the experimental results on the effective coupling obtained by the LEP collaboration [149], $\text{Re}[\delta g_R^{\tau\tau}] \leq 6.2 \times 10^{-4}$, we obtain the $1\,\sigma\,(2\,\sigma)$ limit on the Yukawa coupling as

$$|f'_{33}| \;\leq\; 0.835 \; (1.18) \tag{5.8}$$

for the LQ mass of 900 GeV. Within the context of our model and to find a good fit to $R_{D^{(\star)}}$, we allow this coupling to be in the $2\,\sigma$ range. A similar constraint on f'_{32} can be derived,

$|f'_{23}| \leq 1.7$ from $Z \to \mu^+\mu^-$ decay, which is however much weaker than the constraint that one would obtain from $\tau \to \mu\gamma$, which requires $|f'_{23}f'_{33}| \leq 0.3$.

5.4 Rare D-meson Decays

Rare meson decays also put important constraints on the model parameters. The relevant decays are $D^0 \to \mu^+\mu^-$ and $D^+ \to \pi^+\mu^+\mu^-$.[8]. For effective Lagrangian for these decays mediated by the R_2 and S_3 LQs is given by (cf. Eq. (2.6))

$$\mathcal{L}_Y \supset u^T(V^\star f')e^c\omega^{-5/3} + u^T(V^\star y)e\frac{\rho^{1/3}}{\sqrt{2}} + \text{H.c.} \tag{5.9}$$

There is also a contribution from the f Yukawa, but it does not come with V_{CKM} rotation, so we do not need to consider this contribution for our choice of $f_{1\alpha} = 0$, while deriving the partial decay width for the decay $D^0 \to \mu\mu$. The decay width for $D^0 \to \mu\mu$ proportional to the Yukawa couplings f' and y is given by

$$\Gamma_{D^0 \to \mu\mu} = \frac{|V_{us}V^\star_{cs}|^2 m_\mu^2 f_D^2 m_D}{128\pi} \left(\frac{|f'_{22}|^4}{m_{R_2}^4} + \frac{|y_{22}|^4}{4m_{S_3}^4}\right)\left(1 - \frac{4m_\mu^2}{m_D^2}\right)^{1/2}. \tag{5.10}$$

From Eq. (5.10), one can obtain the constraint on f'_{22} using the experimental limit $\text{BR}(D^0 \to \mu^+\mu^-) < 6.2 \times 10^{-9}$ [1]:

$$|f'_{22}| < 0.564\left(\frac{m_{R_2}}{\text{TeV}}\right). \tag{5.11}$$

The semileptonic decay $D^+ \to \pi^+\mu\mu$ is mediated by the same term as shown in Eq. (5.9) and we implement the calculation of Ref. [16] to obtain the following decay rate:

$$\Gamma_{D^+ \to \pi^+\mu\mu} = \left(\frac{|f'_{22}|^4}{m_{R_2}^4} + \frac{|y_{22}|^4}{4m_{S_3}^4}\right)\left[\frac{f_D}{f_\pi}g_{D^\star D\pi}|V_{us}V^\star_{cs}|\right]^2 \frac{1}{64\pi^3 m_D}\mathcal{F}, \tag{5.12}$$

where the function $\mathcal{F}$ is defined as

$$\mathcal{F} = \frac{m_{D^\star}^2}{12m_D^2}\left[-2m_D^6 + 9m_D^4 m_{D^\star}^2 - 6m_D^2 m_{D^\star}^4 - 6\left(m_{D^\star}^2 - m_D^2\right)^2 m_{D^\star}^2 \log\left(\frac{m_{D^\star}^2 - m_D^2}{m_{D^\star}^2}\right)\right]. \tag{5.13}$$

The numerical value of the function $\mathcal{F} \simeq 2.98\,\text{GeV}$. Using $f_D = 212\,\text{MeV}$, $f_\pi = 130\,\text{MeV}$, $g_{D^\star D\pi} = 0.59$ and the experimental upper limits on the corresponding branching ratio $\text{BR}(D^+ \to \pi^+\mu\mu) < 7.3 \times 10^{-8}$, we obtain bounds on the f' coupling as

$$|f'_{22}| < 0.293\left(\frac{m_{R_2}}{\text{TeV}}\right). \tag{5.14}$$

Similarly, one can find the constraints on Yukawa coupling y_{22}, which is weaker by a factor of $\sqrt{2}$ in comparison to f'_{22} shown in Eqs. (5.11) and (5.14), owing to a Clebsch factor.

---

[8]In general, the decays $B \to K\nu\nu$ and $K \to \pi\nu\nu$ would provide more stringent constraint on the LQ Yukawa couplings [48, 151]. However, these bounds are avoided in our model by the choice of Yukawa coupling matrices

5.5 $D^0 - \bar{D}^0$ Mixing

Both R_2 and S_3 LQs can give rise to $D^0 - \bar{D}^0$ mixing via box diagrams. Explicit calculation of the box diagram involving R_2 LQ gives [152]

$$\Delta m_D = \frac{2}{3} B_1(\mu) m_D f_D^2 C_1' , \qquad (5.15)$$

where $f_D \simeq 212$ MeV is the D meson decay constant, and C_1' is the Wilson coefficient given by

$$C_1' \ (\mu = 1 \text{ TeV}) = \frac{1}{128\pi^2} \frac{(f_{1\alpha} f_{2\alpha}^\star)^2}{m_{R_2}^2} . \qquad (5.16)$$

Here α is the lepton flavor that runs in the box diagrams, which is summed. The renormalized Wilson coefficients C_1' [153–155] and the bag factor B_1 [156], evaluated at $\mu_R = 3$ GeV scale, are given by

$$C_1' \ (\mu_R = 3 \text{ GeV}) \approx 0.8 \, C_1'(\mu_R = 1 \text{ TeV}), \quad B_1(\mu_R = 3 \text{ GeV}) = 0.75 . \qquad (5.17)$$

From the experimental value $|\Delta m_D| = 0.95^{+0.41}_{-0.44} \times 10^{10}$ s^{-1} [1, 157], we obtain the limit

$$|f_{1\alpha} f_{2\alpha}^\star| < 0.0187 \left(\frac{m_{R_2}}{\text{TeV}} \right) . \qquad (5.18)$$

The same constraint applies to the f' coupling as well. However, in addition to the limit quoted in Eq. (5.18), the Yukawa f' is also supplemented by Cabbibo rotation, as seen from Eq. (2.6). Thus, for any nonzero entry in the up-sector $f'_{1\alpha}$ or charm-sector $f'_{2\alpha}$, a nonzero $D^0 - \bar{D}^0$ mixing will be induced by the $(V^\star f')$ term in Eq. (2.6). Consequently, we get a bound on the individual couplings:

$$|f'_{1\alpha}|, \ |f'_{2\alpha}| < 0.305 \left(\frac{m_{R_2}}{\text{TeV}} \right)^{1/2} . \qquad (5.19)$$

Similarly, one can obtain a limit on the individual Yukawa y as well, since a nonzero $y_{1\alpha}$ (or $y_{2\alpha}$) would result in a box diagram contribution to $D^0 - \bar{D}^0$ mixing, owing to the CKM mixing. This has contributions from $u - \nu$ term in addition to the $u - e$ term in Eq. (2.6). Thus for any nonzero entry in the up-sector or charm-sector in the Yukawa matrix y, the bound is slightly stronger than that shown in Eq. (5.19):

$$|y_{1\alpha}|, \ |y_{2\alpha}| < 0.288 \left(\frac{m_{S_3}}{\text{TeV}} \right)^{1/2} . \qquad (5.20)$$

It is worth mentioning that the Yukawa couplings $y_{3\alpha}$ and $f'_{3\alpha}$ also contribute to D-meson mixing. However, these contributions can be safely ignored in the context of our model as they are strongly suppressed by CKM mixing angles by V_{cb} and V_{ub}.

6 LHC Constraints on Leptoquarks

At the LHC, the R_2 and S_3 LQs can be pair-produced through gg and $q\bar{q}$ fusion processes, or can be singly produced in association with charged leptons via s- and t- channel quark-gluon fusion processes. The pair production of the LQs at the LHC is solely dictated by

the LQ mass, irrespective of their Yukawa couplings, whereas the single production rate depends on both mass and the Yukawa coupling of the LQ. Therefore, the single-production limits are relevant only for larger Yukawa couplings $\sim \mathcal{O}(1)$ [16, 158] to the first and second-generation quarks. For the benchmark points studied in Section 7, the Yukawa couplings to the first and second generation quarks are not too large (< 1), hence the collider bounds from single-production are not so significant compared to the limits from QCD-driven LQ pair-production. However, we will show in Section 6.2 that there are stringent limits on the Yukawa couplings of the LQ from the the dilepton processes $pp \to \ell_i^+ \ell_j^-$.

6.1 Pair-production Bounds

Once pair-produced at the LHC, each LQ will decay into a quark and a lepton, and the collider limits on these LQ masses depend on the branching ratios to different decay modes. To impose the bound on the LQ masses, we use the upper limits on the cross-sections from dedicated searches for pair production of first [159, 160], second [160–162] and third generation [162–164] LQs at the LHC and recast them in the context of our model, following the analysis in Ref. [16]. For this purpose, we first implement our model file in `FeynRules` package [165] and then analyze the signal cross sections using `MadGraph5aMC@NLO` [166], which is then compared with the experimental upper limits on the cross section times the branching ratio, assuming that the cut efficiencies are similar in both cases. Our results for the R_2 LQ are shown in Fig. 7, where the black, red, green, blue, cyan, purple, orange, gray, and brown solid colored lines respectively represent the current bounds from the je, $j\mu$, $b\tau$, $t\tau$, $t\nu$, $j\nu$, ce, $c\mu$, and $j\tau$ decay mode of the LQ. Here the branching ratio of each decay mode is varied from 0 to 1 individually without specifying the other decay modes, which compensate for the missing branching ratios to add up to one. As expected, the bounds on the first and second-generation LQs are much more stringent, as compared to the third-generation case. We will use this information to our advantage while choosing our benchmark points in Section 7.

In particular, for the Yukawa ansatz of Eqs. (2.53), the dominant decay modes of the R_2 LQ are:

$$
\begin{aligned}
\omega^{2/3} &\xrightarrow{f} c\bar{\nu}_\mu, \ c\bar{\nu}_\tau, \ t\bar{\nu}_\mu, \ t\bar{\nu}_\tau \,, \\
\omega^{2/3} &\xrightarrow{f'} b\tau^+, \ b\mu^+ \,, \\
\omega^{5/3} &\xrightarrow{f} c\mu^+, \ c\tau^+, \ t\mu^+, \ t\tau^+ \,, \\
\omega^{5/3} &\xrightarrow{f'} t\tau^+, t\mu^+ \,.
\end{aligned}
\tag{6.1}
$$

The branching ratios for these decay modes corresponding to the fits presented in Eqs. (7.3) and (7.4) are shown in Table. III. As we can see, the $\omega^{2/3}$ component of the R_2 LQ dominantly decays to $j\nu$ and $b\tau$ final states, whereas the $\omega^{5/3}$ component mostly decays to $t\tau$, and $j\tau$ final states. Note that the mass of the $\omega^{2/3}$ component cannot be very different from that of the $\omega^{5/3}$ component due to the electroweak precision constraints, and hence, we consider them to be almost degenerate in our analysis. Given the branching ratios in Table. III, the $b\bar{b}\tau^+\tau^-$ final state gives the most stringent constraint on the R_2 LQ mass, which is required to be larger than 859 GeV, as can be seen from Fig. 7.
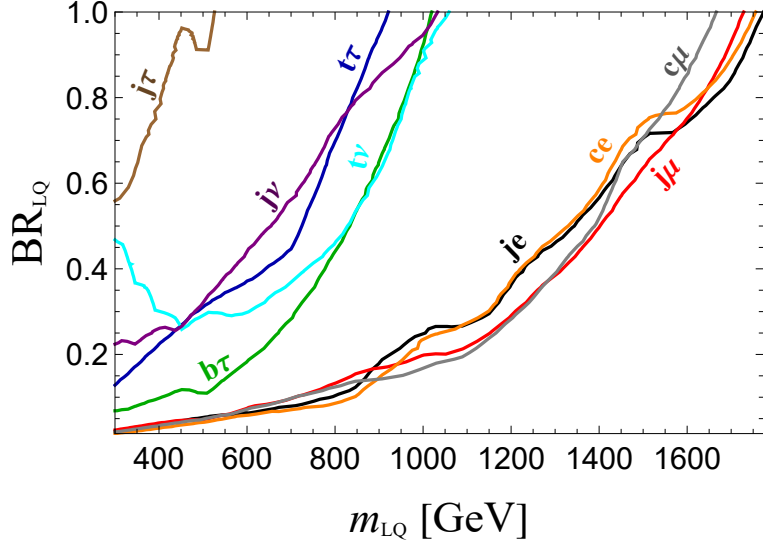
Figure 7: Summary of the updated direct limits from LQ pair-production searches at the LHC for different quark-lepton decay channels of the R_2 LQ. The branching ratio for a specific decay channel of the LQ as indicated in the figure is varied from 0 to 1, while the other decay channels not specified compensate for the missing branching ratios to add up to one. These limits are independent of the LQ Yukawa coupling.

Model Fit	Branching ratio							
	$\omega^{2/3}$				$\omega^{5/3}$			
	νj	$b\tau$	$b\mu$	νt	$t\tau$	μj	τj	$t\mu$
Fit I	41.8%	54.1%	4%	0.04%	54.1%	4%	37.8%	4%
Fit II	41.3%	54%	4%	0.04%	54.1%	4%	37.8%	4%

Table III: Branching ratios for different decay modes of the R_2 LQ corresponding to the fits presented in Eqs. (7.3) and (7.4).

As for the S_3 LQ relevant for $R_{K^{(\star)}}$ anomaly, it can in principle decay to all quark and lepton flavors, due to the CKM-rotations involved in Eq. (2.6). However, the dominant decay modes of the S_3 LQ corresponding to the Yukawa ansatz in Eqs. (7.3) and (7.4) are

$$
\begin{aligned}
\rho^{4/3} &\rightarrow \bar{s}\mu^+ , \\
\rho^{1/3} &\rightarrow \bar{c}\mu^+ , \ \bar{s}\bar{\nu} , \\
\rho^{-2/3} &\rightarrow \bar{c}\bar{\nu} .
\end{aligned}
\tag{6.2}
$$

In addition, for $m_{R_2}, m_\Delta < m_{S_3}$, the S_3 LQ can decay to the R_2 LQ and the quadruplet scalar Δ, mediated by the trilinear coupling μ in Eq. (2.7) that is responsible for neutrino mass in our model. For our numerical analysis, we focus on the scenario with the R_2 (S_3) LQ mass around ~ 1 TeV (2 TeV) and the quadruplet mass also around 1 TeV. In this case,

the $S_3 \to R_2 + \Delta$ decay is the dominant one with $\sim 100\%$ branching ratio. In this case, the various components of S_3 decay as follows:

$$
\begin{aligned}
\rho^{4/3} &\to \omega^{-2/3}\Delta^{++}, \; \omega^{-5/3}\Delta^{+++}, \\
\rho^{1/3} &\to \omega^{-2/3}\Delta^{+}, \; \omega^{-5/3}\Delta^{++}, \\
\rho^{-2/3} &\to \omega^{-5/3}\Delta^{+}, \; \omega^{-2/3}\Delta^{0}.
\end{aligned}
\tag{6.3}
$$

As a consequence, limits on the S_3 LQ mass from the standard LHC searches are not applicable to our scenario. See Section 8 for more details on the S_3 decay signatures at the LHC. For this decay to occur, S_3 mass should exceed that of R_2 LQ.

6.2 Dilepton Bounds

Apart from the direct LHC limits from LQ pair-production, there also exist indirect limits from the cross section measurements on the dilepton process $pp \to \ell_i^+ \ell_j^-$, which could get significantly modified due to a $t-$channel LQ exchange for large Yukawa couplings. Ref. [47] had derived indirect limits on the LQ mass and Yukawa couplings involving the τ lepton using the previous resonant dilepton searches at the LHC. Meanwhile, a dedicated search [167] for the non-resonant signals in dielectron and dimuon final states has been performed at the $\sqrt{s} = 13$ TeV LHC with integrated luminosity 139 fb^{-1}, which is more appropriate for the t-channel LQ search. Therefore, we use this recent non-resonant dilepton study to derive new indirect limits on the LQ mass and Yukawa couplings. For this analysis, we first implement our model file in `FeynRules` package [165], then analyze the cross section for $pp \to \ell_i^+ \ell_j^-$ signal using `MadGraph5aMC@NLO` [166] and compare the quoted observed limits [167] on the cross-section to derive the limits on the Yukawa coupling for a given LQ mass. Our results are shown in Fig. 8 for different Yukawa couplings $f_{i\alpha}$ and $f'_{j\alpha}$ (with $i = 1,2; \; j = 1,2,3; \; \alpha = 1,2$) of the R_2 LQ. Similar bounds can also be derived for the S_3 LQ. There are no bounds on the f_{31} and f_{32} couplings quoted in Fig. 8, because they involve top-quark initial states, whereas the bounds on f'_{31} and f'_{32} come from bottom-quark-initiated processes (cf. Eq. (2.6)). Similarly, we do not report any bounds on the Yukawa couplings involving τ-flavor, as there is no corresponding non-resonant dilepton analysis involving taus available so far. Based on the previous analysis [47], we anyway expect the tau-flavor limits to be weaker than the ones quoted here. Note that the bounds derived in Fig. 8 are independent of the LQ branch ratios, unlike the direct limits shown in Fig. 7. As can be seen from Fig. 8, the flavor-dependent upper limits on the LQ Yukawa couplings for 1 TeV R_2 LQ mass to the first two family leptons and quarks are in the range $(0.15-0.36)$, which get slightly relaxed to $(0.15-0.45)$ if we include the bottom-quark. This precludes a solution of $R_{D^{(\star)}}$ with R_2-mediated decays of the B-meson involving ν_e or ν_μ final states. Therefore, we only focus on the scenario with ν_τ final state in our benchmark points for the explanation of $R_{D^{(\star)}}$.

7 Numerical Fit

In this section, we present our numerical results for the model parameter space that explains the anomalies in $R_{D^{(\star)}}$, $R_{K^{(\star)}}$, and Δa_μ within their 1σ measured values, while being
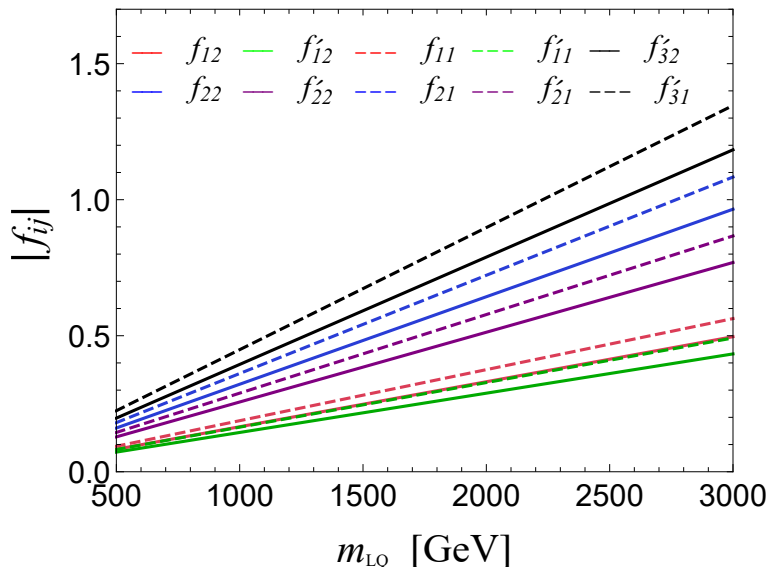
Figure 8: Summary of the new indirect constraints on the Yukawa couplings of the R_2 LQ as a function of its mass from a recent non-resonant dilepton search at the LHC.

consistent with all the low-energy and LHC constraints discussed above. It is beyond the scope of this work to explore the entire parameter space of the theory; instead we implement all the constraints and find a few benchmark points to explain the anomalies. First of all, we fix the R_2 LQ mass at 900 GeV to satisfy the LHC bound obtained from pair-produced $\omega^{2/3}$ decaying to $b\bar{b}\tau^+\tau^-$ (cf. Fig. 7 and Table III). Note that m_{R_2} needs to be around 1 TeV to explain $R_{D^{(\star)}}$; making it larger would require larger f'_{33} and f_{23} coupling values beyond $\mathcal{O}(1)$. For example, with $f'_{33} = \mathrm{Im} f_{23} = 1.5$ and $f_{22} = 0.45$ (to be consistent with the flavor constraints), the maximum m_{R_2} we can have is 1.4 TeV. We also fix the S_3 LQ mass at 2 TeV for our $R_{K^{(\star)}}$ analysis, but it can be scaled up to much higher values without requiring either of the Yukawa couplings y_{22} or y_{32} in Eq. (3.25) to exceed $\mathcal{O}(1)$ values.

7.1 Fit to $R_{D^{(\star)}}$

In Fig. 9, we show the allowed parameter space to explain $R_{D^{(\star)}}$ at $1\,\sigma$ (orange shaded) and $2\,\sigma$ (light blue shaded) CL in the most relevant Yukawa coupling plane $\mathrm{Im}(f_{23}) - |f'_{33}|$ for a fixed R_2 LQ mass at 900 GeV. We have also fixed $f_{22} = 0.29$, which is the maximum allowed value from the dilepton constraint (see Fig. 8). Note that a nonzero f_{22} is required by the neutrino oscillation fit for the textures we have (see Section 7.2), and a larger f_{22} helps widen the $R_{D^{(\star)}}$ region. In our numerical analysis to generate Fig. 9, we have made use of the `Flavio` package [103]. As already noted in Section 3.1 (cf. Fig. 3), the f_{23} coupling needs to be complex to get a good fit to $R_{D^{(\star)}}$. Thus, while doing the minimization to get neutrino oscillation fit, we choose the f_{23} coupling purely imaginary, as shown in Fig. 9.

The dark purple shaded area highlighted in Fig. 9 represents the allowed region that is consistent with all the constraints in our model. The rest of the colored regions are excluded
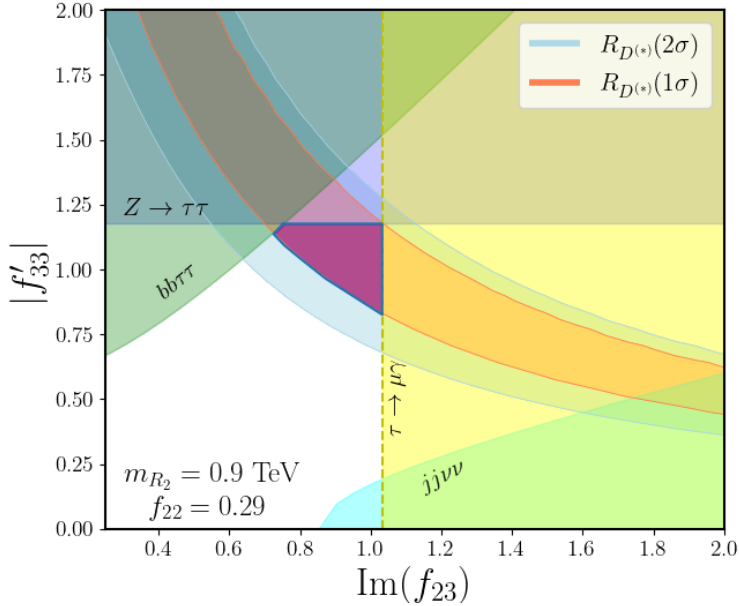
Figure 9: 1σ (light red) and 2σ (light blue) allowed range for $R_{D^{(*)}}$ in the relevant Yukawa coupling plane, with the R_2 LQ mass at 900 GeV and with a fixed $f_{22} = 0.29$. The horizontal purple band is from the $Z \to \tau\tau$ constraint. The curved green band and cyan bands respectively represent exclusion from LQ pair production in $pp \to bb\tau\tau$ and $pp \to jj\nu\nu$ channels at LHC. The vertical yellow band corresponds to the exclusion from LFV decay $\tau \to \mu\gamma$. The dark purple shaded box represents the 1σ allowed region for $R_{D^{(*)}}$ that is consistent with all the constraints in this model.

by various constraints discussed in the previous sections. The horizontal purple band is from $Z \to \tau\tau$ constraint (cf. Eq. 5.8). The green and cyan shaded regions respectively represent LHC exclusion from LQ pair-production in $b\tau$ and $j\nu$ decay modes (cf. Fig. 7). The vertical yellow shaded region corresponds to the exclusion from LFV decay $\tau \to \mu\gamma$ (cf. Table II). In the next subsection, we will choose both f'_{33} and f_{23} values from within the allowed region shown in Fig. 9. Similarly, Fig. 10 shows experimental averages for R_D and R_{D^*} taking correlation into account between the two observables, along with benchmark fits within the model corresponding to the parameters shown in Eq. (7.3) and Eq. (7.4).

We note that Yukawa couplings to the third generation lepton required to explain anomalies in $R_{D^{(*)}}$ can induce $C_9^{\ell\ell}$ and $C_{10}^{\ell\ell}$ operators via penguin diagram [42, 168], with renormalization group equation running down to the B-meson mass scale. For instance, in scenarios with vector LQ, the same Yukawa couplings that explain $R_{D^{(*)}}$ induce such one-loop photon penguin diagrams [169]. Similarly, with scalar LQs, similar log enhanced contribution can be realized [170]. However, within our model, although such contributions exist, the flavor structure we have adopted in Eq. (7.3) and Eq. (7.4) with $f'_{23} = 0$ ($y_{33} = 0$ or $y_{33} \ll 1$) results in these contributions being negligible.
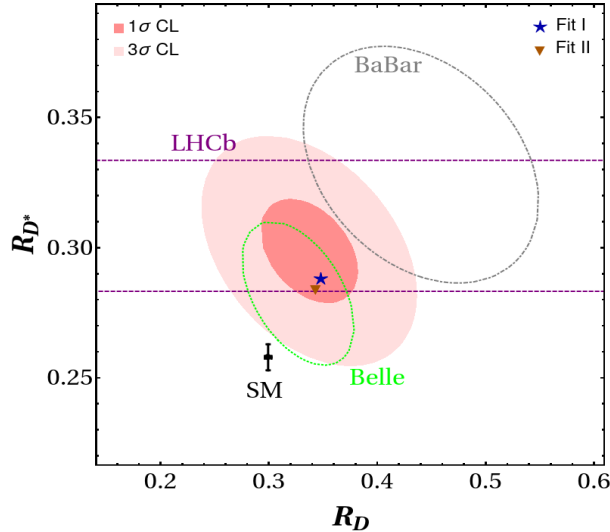
Figure 10: 1σ (dark red) and 3σ (light red) contours for experimental averages from Ref. [171] for the LFUV observables R_D and R_{D^*} observables. Individual 1σ regions from Belle, BarBar, and LHCb are respectively shown by the dotted green, gray, and purple contours. Black error bar represent the SM prediction, whereas black and brown marker corresponds to the two model Fit I and Fit II given by Eq. (7.3) and Eq. (7.4).

7.2 Neutrino Fit

In this section, we explicitly show that the neutrino oscillation data can be explained in our model, while being consistent with the B-anomalies and $(g-2)_\mu$, as well as satisfying all the experimental constraints given in Sections 5 and 6. We have performed a detailed numerical study to find the minimal texture for the Yukawa couplings to fit all the observables. We show our results for two different textures, namely, `Fit I` and `Fit II` as given in Eqs. (2.53) and (2.54). For this analysis, we fix the R_2 and S_3 LQ masses at 900 GeV and 2 TeV respectively. Furthermore, the masses of the up-type quarks entering the neutrino mass matrix (cf. Eq. (2.49)) are fixed at [1, 100, 173]

$$ m_u(2\,\text{GeV}) \;=\; 2.16\,\text{MeV}, \qquad m_c(m_c) \;=\; 1.27\,\text{GeV}, \qquad m_t(m_t) \;=\; 160\,\text{GeV}. \quad (7.1) $$

We have used these input values of the running up-type quarks given in Eq. (7.1) and then extrapolate them to the LQ mass scale at 1 TeV in doing the numerical fit for the neutrino oscillation data. We obtain $m_u(1\,\text{TeV}) = 1.10$ MeV, $m_c(1\,\text{TeV}) = 0.532$ GeV, and $m_t(1\,\text{TeV}) = 150.7$ GeV [100, 174]. The neutrino mass matrix given by Eq. (2.49) is diagonalized by a unitary transformation

$$ U^T_{\text{PMNS}} M_\nu U_{\text{PNMS}} \;=\; \widehat{M_\nu}\,, \tag{7.2} $$

where $\widehat{M_\nu}$ is the diagonal mass matrix and U_{PMNS} is the 3×3 PMNS lepton mixing matrix. We numerically diagonalize Eq. (7.2) by scanning over the input parameters with two different textures as shown in Eqs. (2.53) and (2.54). For ease of finding the fits to oscillation data, we factor out m_t into the overall factor and define $m_0 = m_t \kappa_1$, where κ_1 is given

Oscillation parameters	3 σ allowed range from NuFit5.0 [172]	Model Fit I	Model Fit II
$\sin^2\theta_{12}$	$0.269 - 0.343$	0.290	0.324
$\sin^2\theta_{13}$	$0.02032 - 0.02410$	0.0235	0.0210
$\sin^2\theta_{23}$	$0.415 - 0.616$	0.472	0.430
Δm_{21}^2 $(10^{-5}$ eV$^2)$	$6.82 - 8.04$	7.39	7.45
Δm_{23}^2 $(10^{-3}$ eV$^2)$	$2.435 - 2.598$	2.54	2.49
δ (degree)	$107 - 403$	329.6	322.7
Observable	**1 σ allowed range**		
R_D	$0.310 - 0.367$ [38]	0.348	0.343
$R_{D\star}$	$0.281 - 0.308$ [38]	0.288	0.284
$C_9 = -C_{10}$	$[-0.61, -0.45]$ [42]	-0.52	-0.51
$(g-2)_\mu$ (10^{-10})	27.4 ± 7.3 [20]	29.7	34.4

Table IV: Fits to the the neutrino oscillation parameters in the model with normal hierarchy, along with the B-anomalies, and muon $g - 2$ for two benchmark fits given in Eq. (7.3) and Eq. (7.4). For comparison, the $3\,\sigma$ allowed range for the oscillation parameters and the $1\,\sigma$ range for the other observables are also given. Note that correlation between R_D and R_{D^*} is not taken into account here (see Fig. 10 to see such correlation).

in Eq. (2.50). Furthermore, we perform constrained minimization in which the neutrino observables are restricted to lie within $3\,\sigma$ of their experimental measured values, for which we use the recent NuFit5.0 values (with SK atmospheric data included) [172].

Our fit results for the two textures given in Eqs. (2.53) and (2.54) are shown below:

Fit I: With $m_0 = 9.9$ eV,

$$
f' = \begin{pmatrix} 0 & 0 & 0 \\ 0 & 0 & 0 \\ 0 & 0.29 & -1.15 \end{pmatrix}, \quad
f = \begin{pmatrix} 0 & 0 & 0 \\ 0 & 0.29 & 0.886i \\ 0 & 0.0059 & 0.0226 \end{pmatrix}, \quad
y = \begin{pmatrix} 0 & 0 & 0 \\ 0 & 0.124 & 0.064 \\ -0.016 & 0.028 & 0 \end{pmatrix}.
$$
(7.3)

Fit II: With $m_0 = 15.1$ eV,

$$
f' = \begin{pmatrix} 0 & 0 & 0 \\ 0 & 0 & 0 \\ 0 & 0.29 & -1.10 \end{pmatrix}, \quad
f = \begin{pmatrix} 0 & 0 & 0 \\ 0 & 0.29 & 0.887i \\ 0 & 0.0061 & 0.0215 \end{pmatrix}, \quad
y = \begin{pmatrix} 0 & 0 & 0 \\ 0 & 0.22 & 0 \\ 0.026 & 0.0155 & -0.035 \end{pmatrix}.
$$
(7.4)

For each of these Yukawa textures, the corresponding fit results for the neutrino oscillation parameters are shown in Table IV. It is clear that both fits are in excellent agreement with the observed experimental values. The f_{33} entry in the benchmark texture shown above is required for fine-tuning at the level of 7% the $\tau \to \mu\gamma$ amplitude arising from top

quark loop with a chiral enhancement (cf. Section 5.1). Note that the input parameter f_{23} in both `Fit I` and `Fit IIa` is purely complex, which is required to get $R_{D^{(\star)}}$ correct (cf. Fig. 9). Furthermore, the same coupling leads to a significant Dirac CP phase, as can be seen from Table IV, consistent with the recent T2K result [175].

We note that the structures of f and f' do not change significantly from Fit-I to Fit-II. This happens due to the various flavor violating constraints. In this sense, the parameter space is rather limited for f and f'. However, the structure of y is different for Fits-I and II, and there is also some freedom in the overall scale of y, as illustrated in Eqs. (7.3) and (7.4).

We shown in Table IV the fit results for R_D, $R_{D^{(\star)}}$, $R_{K^{(\star)}}$ and $(g-2)_\mu$, all of which are within $1\,\sigma$ of the experimentally allowed range.

7.3 Non-standard Neutrino Interactions

The LQs $\omega^{2/3}$ from R_2 and $\rho^{-2/3}$, $\rho^{1/3}$ from S_3 have couplings with neutrinos and quarks (cf. Eq. (2.6)). These couplings can induce charged-current NSI at tree-level [16]. Using the effective dimension-6 operators for NSI introduced in Ref. [176], the effective NSI parameters in our model are given by

$$\varepsilon_{\alpha\beta} \;=\; \frac{3}{4\sqrt{2}G_F} \left(\frac{f_{1\alpha}^\star f_{1\beta}}{m_{\omega^{2/3}}^2} + \frac{(Vy^\star)_{1\alpha}(V^\star y)_{1\beta}}{m_{\rho^{-2/3}}^2} + \frac{y_{1\alpha}^\star y_{1\beta}}{2m_{\rho^{1/3}}^2} \right) . \tag{7.5}$$

Any non zero entry in the up-sector $f_{1\alpha}$ and $y_{1\alpha}$, relevant for generating tree-level NSI, does not affect the neutrino oscillation fit, as it is suppressed by the up-quark mass. However, Yukawa couplings to the electron and muon sector $f_{1\alpha}$ and $y_{1\alpha}$ ($\alpha = 1,2$) are highly constrained by the non-resonant dilepton searches at the LHC. The limit on f_{11} and f_{12} are 0.19 and 0.16, respectively, for 1 TeV LQ mass (cf. Fig. 8). Also, the limit on y_{11} and y_{12} are 0.16 and 0.15. Thus ε_{11} and ε_{22} are sub-percent level, and far beyond the reach of forthcoming neutrino experiments. Furthermore, any nonzero $y_{1\alpha}$ is in conjunction to Cabibbo rotation and induces $(V^\star y)_{2\alpha}$ leading to $D^0 - \bar{D}^0$ mixing with a constraint given in Eq. (5.20).

As noted in Section 6.2, the LHC limits on the LQ Yukawa couplings in the tau sector are weaker, and in principle, one can allow $\mathcal{O}(1)$ Yukawa coupling for f_{13} and generate a ε_{33} which can be as large as 5.6%. However, we require f_{23} to be nonzero and $\mathcal{O}(1)$ to explain $R_{D^{(\star)}}$, and the constraint on the product of Yukawa couplings $f_{13}f_{23}$ is severe due to the $D^0 - \bar{D}^0$ bound, see Eq. (5.18). Thus the induced NSI will again be at a sub-percent level. For simplicity, we choose $f_{1\alpha} = y_{1\alpha} = 0$ for all $\alpha = 1, 2, 3$ (cf. Eq. (2.54)) in both the numerical fits discussed in Section 7.2.

8 Collider Implications

This model provides an avenue to test a unified description of B-anomalies, muon anomalous magnetic moment and neutrino masses at the LHC through a new decay channel of the S_3 LQ. The presence of the two scalar LQs R_2 and S_3 and the isospin-3/2 scalar multiplet Δ (especially its triply- and doubly-charged components) give rise to a rich phenomenology for
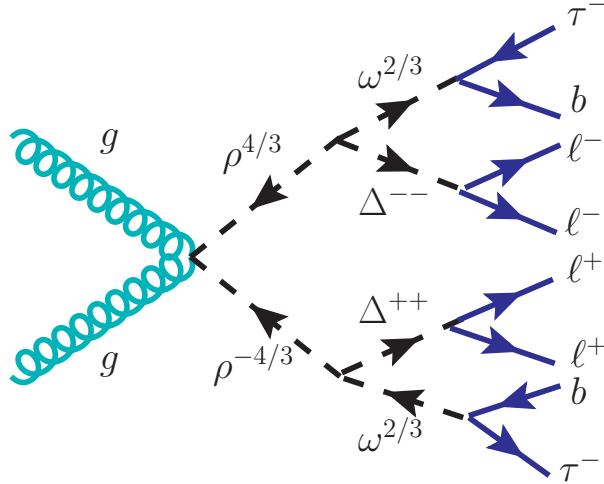
Figure 11: Feynman diagram for the pair-production of the $\rho^{4/3}$ component of the S_3 LQ ($pp \to \rho^{4/3}\rho^{-4/3}$), followed by ρ decay to the $\omega^{2/3}$ component of the R_2 LQ and the doubly-charged component of the Δ quadruplet ($\rho^{\mp 4/3} \to \omega^{\pm 2/3}\Delta^{\mp\mp}$). The $\omega^{2/3}$ component can then decay to $b\tau$ (or $j\nu$) final state, while the doubly-charged scalar mostly decays to same-sign lepton pair (for small v_Δ). This leads to the striking signal of this model: $pp \to \ell^+\ell^+\ell^-\ell^- + \tau^+\tau^- + b\bar{b}$ (where $\ell = e$ or μ).

the LHC. In this section, we analyze the production and decay of the doubly-charged component of the scalar multiplet at the LHC and prospective smoking gun signals correlated with the B-anomalies.

8.1 Production of Doubly-charged Scalars via LQ Decay

Being part of the $SU(2)_L$-quadruplet, the charged scalars ($\Delta^{\pm\pm\pm}, \Delta^{\pm\pm}, \Delta^{\pm}$) can be pair-produced at the LHC by standard DY processes mediated by s-channel Z/γ exchange. In addition, s-channel W exchange can lead to associated production of $\Delta^{\pm\pm\pm}\Delta^{\mp\mp}$ ($\Delta^{\pm\pm}\Delta^{\mp}$). It is important to note that being s-channel processes, the DY pair production cross-sections are highly suppressed for large $\Delta^{\pm\pm\pm}$ ($\Delta^{\pm\pm}$) masses (similar to the doubly-charged scalar production in the type-II seesaw [177–179]). The collider phenomenology of $SU(2)_L$-quadruplet scalars with DY production and the same-sign dilepton (trilepton) signals from doubly (triply)-charged scalars has been studied extensively in different contexts [69–72, 180, 181].

Here we propose a unique production mechanism for the doubly-charged scalars at the LHC via the gluon fusion process, as shown in Fig. 11. In the gluon-gluon fusion process, the S_3 LQ can be pair-produced copiously. Once produced, the various components of the S_3 LQ would decay dominantly to the components of the R_2 LQ and Δ quadruplet, if kinematically allowed (cf. Eq. (6.3)). Here we will mainly focus on the $\rho^{\mp 4/3} \to \omega^{\pm 2/3}\Delta^{\mp\mp}$ decay channel, as $\rho^{4/3}$ and $\omega^{2/3}$ are respectively the components responsible for the $R_{K^{(\star)}}$ and $R_{D^{(\star)}}$ anomalies in our model. Therefore, the signal shown in Fig. 11 provides a direct test of the $R_{K^{(\star)}}$ and $R_{D^{(\star)}}$ explanations at the high-energy LHC.
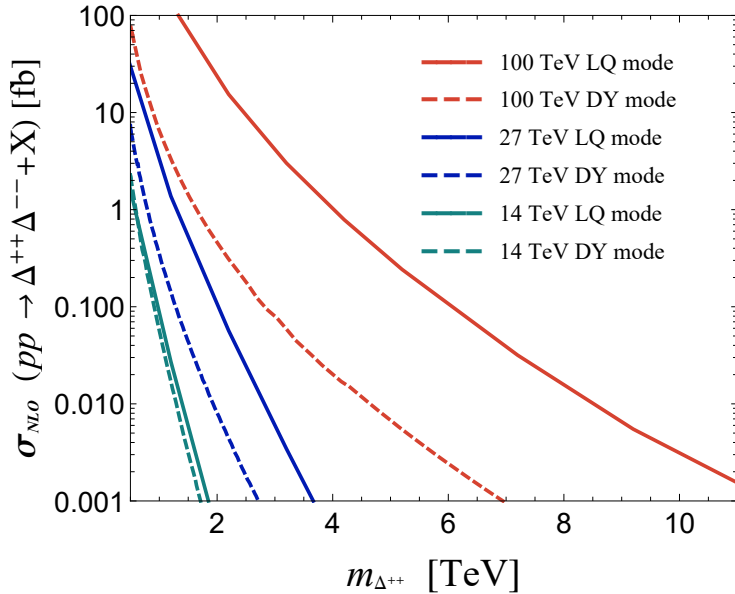
Figure 12: Comparison of the NLO pair-production cross-sections for the doubly-charged scalars in the DY channel ($pp \to \Delta^{++}\Delta^{--}$) versus the LQ channel ($pp \to \Delta^{++}\Delta^{--} + \omega^{2/3}\omega^{-2/3}$) as a function of the doubly-charged scalar mass at $\sqrt{s} = 14$, 27 and 100 TeV.

Another reason we consider the $\Delta^{\pm\pm}$ production via S_3 decay is that the LQ-induced charged-scalar pair-production rate is not as highly suppressed as the DY rate for higher masses. In addition, there will be an enhancement factor for gluon luminosity compared to the quark luminosity, which becomes even more pronounced at higher center-of-mass energies. This can be seen from Fig. 12, where we compare the doubly-charged scalar pair-production cross-sections at NLO in the DY mode $pp \to \Delta^{++}\Delta^{--}$ and in the new LQ mode $pp \to \Delta^{++}\Delta^{--} + \omega^{2/3}\omega^{-2/3}$ (in Fig. 12, $\omega^{2/3}\omega^{-2/3}$ is collectively denoted as X) for center-of-mass energies $\sqrt{s} = 14$, 27 and 100 TeV. Note that for the LQ mode, the cross section only depends on the $\rho^{4/3}$ LQ mass; however, to make a direct comparison with the DY mode, we have fixed the $\omega^{2/3}$ mass at 900 GeV (the preferred value for $R_D^{(\star)}$ explanation), and for a given $\Delta^{\pm\pm}$ mass in Fig. 12, have chosen the $\rho^{4/3}$ mass such that the $\rho^{\mp 4/3} \to \omega^{\pm 2/3}\Delta^{\mp\mp}$ decay branching ratio is $\sim 50\%$ (with the other 50% going to $\omega^{\pm 5/3}\Delta^{\mp\mp\mp}$). From Fig. 12, we infer that the production cross-sections for the doubly-charged scalar in the LQ mode are sizable up to the multi-TeV mass range, and the collider reach in the inclusive mode $pp \to \Delta^{++}\Delta^{--} + X$ can be significantly enhanced, compared to the pure DY mode (see Section 8.4 for more details).

8.2 Decay of Doubly-Charged Scalars

Now we turn to the decay modes of the quadruplet scalar Δ. The doubly charged scalar $\Delta^{\pm\pm}$ can decay to $\ell^{\pm}\ell^{\pm}$ via the leptonic coupling given by Eq. (2.52). In addition, being a part of the $SU(2)_L$-quadruplet, the covariant derivative term leads to bosonic decay

modes ($W^\pm W^\pm$) of $\Delta^{\pm\pm}$. On the other hand, when the mass-splitting between consecutive members of the quadruplet are nonzero, cascade decays also open up. One should note that depending on the quartic coupling $\lambda'_{H\Delta}$, there could be two different hierarchies: (a) when $\lambda'_{H\Delta} > 0$, we have $m_{\Delta^{\pm\pm\pm}} < m_{\Delta^{\pm\pm}} < m_{\Delta^{\pm}} < m_{\Delta^0}$ and (b) when $\lambda'_{H\Delta} < 0$, we have $m_{\Delta^{\pm\pm\pm}} > m_{\Delta^{\pm\pm}} > m_{\Delta^{\pm}} < m_{\Delta^0}$ (cf. Eq. (2.52)). Therefore, due to mass-splitting, it can decay in cascades via $\Delta^{\pm\pm\pm}X^\mp$ or $\Delta^\pm X^\pm$ (where $X = \pi, W^\star$) depending on whether $\Delta m > 0$ or $\Delta m < 0$. For simplicity, we consider $\Delta^{\pm\pm\pm}$ to be the lightest member of the Δ multiplet throughout our analysis. The partial decay widths for different decay modes of $\Delta^{\pm\pm}$ can be written as [71, 72]:

$$\Gamma\left(\Delta^{\pm\pm} \to \ell_i^\pm \ell_j^\pm\right) = \frac{m_{\Delta^{\pm\pm}} (m_\nu)_{ij}^2}{6\pi (1+\delta_{ij}) v_\Delta^2} \left(1 - \frac{m_i^2}{m_{\Delta^{\pm\pm}}^2} - \frac{m_j^2}{m_{\Delta^{\pm\pm}}^2}\right) \left[\lambda\left(\frac{m_i^2}{m_{\Delta^{\pm\pm}}^2}, \frac{m_j^2}{m_{\Delta^{\pm\pm}}^2}\right)\right]^{1/2},$$
(8.1)

$$\Gamma\left(\Delta^{\pm\pm} \to W^\pm W^\pm\right) = \frac{3g^4 v_\Delta^2 m_{\Delta^{\pm\pm}}^3}{16\pi m_W^4} \left(\frac{3m_W^4}{m_{\Delta^{\pm\pm}}^4} + \frac{m_W^2}{m_{\Delta^{\pm\pm}}^2} + \frac{1}{4}\right) \beta\left(\frac{m_W^2}{m_{\Delta^{\pm\pm}}^2}\right),$$
(8.2)

$$\Gamma\left(\Delta^{\pm\pm} \to \Delta^{\pm\pm\pm}\pi^\mp\right) = \frac{g^4 |V_{ud}|^2 (\Delta m)^3 f_\pi^2}{8\pi m_W^4},$$
(8.3)

$$\Gamma\left(\Delta^{\pm\pm} \to \Delta^{\pm\pm\pm}\ell^\mp \nu_\ell\right) = \frac{g^4 (\Delta m)^5}{120\pi^3 m_W^4},$$
(8.4)

$$\Gamma\left(\Delta^{\pm\pm} \to \Delta^{\pm\pm\pm}q\bar{q}'\right) = 3\Gamma\left(\Delta^{\pm\pm} \to \Delta^{\pm\pm\pm}\ell^\mp \nu_\ell\right),$$
(8.5)

$$\Gamma\left(\Delta^{\pm\pm} \to W^\pm W^{\pm\star}\right) = \frac{9g^6 m_{\Delta^{\pm\pm}}}{512\pi^3} \frac{v_\Delta^2}{m_W^2} F\left(\frac{m_W^2}{m_{\Delta^{\pm\pm}}^2}\right),$$
(8.6)

where the kinematic functions are given by [72]

$$\lambda(x,y) = 1 + x^2 + y^2 - 2xy - 2x - 2z,$$
(8.7)

$$\beta(x) = \sqrt{1 - 4x},$$
(8.8)

$$F(x) = -|1-x|\left(\frac{47}{2}x - \frac{13}{2} + \frac{1}{x}\right) + 3\left(1 - 6x + 4x^2\right)|\log\sqrt{x}|$$
$$+ \frac{3\left(1 - 8x + 20x^2\right)}{\sqrt{4x-1}} \cos^{-1}\left(\frac{3x-1}{2x^{3/2}}\right).$$
(8.9)

If $\Delta^{\pm\pm}$ decay to $\Delta^\pm X^\pm$ is allowed, the corresponding partial widths will be the same as in Eqs. (8.3)-(8.5). The different scaling factor due to the Clebsch-Gordon coefficient for the quadruplet scalar is taken into account properly for the partial decay width formulae of the doubly charged Higgs given above. For example, the leptonic decay width given in Eq. (8.1) is suppressed by a factor of 2/3, compared to the type-II seesaw scenario [182, 183]. On the other hand, the bosonic and cascade decay modes are enhanced by a factor 3/2 in the quadruplet case compared to the triplet scenario [182–184].

In Fig. 13, we show the generic decay phase diagram for $\Delta^{\pm\pm}$ in our model, with $m_{\Delta^{\pm\pm}} = 1$ TeV. The dotted, dot-dashed, dashed and thick solid contours correspond to 99%, 90%, 50% and 10% branching ratios into the leptonic, bosonic or cascade decay modes. The decay phase diagram clearly depicts that the branching ratio to leptonic decay
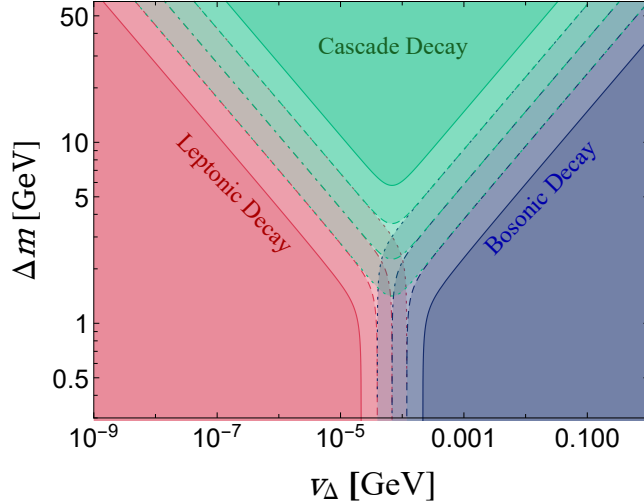
Figure 13: Generic decay phase diagram for $\Delta^{\pm\pm}$ in our model, with $m_{\Delta^{\pm\pm}} = 1\,\mathrm{TeV}$. The dotted, dot-dashed, dashed and thick solid contours correspond to 99%, 90%, 50% and 10% branching ratios respectively for the leptonic, bosonic or cascade decays, whereas Δm is the mass splitting between the Δ^{++} and the next lightest scalar component.

modes of $\Delta^{\pm\pm}$ decreases with v_Δ, whereas the branching ratio to gauge boson decay mode increases with v_Δ. The cross-over happens at $v_\Delta = 10^{-4}$ GeV with $\Delta m \sim 0$, similar to the type-II seesaw case [182, 183]. As soon as the mass splitting is set to ≥ 10 GeV, cascade decays open up and start dominating depending on the exact value of v_Δ. Note that the mass splitting $|\Delta m|$ between any two components of Δ cannot be larger than ~ 50 GeV due to stringent constraints from electroweak precision data [72].

8.3 Comment on 4-body Decay of Δ

In addition to the two-body decays given in Eqs. (8.1)-(8.6), there will also be four-body decay modes of the doubly-charged scalar via the virtual exchange of R_2 and S_3 LQs proportional to the μ term in Eq. (2.7): $\Delta^{\pm\pm} \to (\omega^{\pm 2/3})^\star (\rho^{\pm 4/3})^\star$, with each LQ decaying to two fermions. These decays will depend on the same parameters that lead to $\Delta^{\pm\pm} \to \ell^\pm \ell^\pm$ decays. The phase space for these decays would appear to be comparable to the two-body decays, since the latter has a suppression of a loop factor, $1/(16\pi^2)^2$. We have evaluated these four-body decays of Δ^{++} semi-analytically following the procedure outline in Ref. [185], as well as numerically. The two methods gave very similar results. As an example, for a benchmark values of $m_{\Delta^{++}} = 800$ GeV, $m_{R_2} = 1$ TeV, $m_{S_3} = 2$ TeV, $\mu = 246$ GeV, $v_\Delta = 10^{-4}$ GeV, and the values of the Yukawa couplings given in Fit I (cf. Eq. (7.3)), the four-body decay width is 2.3×10^{-15} GeV, which turns out to be much smaller than that for the dileptonic decay, which is 2×10^{-9} GeV. As v_Δ is increased, the four-body decay may compete with the dileptonic decay; however, in this case $\Delta^{++} \to W^+ W^+$ decay would dominate. Consequently, the four-body decay of Δ^{++} can be safely ignored in our discussions.

Production	$\Delta^{\pm\pm}$ mass reach for $\mathcal{L} = 3$ ab^{-1}		
Channel	$\sqrt{s} = 14$ TeV	$\sqrt{s} = 27$ TeV	$\sqrt{s} = 100$ TeV
LQ-mode	1.1 TeV	2.0 TeV	6.2 TeV
DY-mode	0.9 TeV	1.3 TeV	2.9 TeV

Table V: Comparison of the doubly-charged scalar mass reach in the LQ and DY modes (with same-sign di-muon pair final states only) for 3 ab^{-1} integrated luminosity.

8.4 Signal Sensitivity

We focus on the small v_Δ region which gives same-sign dilepton final states from the $\Delta^{\pm\pm}$ decay, because charged leptons with large transverse momenta can be cleanly identified with good resolution and the charge of the leptons can be identified with fairly good accuracy at hadron colliders. For the benchmark fits given in Section 7.2 with normal hierarchy, the dilepton branching ratios of the $\Delta^{\pm\pm} \to \ell_i \ell_j$ for different flavors are as follows:

$$\text{BR}(ee) \; = \; 0 \,, \quad \text{BR}(\mu\mu) \; = \; 0.22 \,, \quad \text{BR}(\tau\tau) \; = \; 0.23 \,,$$
$$\text{BR}(e\mu) \; = \; 0.01 \,, \quad \text{BR}(\mu\tau) \; = \; 0.39 \,, \quad \text{BR}(e\tau) \; = \; 0.16 \,. \tag{8.10}$$

For simplicity, we focus on the $\mu\mu$ final states and consider the signal $pp \to \Delta^{++}\Delta^{--} + X \to \mu^+\mu^+\mu^-\mu^- + X$ to derive the sensitivity at future hadron colliders. The relevant SM background is mainly from the multi-top and multi-gauge boson production [186, 187]. However, there are several discriminating characteristics of our signal: (a) the invariant mass distributions for same-sign lepton pair from the $\Delta^{\pm\pm}$ decay would peak at a mass value much higher than the SM Z boson mass; and (b) the outgoing leptons will be more energetic compared to the ones produced in the decay of SM gauge bosons, since these leptons are produced from heavy particle $\Delta^{\pm\pm}$ decay. To derive the signal sensitivity, we first implement our model file in `FeynRules` package [165], then analyze the cross section for the signal using `MadGraph5aMC@NLO` [166], simulating the hadronization effects with Pythia8 [188] and detector effects with the `Delphes3` package [189]. In order to optimize the signal efficiency over the SM background, we impose the following basic acceptance criteria: $p_T^\ell > 15$ GeV for each lepton, pseudorapidity $|\eta^\ell| < 2.5$ and a veto on any opposite sign dilepton pair invariant mass being close to the Z boson mass $|M(\ell^+\ell^-) - m_Z| > 15$ GeV. In addition, events are selected such that the invariant mass for same-sign muon pair is higher than 500 GeV. After passing through all these acceptance criteria, we estimate the required luminosities to observe at least 25 events at different center-of-mass energies ($\sqrt{s}$=14, 27, 100 TeV). Our results are shown in Fig. 14. It is clear that for a given luminosity and a given $\sqrt{s}$, the doubly-charged scalar mass reach in the LQ mode is higher than that in the DY mode. The mass reach for 3 ab^{-1} integrated luminosity is summarized in Table V for different center-of-mass energies.

Once we identify the doubly-charged scalar from the multi-lepton signal, the next step is to distinguish the underlying model. In order to identify whether the $\Delta^{\pm\pm}$'s come from the S_3 LQ decay, accompanied by the $\omega^{2/3}$ LQs, we can consider the decay chain given in
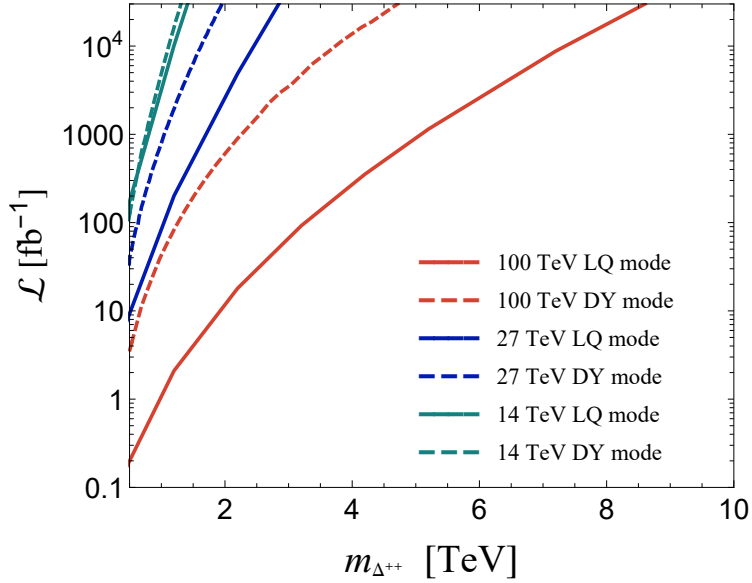
Figure 14: Required integrated luminosities for different center-of-mass energies of the pp collider to observe at least 25 events for the signal $pp \to \Delta^{++}\Delta^{--} + X \to \mu^+\mu^+\mu^-\mu^- + X$ in the LQ and DY production modes.

Fig. 11, i.e.

$$pp \to \rho^{4/3}\rho^{-4/3} \to \omega^{-2/3}\Delta^{++}\omega^{2/3}\Delta^{--} \to \ell^+\ell^+\ell^-\ell^- + \tau^+\tau^- + b\bar{b}. \tag{8.11}$$

In this case, the right combination of the $b\tau$ invariant mass peaks at the $\omega^{2/3}$ LQ mass, if it is produced on-shell from the Δ decay. Considering the fact that the benchmark fits in our model give 54% branching ratio of $\omega^{2/3}$ to $b\tau$ (cf. Table III), and taking into account the b-tagging and τ-identification efficiencies of $\sim 70\%$ each, we find that at least 25 signal events in the channel given by Eq. (8.11) can be obtained with 3 ab^{-1} luminosity for the S_3 LQ masses up to 1.5, 2.4 and 5.5 TeV respectively at $\sqrt{s} = 14$, 27 and 100 TeV. Hence, it is possible to independently test the unified description of B-anomalies, muon $g-2$ and neutrino masses in our model at future colliders.

9 Conclusion

We have presented a radiative neutrino mass model involving TeV-scale scalar leptoquarks R_2 and S_3, which can simultaneously explain the $R_{D^{(\star)}}$, $R_{K^{(\star)}}$, as well as muon $g-2$ anomalies, all within $1\,\sigma$ CL, while being consistent with neutrino oscillation data, as well as all flavor and LHC constraints. The R_2 LQ is responsible for the $R_{D^{(\star)}}$ and $(g-2)_\mu$, while the S_3 LQ explains the $R_{K^{(\star)}}$ anomaly. The model also features a scalar quadruplet Δ, which is required for the radiative neutrino mass generation. The same trilinear $\Delta^\star R_2 S_3$ coupling that is responsible for neutrino mass also leads to interesting collider signatures in the S_3 and Δ decays that can be probed in the forthcoming run of the LHC. Similarly, the

same Yukawa couplings responsible for the chirally-enhanced contribution to Δa_μ give rise to new contributions to the SM Higgs decays to muon and tau pairs, with the modifications to the corresponding branching ratios being at 2-6% level, which could be tested at future hadron colliders, such as HL-LHC and FCC-hh.

Acknowledgments

References

[1] **Particle Data Group** Collaboration, P. Zyla *et al.*, "Review of Particle Physics," *PTEP* **2020** no. 8, (2020) 083C01.

[2] P. Minkowski, "$\mu \to e\gamma$ at a Rate of One Out of 10^9 Muon Decays?," *Phys. Lett. B* **67** (1977) 421–428.

[3] R. N. Mohapatra and G. Senjanović, "Neutrino Mass and Spontaneous Parity Nonconservation," *Phys. Rev. Lett.* **44** (1980) 912.

[4] T. Yanagida, "Horizontal gauge symmetry and masses of neutrinos," *Conf. Proc. C* **7902131** (1979) 95–99.

[5] M. Gell-Mann, P. Ramond, and R. Slansky, "Complex Spinors and Unified Theories," *Conf. Proc. C* **790927** (1979) 315–321, arXiv:1306.4669 [hep-th].

[6] S. Glashow, "The Future of Elementary Particle Physics," *NATO Sci. Ser. B* **61** (1980) 687.

[7] J. Schechter and J. W. F. Valle, "Neutrino Masses in SU(2) x U(1) Theories," *Phys. Rev.* **D22** (1980) 2227.

[8] R. N. Mohapatra and G. Senjanović, "Neutrino Masses and Mixings in Gauge Models with Spontaneous Parity Violation," *Phys. Rev.* **D23** (1981) 165.

[9] G. Lazarides, Q. Shafi, and C. Wetterich, "Proton Lifetime and Fermion Masses in an SO(10) Model," *Nucl. Phys.* **B181** (1981) 287–300.

[10] R. Foot, H. Lew, X. G. He, and G. C. Joshi, "Seesaw Neutrino Masses Induced by a Triplet of Leptons," *Z. Phys.* **C44** (1989) 441.

[11] A. Zee, "A Theory of Lepton Number Violation, Neutrino Majorana Mass, and Oscillation," *Phys. Lett. B* **93** (1980) 389. [Erratum: Phys.Lett.B 95, 461 (1980)].

[12] T. Cheng and L.-F. Li, "Neutrino Masses, Mixings and Oscillations in SU(2) x U(1) Models of Electroweak Interactions," *Phys. Rev. D* **22** (1980) 2860.

[13] A. Zee, "Quantum Numbers of Majorana Neutrino Masses," *Nucl. Phys. B* **264** (1986) 99–110.

[14] K. Babu, "Model of 'Calculable' Majorana Neutrino Masses," *Phys. Lett. B* **203** (1988) 132–136.

[15] Y. Cai, J. Herrero-García, M. A. Schmidt, A. Vicente, and R. R. Volkas, "From the trees to the forest: a review of radiative neutrino mass models," *Front. in Phys.* **5** (2017) 63, arXiv:1706.08524 [hep-ph].

[16] K. S. Babu, P. S. B. Dev, S. Jana, and A. Thapa, "Non-Standard Interactions in Radiative Neutrino Mass Models," *JHEP* **03** (2020) 006, arXiv:1907.09498 [hep-ph].

[17] **Muon g-2** Collaboration, G. Bennett *et al.*, "Final Report of the Muon E821 Anomalous Magnetic Moment Measurement at BNL," *Phys. Rev. D* **73** (2006) 072003, arXiv:hep-ex/0602035.

[18] T. Aoyama *et al.*, "The anomalous magnetic moment of the muon in the Standard Model," arXiv:2006.04822 [hep-ph].

[19] **Muon g-2** Collaboration, J. Grange *et al.*, "Muon (g-2) Technical Design Report," arXiv:1501.06858 [physics.ins-det].

[20] **RBC, UKQCD** Collaboration, T. Blum, P. Boyle, V. Gülpers, T. Izubuchi, L. Jin, C. Jung, A. Jüttner, C. Lehner, A. Portelli, and J. Tsang, "Calculation of the hadronic vacuum polarization contribution to the muon anomalous magnetic moment," *Phys. Rev. Lett.* **121** no. 2, (2018) 022003, arXiv:1801.07224 [hep-lat].

[21] **Fermilab Lattice, LATTICE-HPQCD, MILC** Collaboration, C. Davies *et al.*, "Hadronic-vacuum-polarization contribution to the muon's anomalous magnetic moment from four-flavor lattice QCD," *Phys. Rev. D* **101** no. 3, (2020) 034512, arXiv:1902.04223 [hep-lat].

[22] A. Gérardin, M. Cè, G. von Hippel, B. Hörz, H. B. Meyer, D. Mohler, K. Ottnad, J. Wilhelm, and H. Wittig, "The leading hadronic contribution to $(g-2)_\mu$ from lattice QCD with $N_{\rm f} = 2+1$ flavours of O(a) improved Wilson quarks," *Phys. Rev. D* **100** no. 1, (2019) 014510, arXiv:1904.03120 [hep-lat].

[23] M. Davier, A. Hoecker, B. Malaescu, and Z. Zhang, "A new evaluation of the hadronic vacuum polarisation contributions to the muon anomalous magnetic moment and to $\boldsymbol{\alpha(\mathbf{m_Z^2})}$," *Eur. Phys. J. C* **80** no. 3, (2020) 241, arXiv:1908.00921 [hep-ph]. [Erratum: Eur.Phys.J.C 80, 410 (2020)].

[24] S. Borsanyi *et al.*, "Leading-order hadronic vacuum polarization contribution to the muon magnetic momentfrom lattice QCD," arXiv:2002.12347 [hep-lat].

[25] C. Lehner and A. S. Meyer, "Consistency of hadronic vacuum polarization between lattice QCD and the R-ratio," *Phys. Rev. D* **101** (2020) 074515, arXiv:2003.04177 [hep-lat].

[26] A. Crivellin, M. Hoferichter, C. A. Manzari, and M. Montull, "Hadronic vacuum polarization: $(g-2)_\mu$ versus global electroweak fits," *Phys. Rev. Lett.* **125** no. 9, (2020) 091801, arXiv:2003.04886 [hep-ph].

[27] F. Jegerlehner and A. Nyffeler, "The Muon g-2," *Phys. Rept.* **477** (2009) 1–110, arXiv:0902.3360 [hep-ph].

[28] W. Buchmüller and D. Wyler, "Constraints on SU(5) Type Leptoquarks," *Phys. Lett.* **B177** (1986) 377–382.

[29] **BaBar** Collaboration, J. P. Lees *et al.*, "Evidence for an excess of $\bar{B} \to D^{(*)}\tau^-\bar{\nu}_\tau$ decays," *Phys. Rev. Lett.* **109** (2012) 101802, arXiv:1205.5442 [hep-ex].

[30] **BaBar** Collaboration, J. P. Lees *et al.*, "Measurement of an Excess of $\bar{B} \to D^{(*)}\tau^-\bar{\nu}_\tau$

Decays and Implications for Charged Higgs Bosons," *Phys. Rev.* **D88** no. 7, (2013) 072012, `arXiv:1303.0571 [hep-ex]`.

[31] **Belle** Collaboration, M. Huschle *et al.*, "Measurement of the branching ratio of $\bar{B} \to D^{(*)}\tau^-\bar{\nu}_\tau$ relative to $\bar{B} \to D^{(*)}\ell^-\bar{\nu}_\ell$ decays with hadronic tagging at Belle," *Phys. Rev.* **D92** no. 7, (2015) 072014, `arXiv:1507.03233 [hep-ex]`.

[32] **Belle** Collaboration, S. Hirose *et al.*, "Measurement of the τ lepton polarization and $R(D^*)$ in the decay $\bar{B} \to D^*\tau^-\bar{\nu}_\tau$," *Phys. Rev. Lett.* **118** no. 21, (2017) 211801, `arXiv:1612.00529 [hep-ex]`.

[33] **Belle** Collaboration, A. Abdesselam *et al.*, "Measurement of the branching ratio of $\bar{B}^0 \to D^{*+}\tau^-\bar{\nu}_\tau$ relative to $\bar{B}^0 \to D^{*+}\ell^-\bar{\nu}_\ell$ decays with a semileptonic tagging method," in *Proceedings, 51st Rencontres de Moriond on Electroweak Interactions and Unified Theories: La Thuile, Italy, March 12-19, 2016.* 2016. `arXiv:1603.06711 [hep-ex]`.

[34] **LHCb** Collaboration, R. Aaij *et al.*, "Measurement of the ratio of branching fractions $\mathcal{B}(B_c^+ \to J/\psi\tau^+\nu_\tau)/\mathcal{B}(B_c^+ \to J/\psi\mu^+\nu_\mu)$," *Phys. Rev. Lett.* **120** no. 12, (2018) 121801, `arXiv:1711.05623 [hep-ex]`.

[35] **LHCb** Collaboration, R. Aaij *et al.*, "Measurement of the ratio of the $B^0 \to D^{*-}\tau^+\nu_\tau$ and $B^0 \to D^{*-}\mu^+\nu_\mu$ branching fractions using three-prong τ-lepton decays," *Phys. Rev. Lett.* **120** no. 17, (2018) 171802, `arXiv:1708.08856 [hep-ex]`.

[36] **LHCb** Collaboration, R. Aaij *et al.*, "Search for lepton-universality violation in $B^+ \to K^+\ell^+\ell^-$ decays," `arXiv:1903.09252 [hep-ex]`.

[37] **LHCb** Collaboration, R. Aaij *et al.*, "Test of lepton universality with $B^0 \to K^{*0}\ell^+\ell^-$ decays," *JHEP* **08** (2017) 055, `arXiv:1705.05802 [hep-ex]`.

[38] **HFLAV** Collaboration, Y. S. Amhis *et al.*, "Averages of b-hadron, c-hadron, and τ-lepton properties as of 2018," `arXiv:1909.12524 [hep-ex]`.

[39] M. Bordone, G. Isidori, and A. Pattori, "On the Standard Model predictions for R_K and R_{K^*}," *Eur. Phys. J.* **C76** no. 8, (2016) 440, `arXiv:1605.07633 [hep-ph]`.

[40] B. Capdevila, A. Crivellin, S. Descotes-Genon, J. Matias, and J. Virto, "Patterns of New Physics in $b \to s\ell^+\ell^-$ transitions in the light of recent data," *JHEP* **01** (2018) 093, `arXiv:1704.05340 [hep-ph]`.

[41] W. Altmannshofer, P. Stangl, and D. M. Straub, "Interpreting Hints for Lepton Flavor Universality Violation," *Phys. Rev. D* **96** no. 5, (2017) 055008, `arXiv:1704.05435 [hep-ph]`.

[42] J. Aebischer, W. Altmannshofer, D. Guadagnoli, M. Reboud, P. Stangl, and D. M. Straub, "B-decay discrepancies after Moriond 2019," `arXiv:1903.10434 [hep-ph]`.

[43] M. Bauer and M. Neubert, "Minimal Leptoquark Explanation for the $R_{D^{(*)}}$, R_K, and $(g-2)_g$ Anomalies," *Phys. Rev. Lett.* **116** no. 14, (2016) 141802, `arXiv:1511.01900 [hep-ph]`.

[44] O. Popov and G. A. White, "One Leptoquark to unify them? Neutrino masses and unification in the light of $(g-2)_\mu$, $R_{D^{(*)}}$ and R_K anomalies," *Nucl. Phys. B* **923** (2017) 324–338, `arXiv:1611.04566 [hep-ph]`.

[45] Y. Cai, J. Gargalionis, M. A. Schmidt, and R. R. Volkas, "Reconsidering the One Leptoquark solution: flavor anomalies and neutrino mass," *JHEP* **10** (2017) 047, `arXiv:1704.05849 [hep-ph]`.

[46] O. Popov, M. A. Schmidt, and G. White, "R_2 as a single leptoquark solution to $R_{D^{(*)}}$ and $R_{K^{(*)}}$," *Phys. Rev. D* **100** no. 3, (2019) 035028, `arXiv:1905.06339 [hep-ph]`.

[47] A. Angelescu, D. Bečirević, D. A. Faroughy, and O. Sumensari, "Closing the window on single leptoquark solutions to the B-physics anomalies," *JHEP* **10** (2018) 183, `arXiv:1808.08179 [hep-ph]`.

[48] D. Buttazzo, A. Greljo, G. Isidori, and D. Marzocca, "B-physics anomalies: a guide to combined explanations," *JHEP* **11** (2017) 044, `arXiv:1706.07808 [hep-ph]`.

[49] J. Kumar, D. London, and R. Watanabe, "Combined Explanations of the $b \to s\mu^+\mu^-$ and $b \to c\tau^-\bar{\nu}$ Anomalies: a General Model Analysis," *Phys. Rev. D* **99** no. 1, (2019) 015007, `arXiv:1806.07403 [hep-ph]`.

[50] M. Kohda, H. Sugiyama, and K. Tsumura, "Lepton number violation at the LHC with leptoquark and diquark," *Phys. Lett. B* **718** (2013) 1436–1440, `arXiv:1210.5622 [hep-ph]`.

[51] H. Päs and E. Schumacher, "Common origin of R_K and neutrino masses," *Phys. Rev. D* **92** no. 11, (2015) 114025, `arXiv:1510.08757 [hep-ph]`.

[52] K. Cheung, T. Nomura, and H. Okada, "Testable radiative neutrino mass model without additional symmetries and explanation for the $b \to s\ell^+\ell^-$ anomaly," *Phys. Rev. D* **94** no. 11, (2016) 115024, `arXiv:1610.02322 [hep-ph]`.

[53] S.-Y. Guo, Z.-L. Han, B. Li, Y. Liao, and X.-D. Ma, "Interpreting the $R_{K^{(*)}}$ anomaly in the colored Zee–Babu model," *Nucl. Phys. B* **928** (2018) 435–447, `arXiv:1707.00522 [hep-ph]`.

[54] C. Hati, G. Kumar, J. Orloff, and A. M. Teixeira, "Reconciling B-meson decay anomalies with neutrino masses, dark matter and constraints from flavour violation," *JHEP* **11** (2018) 011, `arXiv:1806.10146 [hep-ph]`.

[55] S. Singirala, S. Sahoo, and R. Mohanta, "Exploring dark matter, neutrino mass and $R_{K^{(*)},\phi}$ anomalies in $L_\mu - L_\tau$ model," *Phys. Rev. D* **99** no. 3, (2019) 035042, `arXiv:1809.03213 [hep-ph]`.

[56] A. Datta, D. Sachdeva, and J. Waite, "Unified explanation of $b \to s\mu^+\mu^-$ anomalies, neutrino masses, and $B \to \pi K$ puzzle," *Phys. Rev. D* **100** no. 5, (2019) 055015, `arXiv:1905.04046 [hep-ph]`.

[57] I. Doršner, S. Fajfer, D. A. Faroughy, and N. Košnik, "The role of the S_3 GUT leptoquark in flavor universality and collider searches," *JHEP* **10** (2017) 188, `arXiv:1706.07779 [hep-ph]`.

[58] S. Saad and A. Thapa, "Common origin of neutrino masses and $R_{D^{(*)}}$, $R_{K^{(*)}}$ anomalies," *Phys. Rev. D* **102** no. 1, (2020) 015014, `arXiv:2004.07880 [hep-ph]`.

[59] C.-H. Chen and T. Nomura, "Electron and muon $g-2$, radiative neutrino mass, and $\ell' \to \ell\gamma$ in a $U(1)_{e-\mu}$ model," `arXiv:2003.07638 [hep-ph]`.

[60] C.-H. Chen, T. Nomura, and H. Okada, "Excesses of muon $g-2$, $R_{D^{(*)}}$, and R_K in a leptoquark model," *Phys. Lett. B* **774** (2017) 456–464, `arXiv:1703.03251 [hep-ph]`.

[61] S. Saad, "Combined explanations of $(g-2)_\mu$, $R_{D^{(*)}}$, $R_{K^{(*)}}$ anomalies in a two-loop radiative neutrino mass model," *Phys. Rev. D* **102** no. 1, (2020) 015019, `arXiv:2005.04352 [hep-ph]`.

[62] I. Bigaran, J. Gargalionis, and R. R. Volkas, "A near-minimal leptoquark model for reconciling flavour anomalies and generating radiative neutrino masses," *JHEP* **10** (2019) 106, `arXiv:1906.01870 [hep-ph]`.

[63] D. Aristizabal Sierra, M. Hirsch, and S. G. Kovalenko, "Leptoquarks: Neutrino masses and accelerator phenomenology," *Phys. Rev.* **D77** (2008) 055011, `arXiv:0710.5699 [hep-ph]`.

[64] K. Babu and J. Julio, "Two-Loop Neutrino Mass Generation through Leptoquarks," *Nucl. Phys. B* **841** (2010) 130–156, `arXiv:1006.1092 [hep-ph]`.

[65] K. S. Babu and J. Julio, "Radiative Neutrino Mass Generation through Vector-like Quarks," *Phys. Rev.* **D85** (2012) 073005, `arXiv:1112.5452 [hep-ph]`.

[66] P. W. Angel, Y. Cai, N. L. Rodd, M. A. Schmidt, and R. R. Volkas, "Testable two-loop radiative neutrino mass model based on an $LLQd^cQd^c$ effective operator," *JHEP* **10** (2013) 118, `arXiv:1308.0463 [hep-ph]`. [Erratum: JHEP11,092(2014)].

[67] Y. Cai, J. D. Clarke, M. A. Schmidt, and R. R. Volkas, "Testing Radiative Neutrino Mass Models at the LHC," *JHEP* **02** (2015) 161, `arXiv:1410.0689 [hep-ph]`.

[68] O. Catà and T. Mannel, "Linking lepton number violation with B anomalies," `arXiv:1903.01799 [hep-ph]`.

[69] K. Babu, S. Nandi, and Z. Tavartkiladze, "New Mechanism for Neutrino Mass Generation and Triply Charged Higgs Bosons at the LHC," *Phys. Rev. D* **80** (2009) 071702, `arXiv:0905.2710 [hep-ph]`.

[70] G. Bambhaniya, J. Chakrabortty, S. Goswami, and P. Konar, "Generation of neutrino mass from new physics at TeV scale and multilepton signatures at the LHC," *Phys. Rev. D* **88** no. 7, (2013) 075006, `arXiv:1305.2795 [hep-ph]`.

[71] K. Ghosh, S. Jana, and S. Nandi, "Neutrino Mass Generation at TeV Scale and New Physics Signatures from Charged Higgs at the LHC for Photon Initiated Processes," *JHEP* **03** (2018) 180, `arXiv:1705.01121 [hep-ph]`.

[72] T. Ghosh, S. Jana, and S. Nandi, "Neutrino mass from Higgs quadruplet and multicharged Higgs searches at the LHC," *Phys. Rev.* **D97** no. 11, (2018) 115037, `arXiv:1802.09251 [hep-ph]`.

[73] K. P. Hadeler, "On copositive matrices," *Linear Algebra and its Applications* **49** (1983) 79–89.

[74] K. Klimenko, "On Necessary and Sufficient Conditions for Some Higgs Potentials to Be Bounded From Below," *Theor. Math. Phys.* **62** (1985) 58–65.

[75] K. S. Babu and J. Julio, "Renormalization of a two-loop neutrino mass model," *AIP Conf. Proc.* **1604** no. 1, (2015) 134–141.

[76] K. S. Babu and C. N. Leung, "Classification of effective neutrino mass operators," *Nucl. Phys.* **B619** (2001) 667–689, `arXiv:hep-ph/0106054 [hep-ph]`.

[77] A. de Gouvêa and J. Jenkins, "A Survey of Lepton Number Violation Via Effective Operators," *Phys. Rev.* **D77** (2008) 013008, `arXiv:0708.1344 [hep-ph]`.

[78] R. Cepedello, M. Hirsch, and J. Helo, "Lepton number violating phenomenology of d = 7 neutrino mass models," *JHEP* **01** (2018) 009, `arXiv:1709.03397 [hep-ph]`.

[79] **LHCb** Collaboration, R. Aaij *et al.*, "Measurement of the ratio of branching fractions

$\mathcal{B}(\bar{B}^0 \to D^{*+}\tau^-\bar{\nu}_\tau)/\mathcal{B}(\bar{B}^0 \to D^{*+}\mu^-\bar{\nu}_\mu)$," *Phys. Rev. Lett.* **115** no. 11, (2015) 111803, `arXiv:1506.08614 [hep-ex]`. [Erratum: Phys. Rev. Lett.115,no.15,159901(2015)].

[80] S. Fajfer, J. F. Kamenik, and I. Nišandžić, "On the $B \to D^*\tau\bar{\nu}_\tau$ Sensitivity to New Physics," *Phys. Rev.* **D85** (2012) 094025, `arXiv:1203.2654 [hep-ph]`.

[81] S. Fajfer, J. F. Kamenik, I. Nišandžić, and J. Zupan, "Implications of Lepton Flavor Universality Violations in B Decays," *Phys. Rev. Lett.* **109** (2012) 161801, `arXiv:1206.1872 [hep-ph]`.

[82] **MILC** Collaboration, J. A. Bailey *et al.*, "$B \to D\ell\nu$ form factors at nonzero recoil and $|V_{cb}|$ from 2+1-flavor lattice QCD," *Phys. Rev.* **D92** no. 3, (2015) 034506, `arXiv:1503.07237 [hep-lat]`.

[83] **HPQCD** Collaboration, H. Na, C. M. Bouchard, G. P. Lepage, C. Monahan, and J. Shigemitsu, "$B \to Dl\nu$ form factors at nonzero recoil and extraction of $|V_{cb}|$," *Phys. Rev.* **D92** no. 5, (2015) 054510, `arXiv:1505.03925 [hep-lat]`. [Erratum: Phys. Rev.D93,no.11,119906(2016)].

[84] D. Bigi, P. Gambino, and S. Schacht, "$R(D^*)$, $|V_{cb}|$, and the Heavy Quark Symmetry relations between form factors," *JHEP* **11** (2017) 061, `arXiv:1707.09509 [hep-ph]`.

[85] F. U. Bernlochner, Z. Ligeti, M. Papucci, and D. J. Robinson, "Combined analysis of semileptonic B decays to D and D^*: $R(D^{(*)})$, $|V_{cb}|$, and new physics," *Phys. Rev.* **D95** no. 11, (2017) 115008, `arXiv:1703.05330 [hep-ph]`. [erratum: Phys. Rev.D97,no.5,059902(2018)].

[86] S. Jaiswal, S. Nandi, and S. K. Patra, "Extraction of $|V_{cb}|$ from $B \to D^{(*)}\ell\nu_\ell$ and the Standard Model predictions of $R(D^{(*)})$," *JHEP* **12** (2017) 060, `arXiv:1707.09977 [hep-ph]`.

[87] F. U. Bernlochner, S. Duell, Z. Ligeti, M. Papucci, and D. J. Robinson, "Das ist der HAMMER: Consistent new physics interpretations of semileptonic decays," `arXiv:2002.00020 [hep-ph]`.

[88] S. Jaiswal, S. Nandi, and S. K. Patra, "Updates on SM predictions of $|V_{cb}|$ and $R(D^*)$ in $B \to D^*\ell\nu_\ell$ decays," `arXiv:2002.05726 [hep-ph]`.

[89] M. A. Ivanov, J. G. Korner, and P. Santorelli, "Semileptonic decays of B_c mesons into charmonium states in a relativistic quark model," *Phys. Rev.* **D71** (2005) 094006, `arXiv:hep-ph/0501051 [hep-ph]`. [Erratum: Phys. Rev.D75,019901(2007)].

[90] W.-F. Wang, Y.-Y. Fan, and Z.-J. Xiao, "Semileptonic decays $B_c \to (\eta_c, J/\Psi)l\nu$ in the perturbative QCD approach," *Chin. Phys.* **C37** (2013) 093102, `arXiv:1212.5903 [hep-ph]`.

[91] R. Dutta and A. Bhol, "$B_c \to (J/\psi, \eta_c)\tau\nu$ semileptonic decays within the standard model and beyond," *Phys. Rev.* **D96** no. 7, (2017) 076001, `arXiv:1701.08598 [hep-ph]`.

[92] C. W. Murphy and A. Soni, "Model-Independent Determination of $B_c^+ \to \eta_c\,\ell^+\,\nu$ Form Factors," *Phys. Rev.* **D98** no. 9, (2018) 094026, `arXiv:1808.05932 [hep-ph]`.

[93] A. Issadykov and M. A. Ivanov, "The decays $B_c \to J/\psi + \bar{\ell}\nu_\ell$ and $B_c \to J/\psi + \pi(K)$ in covariant confined quark model," *Phys. Lett.* **B783** (2018) 178–182, `arXiv:1804.00472 [hep-ph]`.

[94] R. Watanabe, "New Physics effect on $B_c \to J/\psi\tau\bar{\nu}$ in relation to the $R_{D^{(*)}}$ anomaly," *Phys. Lett.* **B776** (2018) 5–9, `arXiv:1709.08644 [hep-ph]`.

[95] T. D. Cohen, H. Lamm, and R. F. Lebed, "Model-independent bounds on $R(J/\psi)$," *JHEP* **09** (2018) 168, `arXiv:1807.02730 [hep-ph]`.

[96] A. Berns and H. Lamm, "Model-Independent Prediction of $R(\eta_c)$," *JHEP* **12** (2018) 114, `arXiv:1808.07360 [hep-ph]`.

[97] I. Doršner, S. Fajfer, N. Košnik, and I. Nišandžić, "Minimally flavored colored scalar in $\bar{B} \to D^{(*)}\tau\bar{\nu}$ and the mass matrices constraints," *JHEP* **11** (2013) 084, `arXiv:1306.6493 [hep-ph]`.

[98] K. Chetyrkin, "Quark mass anomalous dimension to O (alpha-s**4)," *Phys. Lett. B* **404** (1997) 161–165, `arXiv:hep-ph/9703278`.

[99] J. Gracey, "Three loop MS-bar tensor current anomalous dimension in QCD," *Phys. Lett. B* **488** (2000) 175–181, `arXiv:hep-ph/0007171`.

[100] K. Babu, "TASI Lectures on Flavor Physics," in *Proceedings of Theoretical Advanced Study Institute in Elementary Particle Physics on The dawn of the LHC era (TASI 2008): Boulder, USA, June 2-27, 2008*, pp. 49–123. 2010. `arXiv:0910.2948 [hep-ph]`.

[101] M. González-Alonso, J. Martin Camalich, and K. Mimouni, "Renormalization-group evolution of new physics contributions to (semi)leptonic meson decays," *Phys. Lett. B* **772** (2017) 777–785, `arXiv:1706.00410 [hep-ph]`.

[102] M. Blanke, A. Crivellin, S. de Boer, T. Kitahara, M. Moscati, U. Nierste, and I. Nišandžić, "Impact of polarization observables and $B_c \to \tau\nu$ on new physics explanations of the $b \to c\tau\nu$ anomaly," *Phys. Rev. D* **99** no. 7, (2019) 075006, `arXiv:1811.09603 [hep-ph]`.

[103] D. M. Straub, "flavio: a Python package for flavour and precision phenomenology in the Standard Model and beyond," `arXiv:1810.08132 [hep-ph]`.

[104] Y. Sakaki, M. Tanaka, A. Tayduganov, and R. Watanabe, "Testing leptoquark models in $\bar{B} \to D^{(*)}\tau\bar{\nu}$," *Phys. Rev. D* **88** no. 9, (2013) 094012, `arXiv:1309.0301 [hep-ph]`.

[105] R. Alonso, B. Grinstein, and J. Martin Camalich, "Lifetime of B_c^- Constrains Explanations for Anomalies in $B \to D^{(*)}\tau\nu$," *Phys. Rev. Lett.* **118** no. 8, (2017) 081802, `arXiv:1611.06676 [hep-ph]`.

[106] C.-H. Chang, S.-L. Chen, T.-F. Feng, and X.-Q. Li, "The Lifetime of B_c meson and some relevant problems," *Phys. Rev. D* **64** (2001) 014003, `arXiv:hep-ph/0007162`.

[107] S. Gershtein, V. Kiselev, A. Likhoded, and A. Tkabladze, "Physics of B(c) mesons," *Phys. Usp.* **38** (1995) 1–37, `arXiv:hep-ph/9504319`.

[108] I. I. Bigi, "Inclusive B(c) decays as a QCD lab," *Phys. Lett. B* **371** (1996) 105–110, `arXiv:hep-ph/9510325`.

[109] M. Beneke and G. Buchalla, "The B_c Meson Lifetime," *Phys. Rev. D* **53** (1996) 4991–5000, `arXiv:hep-ph/9601249`.

[110] V. Kiselev, A. Kovalsky, and A. Likhoded, "B_c decays and lifetime in QCD sum rules," *Nucl. Phys. B* **585** (2000) 353–382, `arXiv:hep-ph/0002127`.

[111] A. Akeroyd and C.-H. Chen, "Constraint on the branching ratio of $B_c \to \tau\bar{\nu}$ from LEP1 and consequences for $R(D^{(*)})$ anomaly," *Phys. Rev. D* **96** no. 7, (2017) 075011, `arXiv:1708.04072 [hep-ph]`.

[112] D. Bardhan and D. Ghosh, "B-meson charged current anomalies: The post-Moriond 2019 status," *Phys. Rev. D* **100** no. 1, (2019) 011701, `arXiv:1904.10432 [hep-ph]`.

[113] **LHCb** Collaboration, R. Aaij *et al.*, "Test of lepton universality in beauty-quark decays," arXiv:2103.11769 [hep-ex].

[114] C. Bobeth, G. Hiller, and G. Piranishvili, "Angular distributions of $\bar{B} \to \bar{K}\ell^+\ell^-$ decays," *JHEP* **12** (2007) 040, arXiv:0709.4174 [hep-ph].

[115] **Belle** Collaboration, A. Abdesselam *et al.*, "Test of lepton flavor universality in $B \to K\ell^+\ell^-$ decays," arXiv:1908.01848 [hep-ex].

[116] **Belle** Collaboration, A. Abdesselam *et al.*, "Test of lepton flavor universality in $B \to K^*\ell^+\ell^-$ decays at Belle," arXiv:1904.02440 [hep-ex].

[117] D. Bečirević and O. Sumensari, "A leptoquark model to accommodate $R_K^{\exp} < R_K^{\mathrm{SM}}$ and $R_{K^*}^{\exp} < R_{K^*}^{\mathrm{SM}}$," *JHEP* **08** (2017) 104, arXiv:1704.05835 [hep-ph].

[118] K.-m. Cheung, "Muon anomalous magnetic moment and leptoquark solutions," *Phys. Rev. D* **64** (2001) 033001, arXiv:hep-ph/0102238.

[119] R. Mandal and A. Pich, "Constraints on scalar leptoquarks from lepton and kaon physics," *JHEP* **12** (2019) 089, arXiv:1908.11155 [hep-ph].

[120] I. Doršner, S. Fajfer, A. Greljo, J. F. Kamenik, and N. Košnik, "Physics of leptoquarks in precision experiments and at particle colliders," *Phys. Rept.* **641** (2016) 1–68, arXiv:1603.04993 [hep-ph].

[121] L. Lavoura, "General formulae for $f(1) \to f(2)\gamma$," *Eur. Phys. J. C* **29** (2003) 191–195, arXiv:hep-ph/0302221.

[122] R. H. Parker, C. Yu, W. Zhong, B. Estey, and H. Müller, "Measurement of the fine-structure constant as a test of the Standard Model," *Science* **360** (2018) 191, arXiv:1812.04130 [physics.atom-ph].

[123] A. Crivellin, D. Müller, and F. Saturnino, "Correlating $h \to \mu^+\mu^-$ to the Anomalous Magnetic Moment of the Muon via Leptoquarks," arXiv:2008.02643 [hep-ph].

[124] **ATLAS** Collaboration, G. Aad *et al.*, "A search for the dimuon decay of the Standard Model Higgs boson with the ATLAS detector," arXiv:2007.07830 [hep-ex].

[125] **CMS** Collaboration, "Measurement of Higgs boson decay to a pair of muons in proton-proton collisions at $\sqrt{s} = 13\,\mathrm{TeV}$," Tech. Rep. CMS-PAS-HIG-19-006, 2020.

[126] J. de Blas *et al.*, "Higgs Boson Studies at Future Particle Colliders," *JHEP* **01** (2020) 139, arXiv:1905.03764 [hep-ph].

[127] M. Cepeda *et al.*, *Report from Working Group 2: Higgs Physics at the HL-LHC and HE-LHC*, vol. 7, pp. 221–584. 12, 2019. arXiv:1902.00134 [hep-ph].

[128] **LCC Physics Working Group** Collaboration, K. Fujii *et al.*, "Tests of the Standard Model at the International Linear Collider," arXiv:1908.11299 [hep-ex].

[129] **CLIC, CLICdp** Collaboration, "The Compact Linear e$^+$e$^-$ Collider (CLIC): Physics Potential," arXiv:1812.07986 [hep-ex].

[130] **CEPC Study Group** Collaboration, M. Dong *et al.*, "CEPC Conceptual Design Report: Volume 2 - Physics & Detector," arXiv:1811.10545 [hep-ex].

[131] **FCC** Collaboration, A. Abada *et al.*, "FCC Physics Opportunities: Future Circular Collider Conceptual Design Report Volume 1," *Eur. Phys. J. C* **79** no. 6, (2019) 474.

[132] **ATLAS** Collaboration, M. Aaboud *et al.*, "Cross-section measurements of the Higgs boson decaying into a pair of τ-leptons in proton-proton collisions at $\sqrt{s} = 13$ TeV with the ATLAS detector," *Phys. Rev.* **D99** (2019) 072001, `arXiv:1811.08856 [hep-ex]`.

[133] **CMS** Collaboration, "Measurement of Higgs boson production in the decay channel with a pair of τ leptons," Tech. Rep. CMS-PAS-HIG-19-010, 2020.

[134] K. Fuyuto, M. Ramsey-Musolf, and T. Shen, "Electric Dipole Moments from CP-Violating Scalar Leptoquark Interactions," *Phys. Lett. B* **788** (2019) 52–57, `arXiv:1804.01137 [hep-ph]`.

[135] W. Dekens, J. de Vries, M. Jung, and K. Vos, "The phenomenology of electric dipole moments in models of scalar leptoquarks," *JHEP* **01** (2019) 069, `arXiv:1809.09114 [hep-ph]`.

[136] **ACME** Collaboration, V. Andreev *et al.*, "Improved limit on the electric dipole moment of the electron," *Nature* **562** no. 7727, (2018) 355–360.

[137] **Muon (g-2)** Collaboration, G. Bennett *et al.*, "An Improved Limit on the Muon Electric Dipole Moment," *Phys. Rev. D* **80** (2009) 052008, `arXiv:0811.1207 [hep-ex]`.

[138] M. Abe *et al.*, "A New Approach for Measuring the Muon Anomalous Magnetic Moment and Electric Dipole Moment," *PTEP* **2019** no. 5, (2019) 053C02, `arXiv:1901.03047 [physics.ins-det]`.

[139] T. Kishishita *et al.*, "SliT: A Strip-sensor Readout Chip with Subnanosecond Time-walk for the J-PARC Muon $g - 2$/EDM Experiment," `arXiv:2006.08095 [physics.ins-det]`.

[140] R. Janish and H. Ramani, "Muon g-2 and EDM experiments as muonic dark matter detectors," `arXiv:2006.10069 [hep-ph]`.

[141] **Belle** Collaboration, K. Inami *et al.*, "Search for the electric dipole moment of the tau lepton," *Phys. Lett. B* **551** (2003) 16–26, `arXiv:hep-ex/0210066`.

[142] H. Gisbert and J. Ruiz Vidal, "Improved bounds on heavy quark electric dipole moments," *Phys. Rev. D* **101** no. 11, (2020) 115010, `arXiv:1905.02513 [hep-ph]`.

[143] J. M. Pendlebury *et al.*, "Revised experimental upper limit on the electric dipole moment of the neutron," *Phys. Rev. D* **92** no. 9, (2015) 092003, `arXiv:1509.04411 [hep-ex]`.

[144] R. Benbrik and C.-K. Chua, "Lepton Flavor Violating $l \to l' gamma$ and $Z \to l \bar{l}'$ Decays Induced by Scalar Leptoquarks," *Phys. Rev. D* **78** (2008) 075025, `arXiv:0807.4240 [hep-ph]`.

[145] **MEG** Collaboration, A. M. Baldini *et al.*, "Search for the lepton flavour violating decay $\mu^+ \to e^+ \gamma$ with the full dataset of the MEG experiment," *Eur. Phys. J.* **C76** no. 8, (2016) 434, `arXiv:1605.05081 [hep-ex]`.

[146] **BaBar** Collaboration, B. Aubert *et al.*, "Searches for Lepton Flavor Violation in the Decays $\tau^{\pm} \to e^{\pm}\gamma$ and $\tau^{\pm} \to \mu^{\pm}\gamma$," *Phys. Rev. Lett.* **104** (2010) 021802, `arXiv:0908.2381 [hep-ex]`.

[147] Y. Kuno and Y. Okada, "Muon decay and physics beyond the standard model," *Rev. Mod. Phys.* **73** (2001) 151–202, `arXiv:hep-ph/9909265`.

[148] **SINDRUM II** Collaboration, W. H. Bertl *et al.*, "A Search for muon to electron conversion in muonic gold," *Eur. Phys. J. C* **47** (2006) 337–346.

[149] **ALEPH, DELPHI, L3, OPAL, SLD, LEP Electroweak Working Group, SLD Electroweak Group, SLD Heavy Flavour Group** Collaboration, S. Schael *et al.*, "Precision electroweak measurements on the Z resonance," *Phys. Rept.* **427** (2006) 257–454, `arXiv:hep-ex/0509008`.

[150] P. Arnan, D. Bečirević, F. Mescia, and O. Sumensari, "Probing low energy scalar leptoquarks by the leptonic W and Z couplings," *JHEP* **02** (2019) 109, `arXiv:1901.06315 [hep-ph]`.

[151] L. Da Rold and F. Lamagna, "Composite Higgs and leptoquarks from a simple group," *JHEP* **03** (2019) 135, `arXiv:1812.08678 [hep-ph]`.

[152] A. Crivellin and F. Saturnino, "Correlating tauonic B decays with the neutron electric dipole moment via a scalar leptoquark," *Phys. Rev. D* **100** no. 11, (2019) 115014, `arXiv:1905.08257 [hep-ph]`.

[153] A. J. Buras, M. Misiak, and J. Urban, "Two loop QCD anomalous dimensions of flavor changing four quark operators within and beyond the standard model," *Nucl. Phys. B* **586** (2000) 397–426, `arXiv:hep-ph/0005183`.

[154] M. Ciuchini, E. Franco, V. Lubicz, G. Martinelli, I. Scimemi, and L. Silvestrini, "Next-to-leading order QCD corrections to Delta F = 2 effective Hamiltonians," *Nucl. Phys. B* **523** (1998) 501–525, `arXiv:hep-ph/9711402`.

[155] E. Golowich, J. Hewett, S. Pakvasa, and A. A. Petrov, "Implications of D^0 - $\bar{D}^0$ Mixing for New Physics," *Phys. Rev. D* **76** (2007) 095009, `arXiv:0705.3650 [hep-ph]`.

[156] N. Carrasco *et al.*, "$D^0 - \bar{D}^0$ mixing in the standard model and beyond from $N_f =2$ twisted mass QCD," *Phys. Rev. D* **90** no. 1, (2014) 014502, `arXiv:1403.7302 [hep-lat]`.

[157] A. Bazavov *et al.*, "B- and D-meson leptonic decay constants from four-flavor lattice QCD," *Phys. Rev. D* **98** no. 7, (2018) 074512, `arXiv:1712.09262 [hep-lat]`.

[158] L. Buonocore, U. Haisch, P. Nason, F. Tramontano, and G. Zanderighi, "Resonant single leptoquark production at hadron colliders," `arXiv:2005.06475 [hep-ph]`.

[159] **CMS** Collaboration, "Search for pair production of first generation scalar leptoquarks at $\sqrt{s} = 13$ TeV," Tech. Rep. CMS-PAS-EXO-17-009, 2018.

[160] **CMS** Collaboration, V. Khachatryan *et al.*, "Search for pair production of first and second generation leptoquarks in proton-proton collisions at $\sqrt{s} = 8$ TeV," *Phys. Rev.* **D93** no. 3, (2016) 032004, `arXiv:1509.03744 [hep-ex]`.

[161] **ATLAS** Collaboration, M. Aaboud *et al.*, "Searches for scalar leptoquarks and differential cross-section measurements in dilepton-dijet events in proton-proton collisions at a centre-of-mass energy of $\sqrt{s} = 13$ TeV with the ATLAS experiment," `arXiv:1902.00377 [hep-ex]`.

[162] **CMS** Collaboration, A. M. Sirunyan *et al.*, "Constraints on models of scalar and vector leptoquarks decaying to a quark and a neutrino at $\sqrt{s} = 13$ TeV," *Phys. Rev.* **D98** no. 3, (2018) 032005, `arXiv:1805.10228 [hep-ex]`.

[163] **CMS** Collaboration, A. M. Sirunyan *et al.*, "Search for heavy neutrinos and third-generation leptoquarks in hadronic states of two τ leptons and two jets in proton-proton collisions at $\sqrt{s} = 13$ TeV," *JHEP* **03** (2019) 170, `arXiv:1811.00806 [hep-ex]`.

[164] **ATLAS** Collaboration, M. Aaboud *et al.*, "Searches for third-generation scalar leptoquarks in $\sqrt{s} = 13$ TeV pp collisions with the ATLAS detector," `arXiv:1902.08103 [hep-ex]`.

[165] N. D. Christensen and C. Duhr, "FeynRules - Feynman rules made easy," *Comput. Phys. Commun.* **180** (2009) 1614–1641, `arXiv:0806.4194 [hep-ph]`.

[166] J. Alwall, R. Frederix, S. Frixione, V. Hirschi, F. Maltoni, O. Mattelaer, H. S. Shao, T. Stelzer, P. Torrielli, and M. Zaro, "The automated computation of tree-level and next-to-leading order differential cross sections, and their matching to parton shower simulations," *JHEP* **07** (2014) 079, `arXiv:1405.0301 [hep-ph]`.

[167] **ATLAS** Collaboration, G. Aad *et al.*, "Search for new non-resonant phenomena in high-mass dilepton final states with the ATLAS detector," `arXiv:2006.12946 [hep-ex]`.

[168] C. Bobeth, U. Haisch, A. Lenz, B. Pecjak, and G. Tetlalmatzi-Xolocotzi, "On new physics in $\Delta\Gamma_d$," *JHEP* **06** (2014) 040, `arXiv:1404.2531 [hep-ph]`.

[169] A. Crivellin, C. Greub, D. Müller, and F. Saturnino, "Importance of Loop Effects in Explaining the Accumulated Evidence for New Physics in B Decays with a Vector Leptoquark," *Phys. Rev. Lett.* **122** no. 1, (2019) 011805, `arXiv:1807.02068 [hep-ph]`.

[170] A. Crivellin, D. Müller, and F. Saturnino, "Flavor Phenomenology of the Leptoquark Singlet-Triplet Model," *JHEP* **06** (2020) 020, `arXiv:1912.04224 [hep-ph]`.

[171] W. Altmannshofer, P. B. Dev, A. Soni, and Y. Sui, "Addressing $R_{D^{(*)}}$, $R_{K^{(*)}}$, muon $g-2$ and ANITA anomalies in a minimal R-parity violating supersymmetric framework," *Phys. Rev. D* **102** no. 1, (2020) 015031, `arXiv:2002.12910 [hep-ph]`.

[172] I. Esteban, M. Gonzalez-Garcia, M. Maltoni, T. Schwetz, and A. Zhou, "The fate of hints: updated global analysis of three-flavor neutrino oscillations," `arXiv:2007.14792 [hep-ph]`.

[173] Z.-z. Xing, "Flavor structures of charged fermions and massive neutrinos," `arXiv:1909.09610 [hep-ph]`.

[174] Z.-z. Xing, H. Zhang, and S. Zhou, "Updated Values of Running Quark and Lepton Masses," *Phys. Rev. D* **77** (2008) 113016, `arXiv:0712.1419 [hep-ph]`.

[175] **T2K** Collaboration, K. Abe *et al.*, "Constraint on the Matter-Antimatter Symmetry-Violating Phase in Neutrino Oscillations," *Nature* **580** (2020) 339–344, `arXiv:1910.03887 [hep-ex]`.

[176] L. Wolfenstein, "Neutrino Oscillations in Matter," *Phys. Rev.* **D17** (1978) 2369–2374.

[177] P. B. Dev and Y. Zhang, "Displaced vertex signatures of doubly charged scalars in the type-II seesaw and its left-right extensions," *JHEP* **10** (2018) 199, `arXiv:1808.00943 [hep-ph]`.

[178] Y. Du, A. Dunbrack, M. J. Ramsey-Musolf, and J.-H. Yu, "Type-II Seesaw Scalar Triplet Model at a 100 TeV pp Collider: Discovery and Higgs Portal Coupling Determination," *JHEP* **01** (2019) 101, `arXiv:1810.09450 [hep-ph]`.

[179] K. Babu and S. Jana, "Probing Doubly Charged Higgs Bosons at the LHC through Photon Initiated Processes," *Phys. Rev. D* **95** no. 5, (2017) 055020, `arXiv:1612.09224 [hep-ph]`.

[180] S. Bhattacharya, S. Jana, and S. Nandi, "Neutrino Masses and Scalar Singlet Dark Matter," *Phys. Rev. D* **95** no. 5, (2017) 055003, `arXiv:1609.03274 [hep-ph]`.

[181] C. Arbeláez R, G. Cottin, J. C. Helo, and M. Hirsch, "Long-lived charged particles and

multi-lepton signatures from neutrino mass models," *Phys. Rev.* **D101** no. 9, (2020) 095033, arXiv:2003.11494 [hep-ph].

[182] P. Fileviez Perez, T. Han, G.-y. Huang, T. Li, and K. Wang, "Neutrino Masses and the CERN LHC: Testing Type II Seesaw," *Phys. Rev. D* **78** (2008) 015018, arXiv:0805.3536 [hep-ph].

[183] A. Melfo, M. Nemevsek, F. Nesti, G. Senjanović, and Y. Zhang, "Type II Seesaw at LHC: The Roadmap," *Phys. Rev. D* **85** (2012) 055018, arXiv:1108.4416 [hep-ph].

[184] M. Aoki, S. Kanemura, and K. Yagyu, "Testing the Higgs triplet model with the mass difference at the LHC," *Phys. Rev. D* **85** (2012) 055007, arXiv:1110.4625 [hep-ph].

[185] H. Pois, T. J. Weiler, and T. C. Yuan, "Higgs boson decay to four fermions including a single top quark below $t\bar{t}$ threshold," *Phys. Rev. D* **47** (1993) 3886–3897, arXiv:hep-ph/9303277.

[186] **ATLAS** Collaboration, M. Aaboud *et al.*, "Search for doubly charged Higgs boson production in multi-lepton final states with the ATLAS detector using proton–proton collisions at $\sqrt{s} = 13\,\mathrm{TeV}$," *Eur. Phys. J. C* **78** no. 3, (2018) 199, arXiv:1710.09748 [hep-ex].

[187] **CMS** Collaboration, "A search for doubly-charged Higgs boson production in three and four lepton final states at $\sqrt{s} = 13$ TeV,". CMS-PAS-HIG-16-036.

[188] T. Sjostrand, S. Mrenna, and P. Z. Skands, "A Brief Introduction to PYTHIA 8.1," *Comput. Phys. Commun.* **178** (2008) 852–867, arXiv:0710.3820 [hep-ph].

[189] **DELPHES 3** Collaboration, J. de Favereau, C. Delaere, P. Demin, A. Giammanco, V. Lemaître, A. Mertens, and M. Selvaggi, "DELPHES 3, A modular framework for fast simulation of a generic collider experiment," *JHEP* **02** (2014) 057, arXiv:1307.6346 [hep-ex].